Republic of Iraq
Ministry of Higher Education
and Scientific Research
University of Babylon
College of Engineering

Performance Analysis of Multiple-Input and Multiple-Output Channels with Transceiver Impairments

A Thesis
Submitted to the Department of Electrical Engineering / College of Engineering / University of Babylon in Partial Fulfillment of the Requirements for the Degree of Master in Engineering /Electrical Engineering / Electronic.

By

Mohammed Odai Abdullah Hason

Supervised by

Dr. Wasan Hashim Jacob

2022 A.D. 1444 A.H.

بِسْمِ اللَّـهِ الرَّحْمَـٰنِ الرَّحِيمِ

3.1

﴿ يَرْفَعِ اللَّهُ الَّذِينَ آمَنـــــــوا مِنكُمْ
وَالَّذِينَ أُوتُـــــــوا الْعِلْمَ دَرَجَاتٍ ﴾

صدق الله العظيم

سورة المجادلة : 11

Supervisors Certification

We certify that this thesis, titled **"Performance Analysis of Multiple-Input and Multiple-Output Channels with Transceiver Impairments"** was prepared by **(Mohammed Odai Abdullah)** under our supervision at the Electrical Engineering Department, College of Engineering at University of Babylon, in a partial fulfillment of the requirements for the degree of Master of Science in Engineering /Electrical Engineering/ Electronic.

Supervisors

Signature:

Name: Dr. Wasan Hashim Jacob

Date: / / 2022

In view of the available recommendation, we forward this thesis for debate by the examining committee.

Head of the Electrical Engineering Department

Signature:

Name:

Date: / / 2022

Acknowledgements

Thanks be to God for the insight that inspired me, and praise be to Him for the blessings He has bestowed upon me, and to Him is the credit for achieving what I aspire to in this research. Praise be to God, who by His praise opens every book and by His remembrance every speech is issued, and by His praise the people of blessings enjoy the abode of reward.

*It gives me great pleasure to extend my thanks and gratitude to (**Dr. Wasan Hashim Al-Masoody**), who provided me with the information I needed in my research*

And for the great efforts she made for me since she proposed the subject of the research and her continuous supervision, and for her advice that helped me a lot in overcoming the difficulties, I faced, calling from God success and brilliance in the scientific career.

I would like to extend my thanks and gratitude to the Deanship of the College of Engineering and the Presidency of the Electrical Engineering Department for the facilities and administrative procedures they provided me, which effectively contributed to the completion of the requirements of this research.

.

Researcher

Dedication

To my kind father.... *who taught me how to stand firmly above the earth, my role model, and my ideal in life; He is the one who taught me how to live with dignity and honor.*

To my tender mother... *the source of love, altruism, and generosity, I cannot find words that can give her her due, for she is the epic of love and the joy of a lifetime, and an example of dedication and giving.*

To my brother... *my support and who shares me the joys and sorrows.*

To all my friends and to all those from whom I received advice and support;

I dedicate to you the summary of my scientific effort.

Abstract

Multiple-input-multiple-output (MIMO) is one of the most promising directions in wireless communication systems with several attractive features for decades. The deployment of MIMO systems offers key advantages to their performance in many ways such as system capacity and multiplexing gain. However, the applicability of these systems especially in cellular network has have many drawbacks such as the observation of some modest gain in addition to the slight decrease in the throughput due to the extra overhead. Although these issues have a substantial role in degrading the system performance, there is another non-ideality which affects the performance of the MIMO systems. This non-ideality is called the transceiver impairments which is the focus of this thesis.

This thesis proposes two algorithms for analyzing the performance of MIMO channels affected by Rayleigh flat fading in the existence of the actual transceiver (physical transceiver). The first algorithm analyzes the performance of the correlated MIMO channel and the uncorrelated MIMO channel in the presence of the actual transmitter in four different scenarios: multi-carrier multiple-input and multiple-output (MC-MIMO) system with channel state information available to the transmitter (CSIT), MC-MIMO system with channel state information available to the receiver (CSIR), single-carrier multiple-input and multiple-output (SC-MIMO) system with CSIT, and SC-MIMO system with CSIR. This algorithm takes the effect of the physical transmitter to be additive Gaussian distortion noise with zero mean and variance. While, the second algorithm analyzes the performance of the correlated MIMO channel and the uncorrelated MIMO channel in the existence of the actual transmitter and actual receiver in one scenario, namely, the SC-MIMO system with CSIR. This method evaluates the

influence of the physical receiver as additive uncorrelated Gaussian distortion noise with zero mean and variance.

The work's most important result is that the MIMO channel's capacity in the first and second algorithms at the high SNR rates stops growing at a value called the capacity limit. In the meantime, the correlation coefficient in the first algorithm does not own an effect on the value of the capacity limit, while the correlation coefficient in the second algorithm plays an important role in determining the capacity limit. More clearly, The capacity limit of the 4*4 MIMO system is 29.19 bit/second/hertz for an impairment level of 0.08 and any value of correlation coefficient in the first algorithm. For the second algorithm, the capacity limit of the 4*4 MIMO system is 21.23 bit/second/hertz for an impairment level equal to 0.08 and value of correlation coefficient equal to zero, and its equal to 19.98 for an impairment level equal to 0.08 and value of correlation coefficient equal to 0.4.

List of Contents

List of Contents

List of Tables

List of Tables

List of Tables

List of Figures

List of Figures

List of Figures

List of Figures

List of Abbreviations

Abbreviation	Definition
ADCs	Analogue-to-Digital Converters
AF	Amplify-and-Forward
BER	Bit Error Rate.
CMIMOC	Correlated MIMO channel
CSI	Channel State Information
CSIR	Channel State Information Available to the Receiver
CSIT	Channel State Information Available to the Receiver and Transmitter
DACs	Digital-to-Analogue Converters
DF	Decode-and-Forward
DFS	Doppler Frequency Shift
DH	Dual-Hop
DS	Doppler Spread.
EC	Ergodic Capacity
FFF	Frequency-Flat Fading
FSF	Frequency-Selective Fading
F-SNRMG	Finite-SNR Multiplexing Gain
I	In-phase
IQ mixer	In-phase and Quadrature-phase mixer
ISI	Intersymbol interference.
ISR	Image-to-Signal-Power-Ratio
LNA	Low Noise Amplifier
LO	Local Oscillator
low-IF TX	Low Intermediate Frequency Transmitter.
LTE	Long-Term Evolution
MC	Multi-Carrier
MC-MIMO	Multi-carrier Multiple-input and Multiple-output System
MG	Multiplexing Gain
MIMO	Multiple-input and Multiple-output

List of Abbreviations

Abbreviation	Definition
MISO	Multiple-input and Single-output
PA	Power Amplifier
PN	Phase Noise
Q	Quadrature-phase
RF	Radio Frequency
RFT	Radio Frequency Transceiver
SC	Single- Carrier.
SC-MIMO	Single- Carrier Multiple-input and Multiple-output System
SD	Spatial Diversity
SER	Symbol Error Rate.
SIMO	Single-input and Multiple-output
SISO	Single-input and Single-output
SM	Spatial Multiplexing
SNR	Signal-to-Noise Ratio
SNRs	Signal-to-Noise Ratios
SVD	Singular Value Decomposition
UMIMOC	Uncorrelated MIMO channel
zero-IF TX	Zero Intermediate Frequency Transmitter.
ZMCSCG	Zero Mean Circular Symmetric Complex Gaussian.
IF	Intermediate Frequency.

List of Symbols

Symbol	Definition
$u_{n_t}(t)$	Digital Baseband Signal in Figure (1.1).
$y_{RF,nr}(t)$	Radio Frequency Signal in Figure (1.1).
τ_c	Coherence time.
B_D	Doppler spread.
F_D	Doppler frequency shift.
v_e	Velocity of the Moving Body.
C_e	Light's Speed.
f_c	Carrier Frequency.
Θ	The Angle Between the Direction of Movement of the Object and the Line Connecting the Receiver to the Transmitter.
B_C	Coherence Bandwidth.
H	Uncorrelated MIMO Channel Matrix.
$h_{i,j}(t,\tau)$	Impulse Responses from the ith Transmit Antenna to the jth Receive Antenna.
Y	Received Signal Vector in Ideal MIMO Channel Model.
S	Transmitted Signal Vector in Ideal MIMO Channel Model.
Q	Covariance Matrix of the Transmitted Signal Vector in Ideal MIMO Channel Model.
Z	Gaussian Noise Vector.
N	Number of Transmitting Antennas.
M	Number of Receiving Antennas.
U	Unitary Matrix with $M \times M$ in the Singular Value Decomposition Analysis.
V	Unitary Matrix with $N \times N$ in the Singular Value Decomposition Analysis.
Σ	Singular Values Matrix.
Ra_H	Rank degree of the MIMO Channel Matrix.
C_{id}	Deterministic Uncorrelated MIMO Channel Capacity in Ideal Model.
$I(.,.)$	Mutual Information Between Two Vectors of Random Variables.
$\mathcal{H}(Y)$	Differential Entropy of Y.

List of Symbols

Symbol	Definition
$\mathcal{H}(Y/S)$	Conditional Differential Entropy of Y when S is Known.
$\mathcal{H}(Z)$	Differential Entropy of Z.
Q_Y	Covariance Matrix of the Received Signal Vector in Ideal MIMO Channel Model.
Q_Z	Covariance Matrix of the Noise Vector in Ideal MIMO Channel Model.
I_M	Unity Matrix with Size M × M.
$\mathbb{E}(.)$	Expectation Operator
$(.)^H$	Performing the Hermitian Operation on the Matrix Within the Bows
D_{M*M}	A Diagonal Matrix with Size M × M, its Diagonal Element Values Represent the Power for the SISO Channels (Effective Channels).
λ	A Diagonal Matrix with Size M × M, its Diagonal Element Values Represent the Eigenvalues of H H^H.
D_i	The Power of the ith Effective Channel.
λ_i	The Channel Gain (Eigenvalue) of the ith Effective Channel.
Ω	Water Level Value.
C_{eid}	Ergodic Capacity of Uncorrelated MIMO Channel in Ideal Model.
L	Number of Realizations of the Channel.
H_k	Correlated MIMO Channel Matrix.
D_t	The Transmit Correlation Matrix with Size N × N.
D_r	The Receive Correlation Matrix with Size M × M.
α_t	The Correlation Coefficient on the Transmitting Side.
α_r	The Correlation Coefficient on the Receiving Side.
$\lambda_{k\,i}$	The Channel Gain of the ith Effective Channel in Correlated MIMO Channel.
$D_{k\,i}$	The Power Assigned to ith Effective Channel in the Correlated MIMO Channel.
r	Multiplexing Gain in Ideal MIMO Channel Model.
R	Data Rate (bps) per Unit Hertz.
C_{Seid}	Ergodic Capacity of the SISO channel in Ideal Model.

List of Symbols

Symbol	Definition
x_I and x_Q	The Real Part and Imaginary Part of the Input Signal, Respectively.
ΔG	Gain Imbalance.
G_I	The Gain of I Branch.
G_Q	Gain of Q Branch.
$\Delta\Phi$	The Phase Error Between I and Q Branches.
Δf	The Frequency of Baseband Signal.
B_a	Bandwidth for the Desired signal.
$y_{BB}(t)$	Baseband Frequency Signal FIG. (2.11)
∇f	Offset Frequency.
$v(t)$	Voltage of the Input Signal in the Sampling Jitter.
A_a	The signal's Amplitude in the Sampling Jitter.
Δv_{j_rms}	RMS Jitter Noise.
Δt_{j_rms}	RMS Time of Jitter.
L_q	Number of Quantization Levels
w	Number of Bits for Each Level
Υ_{tDF}	Variance of the Distortion of the Transmitter in the DF Relay System with Multi-antenna Terminals
κ_{tDF}	Level of the Degradation of the Transmitter that is used in the DF Relay System with Multi-antenna Terminals.
σ_t	Transmitter Distortion.
σ_r	Receiver Distortion.
Υ_t	Variance of the Transmitter Distortion in the MIMO System.
Υ_r	Variance of the Receiver Distortion in the MIMO System.
Y_{a1}	Received Signal Vector of the Uncorrelated MIMO channel in the First Algorithm.
R_{XX}	Covariance Matrix of the Transmitted Signal Vector in Physical MIMO Channel Model.
κ_t	Level of the Degradation of the Transmitter that is used in the MIMO System.
C_{a1}	Deterministic MIMO Channel Capacity in the First Algorithm.

List of Symbols

Symbol	Definition
$\mathcal{H}(\mathrm{Y_{a1}})$	**Entropy of the Received Signal Vector ($\mathrm{Y_{a1}}$).**
$\mathcal{H}(\mathrm{Y_{a1}/X})$	**Entropy of the Received Signal Vector ($\mathrm{Y_{a1}}$) Given the Transmitted Signal Vector (X).**
$\mathrm{R_{Y_{a1}}}$	**Covariance Matrix of the Received Signal Vector $\mathrm{Y_{a1}}$ in Physical MIMO Channel Model.**
$\mathrm{R_{Y_{a1}/X}}$	**Covariance Matrix of the Received Signal Given the Transmitted Signal ($\mathrm{Y_{a1}}$ / X) in Physical MIMO Channel Model.**
$\mathrm{C_{ea1}}$	**Ergodic Capacity of Uncorrelated MIMO Channel in the First Algorithm**
A, C, F	***A* is a square matrix with any size, *C* is a diagonal matrix with a size similar to the size of *A*, and *F* is a diagonal matrix with a size similar to the size of *C*.**
μ_{a1}	**Finite-SNR Multiplexing Gain of the Uncorrelated MIMO Channel in the First Algorithm.**
μ_{ca1}	**Finite-SNR Multiplexing Gain of the Correlated MIMO Channel in the First Algorithm.**
$\mathrm{C_{Sea1}}$	**Ergodic Capacity of the SISO channel in the First Algorithm.**
$\mathrm{Y_{ca1}}$	**Received Signal Vector of the Correlated MIMO channel in the First Algorithm.**
$\mathrm{C_{ca1}}$	**Ergodic Capacity of the Correlated MIMO Channel in the First Algorithm**
$\mathrm{Y_{a2}}$	**Received Signal Vector of the Uncorrelated MIMO channel in the Second Algorithm.**
$\mathrm{Y_{ca2}}$	**Received Signal Vector of the Correlated MIMO channel in the Second Algorithm.**
κ_{r}	**Receiver Impairment Level in the MIMO System.**
C_{ea2}	**Ergodic Capacity of the Uncorrelated MIMO Channel in the Second Algorithm.**
$\mathrm{C_{ca2}}$	**Ergodic Capacity of the Correlated MIMO Channel in the Second Algorithm.**
μ_{a2}	**Finite-SNR Multiplexing Gain of the Uncorrelated MIMO Channel in the Second Algorithm.**
μ_{ca2}	**Finite-SNR Multiplexing Gain of the Correlated MIMO Channel in the Second Algorithm.**

Chapter One

General Introduction

CHAPTER ONE
INTRODUCTION

1.1 Overview

In the past decades, most wireless communication systems consisted of one antenna for signal transmission and another for signal reception. Those systems are called the single-input and single-output (SISO) systems. The problem in those systems is represented that there is one link between the transmitting and receiving sides, which means that the probability of a successful transmitting process is not large. Therefore, other systems, such as Single-Input and Multiple-Output (SIMO) system and Multiple-Input and Single-Output (MISO) system, have appeared lately to generate more links between the transmitting side and receiving side, which means increases the probability of the successful transmitting process. However, the demand to obtain a high data rate without increasing the transmitting power or bandwidth led to the emergence of what is known as a multiple-input and multiple-output (MIMO) system, which means having more than one antenna on both the transmitting side and receiving side [1], [2]. In fact, the MIMO system can be used in two different techniques. The first technique aims to fight channel fading to increase reliability and improve the bits error rate. This technique sends the same signal from each transmitting antenna, so it is called the spatial diversity (SD) technique. In contrast, the second technique exploits channel fading to increase the system capacity. This technique divides the transmitted signal bits over the transmitting antennas to send them simultaneously, so this technique is called the spatial multiplexing (SM) technique. The main purpose of this technique is to maximize the MIMO system capacity [3], [4].

In addition, in the spatial multiplexing technique, the channel capacity of the MIMO system increases semi-linearly with the increase in the signal-to-

noise ratio (SNR) and degree of freedom, which means that in high SNRs, the MIMO channel capacity grows unboundedly. Also, the maximum value of the multiplexing gain of the MIMO channel is equal to the minimum number between the number of transmitting antennas and the number of receiving antennas [5]. However, there are many criteria that have a negative influence on the performance of the MIMO capacity, and the most popular of them is the correlation between the channel elements. This correlation depends on the spacing between the antennas used in the system [6]. All these characteristics mentioned are dedicated to the ideal MIMO system, which means that transceivers used in the MIMO system are ideal. In other words, the ideal MIMO system means that the transceivers used in the MIMO system do not affect the signal that passes through them; Figure 1.1 shows the block diagrams of the ideal transmitter and receiver in the wireless system.

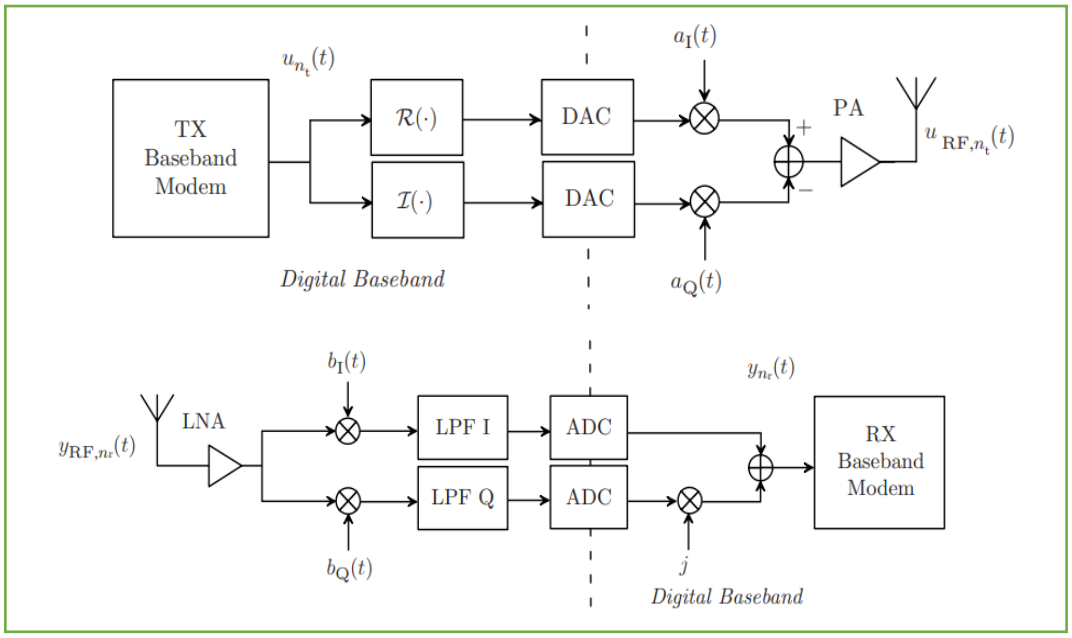

Fig.1.1: Block diagrams for ideal transmitter and receiver in the wireless system [7].

The above figure shows that in the transmitter, the digital-to-analogue converters (DACs) take the real and imaginary parts of the digital baseband signal u_{n_t} (t) and turn them back into an analogue signal. The signal is then turned up to radio frequency (RF), using the structure shown in the figure for

quadrature mixing. Before being sent through the channel, the RF signal goes through the power amplifier (PA), which is assumed to be perfect with a gain of 1. In contrast, Figure (1.1) indicates that in the receiver, the antenna receives the signal and then enters the signal on the low noise amplifier (LNA), which will be assumed to be perfect with unity gain. Then, the RF signal $y_{RF,nr}$ (t) flows through two parallel branches. In the first branch, the RF signal is multiplied by a sinusoidal signal generated by the local oscillator (LO). In the second branch, the RF signal is multiplied by the same signal utilized in the first branch but with a 90-phase shift. Low-pass filtering is employed in both branches to remove higher-order modulation products. Both signals are then transferred through the analogue to-digital converter (ADCs) and merged to generate the baseband signal y_{n_r} (t), which is fed to the baseband RX modem [7].

Moreover, the ideal transceiver has advantages and disadvantages. The most popular advantage is that the quality of the signal that comes out from the ideal transceiver is very high. At the same time, the most popular disadvantage is represented that the ideal transceiver has a high manufacturing cost, which makes the use of the ideal transceiver in practical systems very limited. Therefore, the scientists turned towards designing the transceivers at the lowest possible cost, which reduces the quality of these devices. In other words, in fine conditions, the wireless system (e.g., MIMO system) contains a low-cost transceiver (physical transceiver), which suffers from many defects such as phase noise, quantization noise, non-linear amplifier, IQ imbalance, sampling jitter, etc. These defects affect the signal passing over the transceiver, which degrades the system performance [8]. Therefore, the effect of the physical transceiver cannot be neglected when analyzing the performance of the wireless channel.

In this chapter, some research that analyzes the performance of different wireless systems in the presence of the physical transceiver (non-ideal transceiver) will be offered. The studies that focus on a system containing a MIMO channel will have the largest share because the proposed work here is related to the MIMO channel.

1.2 Problem Statement

The MIMO system is one of the most important communication systems currently relied upon. Compared to other systems, the most important benefit of the MIMO system is the capacity increase without excessive power consumption or expanding bandwidth allocated to the system. The MIMO system contains three main parts: transmitter, channel, and receiver. Both transmitter and receiver contain RF chains. The number of RF chains in the transmitter equals the amount of transferring antennas, and the number of RF chains in the receiver equals the number of receiving antennas. The signal in each RF chain passes through many processes; in the transmitter, the signal passes through a digital process, DAC, IQ mixer, and power amplifier. In the receiver, the signal also passes through the same processes but inversely, and the converter used is ADC. However, in practical reality, the quality of the devices that performs these processes is not high. In other words, the transceiver used in the MIMO system on the transmission side, reception side, or both, suffers from many impairments such as phase noise, quantization noise, non-linear amplifier, IQ imbalance, sampling jitter, etc. These impairments affect the signal that passes through the transceiver, which degrades the system performance. Also, the channel type impacts the system's performance, where if the channel contains the correlation between its elements, its performance degrades. Therefore, to get on results close to the results of real reality, the

performance of the MIMO system must be analyzed and consider all these impacts.

1.3 Literature Survey

Studer et al (2010) [11] derived the ergodic capacity (EC) equation for one realization for the uncorrelated MIMO channel that suffers from Rayleigh flat fading in the presence of the physical transmitter. The researchers assumed that the system used in their work is the multi-carrier (MC) MIMO system (one subcarrier), and the channel state information is available in the receiver only (i.e., CSIR). Also, they considered that the effect of the physical transmitter in the system is modeled as an uncorrelated Gaussian distortion noise with zero mean and variance represented as a unity matrix with size $N \times N$ (where N is the number of the transmitting antennas), which is multiplied by an impairment level of the transmitter. Their research results showed that the capacity of the uncorrelated MIMO channel is affected in a negative form by the distortion of the physical transmitter. Also, they showed that the capacity of the ith eigenmode approaches the traditional capacity (capacity without the effect of the physical transmitter) when the channel gain value of this eigenmode is small. The level of impairment for the transmitter used in their research is 0.025.

Markus Wenk et al. (2011) [12] investigated the effect of the physical transmitter on the ergodic capacities of the uncorrelated MIMO channel with a very long distance between the transmitter and receiver and uncorrelated MIMO channel with a natural or small distance between the transmitter and receiver. They supposed that both channels suffer from Rayleigh flat fading. Also, the researchers assumed that the system employed in their work is the multi-carrier MIMO system (one subcarrier) and that only the receiver has access to channel

state information (i.e., CSIR). In addition, they characterized the effect of the physical transmitter in the system as an uncorrelated Gaussian distortion noise with zero mean and variance represented by a unity matrix of size $N \times N$ multiplied by a transmitter impairment level. They showed by their scientific research that the capacity of the uncorrelated MIMO channel for the very long link approaches the traditional capacity. In contrast, their research illustrates that the distortion of the transmitter affects the capacity of the uncorrelated MIMO channel for the short link or natural link.

Bjornson Emil et al. (2012) [13]. Illustrated the behavior of ergodic capacity and multiplexing gain for the uncorrelated MIMO channel that suffers from Rayleigh flat fading in the presence of the physical transmitter with impairments level 0.05. The researchers assumed that the system used in their work is the multi-carrier MIMO system (one subcarrier), and the channel state information is available in the receiver and transmitter (i.e., CSIT). The authors modeled the effect of the transmitter as an uncorrelated Gaussian distortion noise. In more detail, the authors assumed that the total transmitter distortion is equal to the sum of transmitter distortion power at each transfer antenna, which is proportional to the power of transmitted signal, divided by the number of transmitting antennas. The drawings presented in their paper showed that at the high SNR rates, the capacity of the uncorrelated MIMO channel in the presence of the physical transmitter stopped growing at a particular value. That specific value was called the capacity limit.

Merouane Debbah et al. (2013) [14] showed the behavior of amplify-and-forward (AF) relaying system capacity under Nakagami-m flat fading. The authors assumed that the system used in their work is the multi-carrier system (one subcarrier), and the transmitters used on the source and relay sides are

physical, with an impairment level of 0.05 for both. Their work depends on the fact that the distortion of the transmitter on the source side is proportional to signal power transmitted, and the distortion of the transmitter on the relay side depends on the average signal power transmitted from the relay. The research shows that the capacity of the AF relaying system under the proposed conditions is stopped growing in the high SNRs at a limit that is inversely proportional to the impairment level of the transmitter used on the source and impairment level of the transmitter used on the relay. This work assumed a single antenna on the source, relay, and Destination sides.

Zhang et al. (2014) [15] analyzed the uncorrelated MIMO channel capacity (ergodic capacity) under Rayleigh flat fading in the presence of the physical transmitter and physical receiver, with a degradation level of 0.15 for both. The researchers assumed that the system used in their work is the single-carrier (SC) system, and the channel information is available exclusively in the receiver (i.e. CSIR). Their work is dependent on the fact that the effect of the transmitter at the nth transmit antenna is commensurate to the signal power transmitted through the same antenna and that the effect of the receiver in the mth receive antenna is proportional to the average signal power received through the mth row of the channel matrix (i.e., the receiver distortion at the mth receive antenna is proportional to total received signal power through the same antenna). Their research revealed that in a high SNR regime, the channel capacity with the physical transmitter and the physical receiver stops growing at a particular value called the capacity limit.

Papazafeiropoulos et al. (2015) [16] investigated the impact of hardware impairments on the ergodic capacity of dual hop (DH) amplify and forward (AF) massive MIMO relay systems. The work happens in the presence of the physical hardware (transmitter of users, receiver of relay, transmitter of relay,

and receiver of base station) with different impairment levels $\in \{0, 0.01\}$. The authors assumed that entries of the two channels (channel from users to relay and channel from relay to base station) are independent and have identical distribution (Rayleigh flat distribute). Also, the authors considered that total system channel state information is unknown at the relay station and the users. Their work depended on the fact that the effect of the transmitter at the nth transfer antenna in any channel is proportional to the transmitted signal power through the same antenna, and the impact of the receiver at the mth receive antenna in any channel is proportional to the total received signal power through the same antenna. Their article results showed that capacity saturates after a specific value of SNR, and the point of saturation is affected by the levels of impairment of the hardware used in the system, which is of equal value in their research.

Kefeng Guo and others (2016) [17] derived the instantaneous capacity formula of the dual-hop decode-and-forward (DF) satellite relay system in the Rician fading case. The system they depended on in their work consisted of a source with N antennas, a satellite relay with a single antenna, and a destination with M antennas. Also, their work assumed the presence of the physical transmitters in the receiving process of the uplink signal and receiving process of the downlink signal. The researchers considered that the effect of the transmitters in uplink and downlink is proportional to the average power of the transmitted signal. The graphics presented by their research showed that the capacity of the proposed system is not affected by the hardware impairment in the low SNR rates but is affected by the hardware impairment in the high SNR rates. The levels of impairment used in this work are 0.3 and 0.6.

Sharma et al. (2017) [18] investigated the impact of hardware impairments on the ergodic capacity of dual hop (DH) amplify and forward (AF) MIMO relay systems with both finite and infinite numbers of antennas. The researchers assumed that all hardware used in the system is physical with impairment level 0.05 for all. The authors considered that entries of the two channels (channel from users to relay and channel from relay to base station) are independent and have identical distribution (Rayleigh distribute). Also, they consider that total system channel state information is unknown at the relay station and users. In addition, their work depended on the fact that the effect of the transmitter at the nth transfer antenna in any channel is proportional to the transmitted signal power through the same antenna, and the impact of the receiver at the mth receive antenna in any channel is proportional to the total received signal power through the same antenna. Their result showed that capacity affected by impairments hardware in the high SNR regime for both systems (DHAF MIMO system with finite numbers of antennas and DHAF MIMO system with infinite numbers of antennas). Also, the results showed that the capacity with transceivers impairments is directly proportional to relay gain.

A. Singal and others (2017) [19] examined the behavior of ergodic capacity for the uncorrelated MIMO-OFDM channel with Rayleigh flat fading in the presence of a physical transmitter with an impairments level of 0.05. The researchers assumed that only the receiver has access to channel state information (i.e., CSIR). In addition, the authors believed that transmitter distortion is described as an uncorrelated Gaussian distortion noise with a zero mean and a variance proportionate to the transmitted signal's strength. Drawings shown in their work demonstrated that at high SNR rates, the capacity of the uncorrelated MIMO channel in the presence of the physical transmitter ceased to increase at a certain threshold, which is referred to as the capacity limit.

Singal and Kedia (2018) [20] investigated the energy efficiency of bulk and per-subcarrier antenna selection strategies in the MIMO-OFDM system with and without physical transmitter limitations (distortion of the transmitter). The channel used in their work is the uncorrelated channel that suffers from flat Rayleigh fading. Their work required finding the ergodic capacity of the uncorrelated MIMO-OFDM channel with and without transmitter defects. Also, their work assumed that the channel state information is available at the receiver only (CSIR), and the effect of the transmitter at the nth transfer antenna is proportional to transmitted signal power through the same antenna. From their work, it has been noticed that as the value of these transmitter deficiencies grows, the energy efficiency falls. The impairment level for the transmitter used in their work is 0.05.

Mengyan Huang et al. (2018) [21] showed the behavior of the ergodic capacity of the Large-scale uncorrelated MIMO channel that suffers from the Rician fading in the presence of the physical receiver. The authors assumed that the channel state information is available at the receiver only. Their work depends on the fact that the impact of the receiver at the mth receive antenna is proportional to the total received signal power through the same antenna, which is suffer from path loss and the shadowing.

Papazafeiropoulos and others (2018) [22] shifted their focus on the ergodic capacity of Rayleigh-product MIMO channel with K number of scatters and in the presence of the physical transmitter or a physical receiver. From their research, it can be seen that the channel matrix in Rayleigh-product channel consists of two matrices, the first matrix between the transmitter and scatters and the second between the scatters and receiver. The researchers assumed that the entries of the two matrices are independent of each other and all subject to

Rayleigh distributed. In addition, they considered that the information of both channels is known in the receiver (i.e., CSIR). Their work results showed that at the high SNRs, the performance of capacity of the Rayleigh-product channel in the case of the physical transmitter is better than its performance in the case of the physical receiver. Also, their work results showed that at the medium SNRs, the performance of capacity of the Rayleigh-product channel in the case of the physical receiver is better than its performance in the case of a physical transmitter. The impairment level that the researchers used in their work is 0.15 for both transmitter and receiver when one of them is used as a physical device.

Jingjing and others (2019) [23] studied the ergodic capacity of dual-hop (DH) decode-and-forward (DF) multi-Relay Networks. Their studies depend on a system consisting of a source with a single antenna, N number of relays, each containing a single antenna for transmitting, a single antenna for receiving, and a destination with a single antenna. The researchers used two methods to select a relay used in a communicated process: random relay selection (RRS) and opportunistic relay selection (ORS). Their work happens in the presence of a physical transmitter on the source side and a physical receiver on the destination side. Their research results showed that the capacity of the proposed system in the case of ORS is better than in the case of RRS for any value of SNR. the impairment level used in this work is 0.05.

S. Bharati et al. (2020) [24] investigated the ergodic capacity and multiplexing gain of the uncorrelated MIMO channel that suffers from Rayleigh flat fading in the presence of the physical transmitter with varying values of impairment level (0.01, 0.02, 0.2, 0.3, and 0.4). The authors assumed that the total transmitter distortion is equal to the sum of transmitter distortion power at each transfer antenna, which is proportional to the power of the transmitted signal, divided by the number of transmitting antennas. They

devoted their work to multi-carrier systems (one subcarrier) with channel state information know at the receiver only (CSIT).

1.4 Summary of Literature Review and Contribution

In the previous section, all researches that looked at the wireless channel, which has multiple antennas on the transmission side, the reception side, or both, and a physical transceiver, show that all of the authors focused on the uncorrelated wireless channel.

Moreover, the studies focusing on the natural MIMO system fall into two main groups. The first group analyzes the uncorrelated MIMO channel in the presence of the physical transmitter, with differencing some criteria. This group devoted their work to the multi-carrier system for one subcarrier. The second group analyzes the uncorrelated MIMO channel in the presence of the physical transmitter and physical receiver, with differencing some criteria. This group devoted their work to the single-carrier system. As is known, any MIMO system in practical reality is subject to the impact of the correlation between the channel elements. Also, the practical reality has many MIMO systems, such as single-carrier and multi-carrier MIMO systems. Therefore, it became necessary to develop algorithms to analyze the two types of MIMO channels (correlated MIMO channel and the uncorrelated MIMO channel) in the presence of the physical transceiver. On the other hand, at least an algorithm for analyzing MIMO channels in the presence of the physical transceiver for different systems scenarios should be provided. As a result, this letter presented two algorithms to analyze the MIMO channels that suffer from Rayleigh flat fading in the presence of the physical transceiver. The first algorithm keeps pace with the group that specializes in analyzing the MIMO channel in the presence of a physical transmitter. The second algorithm keeps pace with the group that specializes in analyzing the MIMO channel in the presence of the physical

transmitter and the physical receiver. The two algorithms and the scenarios that each one covers can be summed up as follows:

- The first algorithm analyzes the performance of the correlated MIMO channel and uncorrelated MIMO channel in the presence of the physical transmitter in several scenarios:
  - MC-MIMO system with CSIT
  - MC-MIMO system with CSIR
  - SC-MIMO system with CSIT
  - SC-MIMO system with CSIR

- The second algorithm analyzes the performance of the correlated MIMO channel and uncorrelated MIMO channel in the presence of the physical transmitter and physical receiver in one scenario, namely, SC-MIMO system with CSIR.

The first algorithm considers the effect of the physical transmitter as additive uncorrelated Gaussian distortion noise with zero mean and variance indicated by the symbol Υ_t. This algorithm considers that the distortion power of the physical transmitter at the nth transmit antenna in the SC-MIMO system is proportional to the power assigned to the signal transmitted through the same antenna. While in the MC-MIMO, this algorithm considers that the total distortion power of the physical transmitter is equal to the sum distortion power of each transmit antenna, which is calculated in the same way in the SC-MIMO system, divided by number of transmitting antennas.

In addition, the second algorithm considers the effect of the physical transmitter in the same way as the first algorithm, and it considers the effect of

the physical receiver as additive uncorrelated Gaussian distortion noise with zero mean and variance indicated by the symbol Υ_r. This algorithm considers that the distortion power of the physical receiver at the nth receive antenna in the SC-MIMO system is proportional to the average signal power received through the mth row of the channel matrix.

Finally, the two algorithms proposed in this work analyze the performance of the correlated MIMO channel and uncorrelated MIMO channel in terms of the ergodic capacity (EC) and the finite-SNR multiplexing gain (F-SNRMG), and they use the Kronecker model to calculate the correlation between the channel elements. Also, the value of the impairment level that will be used in the simulation processes of these algorithms is 0.08, 0.175, or both. Due to using these values of impairments level, the work becomes devoted to the LTE system, where the impairments level of the transceiver in LTE systems is in the range from 0.08 to 0.175, as mentioned in [25].

1.5 Work Objectives

This research seeks to investigate the crucial properties and methods appropriate to design a wireless MIMO channel. The objective of this work can be summarized as follows:

1. The physical MIMO system can achieve great results with a finite upper capacity limit, for any channel distribution and SNR.

2. It aims to adapt the suitable number of transmitting / receiving antennas appropriate to achieve great gains from employing MIMO and spatial multiplexing.

3. The practical MIMO gain is shown to be at least as large as with ideal transceivers.

1.6 Thesis Outlines

The first chapter presents an overview of the evolution of communication systems and their gradation from the SISO system to the MIMO system, the structure of the transceiver, a problem statement, and a literature review of related works.

Chapter two introduces the theory of the ideal MIMO system, showing the capacities of the ideal uncorrelated MIMO channel and ideal correlated MIMO channel in the CSIT and CSIR cases. Also, it shows the most important defects that the transceiver used in the MIMIO system suffers from them.

Chapter three introduces the proposed algorithms of the MIMO channels in the physical form. Also it introduces flowcharts to these algorithms.

Chapter four Introduces the results and discussions of the algorithms proposed in the third chapter.

Finally, chapter five concludes the major contributions of the present work and proposes several extensions to our work.

Chapter Two

Background Theory

CHAPTER TWO

Background Theory

2.1 Introduction

This chapter outlines some of the fundamental principles required for comprehension of this work. This chapter begins with an explanation of multipath fading so that the reader may differentiate between slow and rapid fading and understand what frequency flat fading and frequency selective fading mean. Then, this chapter clarifies the conventional MIMO channel model and the SVD technique for analyzing the MIMO channel matrix. This chapter then describes the basic strategies required to implement the MIMO system. This chapter next describes the capacity of the conventional MIMO channel model and the factors that influence it. Then, this chapter begins with an introduction to non-ideal physical transceivers, wherein the eighth section explains some of the transceiver's problems and the final section demonstrates how to simulate the transceiver's defects in communication systems with many antennas.

2.2 Multipath Fading

Multipath fading refers to the accumulation of several different propagation paths within the channel for the same signal transmitted. More clearly, when a signal is sent from the transmitter, it will take different paths on its way to the receiver. These different paths are generated by the reflection, refraction, and scattering of the transmitted signal within the channel, as shown in Fig. (2.1) [26], [27].

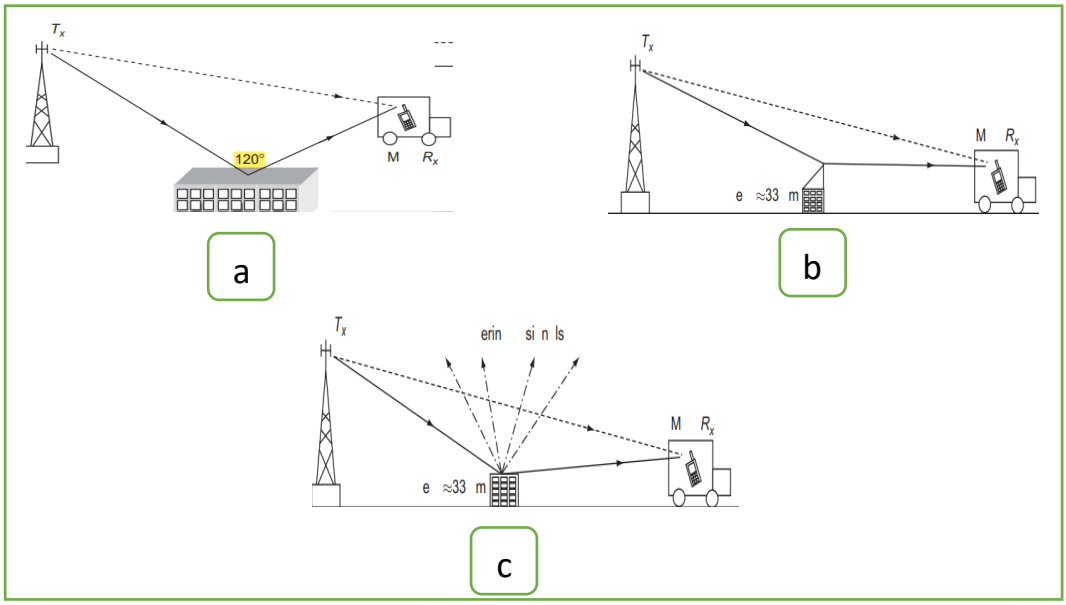

Fig. 2.1: Multipath signals due to: a) Reflection, b) Refraction, c) Scattering [28]

Moreover, multipath signals arrive at the receiver and collect constructively or destructively [29], [30]. The reason for this is that when the signal is sent, it will take several paths, and each path will travel a certain distance. Therefore, each path will have an arrival time and attenuation and based on the access time of each path, the phase of this path changes [30]. Also, the multipath environment induces rapid channel fluctuations and, therefore, small-scale fading; Figure (2.2) shows that if the same impulse is sent from the transmitter at different times, the received signal will be dissimilar due to channel fluctuations [31].

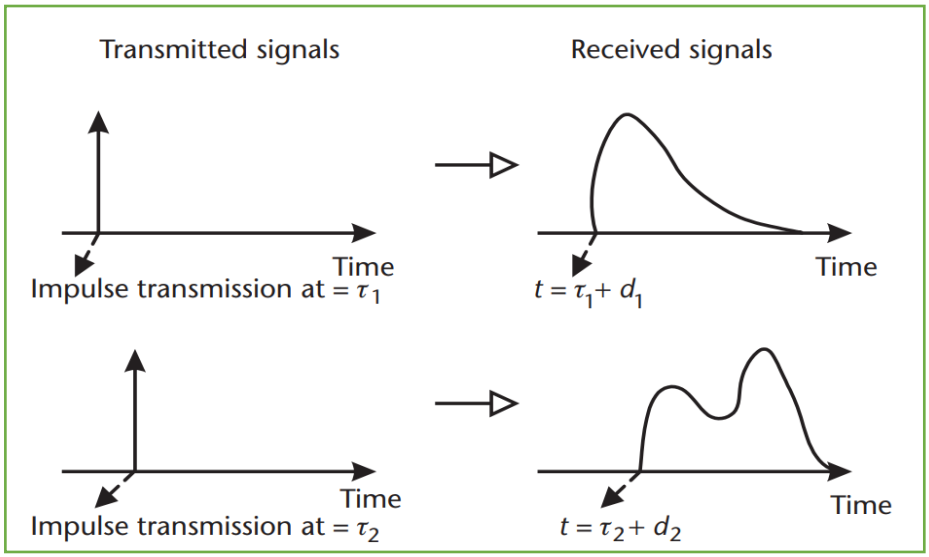

Fig. 2.2: Impulse response of multipath channel [31].

Furthermore, channel fading in the time domain can be described by the Coherence time and Doppler spread, and each can be defined as follows [31]:

- **Coherence time(τ_c):** It is the minimum time after which the form of the channel impulse response becomes unrelated to the previous case. In a clearer sense, it is the minimum time that the channel's impulse response can remain constant [32].
- **Doppler spread (DS):** It describes how the bandwidth of the signal at the receiver is extended [31], [33].

Doppler spread or what is called Doppler bandwidth can be given by the following relationship [31], [34]:

$$B_D = 2F_D \tag{2.1}$$

where F_D represents a Doppler frequency shift (DFS), which refers to the change in carrier frequency at the receiver when the receiver, transmitter, or both are moving [31], [34]. The DFS for single path is given by the following relationship [35]:

$$\mathbf{F_D = \frac{v_e}{C_e} * f_c * \cos\vartheta} \quad (2.2)$$

where v_e is the velocity of the moving body, C_e is the light's speed, f_c is the carrier frequency, and ϑ is the angle between the direction of movement of the object and the line connecting the receiver to the transmitter. In the case of multipath reception, the signals arrive by the individual paths to the receiving antenna with different Doppler shifts. This difference in the Doppler shifts happens due to the change of angle ϑ at every moment during the body's movement, so the received spectrum will be spread [35]. In light of these definitions, it can be concluded that coherence time is inversely proportional to the Doppler spread [36]:

$$\mathbf{\tau_c \approx \frac{1}{B_D}} \quad (2.3)$$

The above equation indicates that the Doppler shift frequency is zero in the absence of movement. Thus, the coherence time will be equal to infinity.

Additionally, through the two terms coherence time and Doppler spread, fading can be classified into two types [37]:

- **Slow fading:** The channel will have slow fading if the coherence time is large, where it will be greater than the time of sending the unit data, which means that the channel fading does not change during the transmission of the unit data [37].
- **Fast fading:** Unlike the previous case in slow fading, here, the channel will have a fast fade if the coherence time is short, where it will be smaller than the time of sending the unit data, which means that the channel fading will change during the transmission of the unit data [37]. The contrast between fast and slow fading paths is adorned in Fig. (2.3) [38].

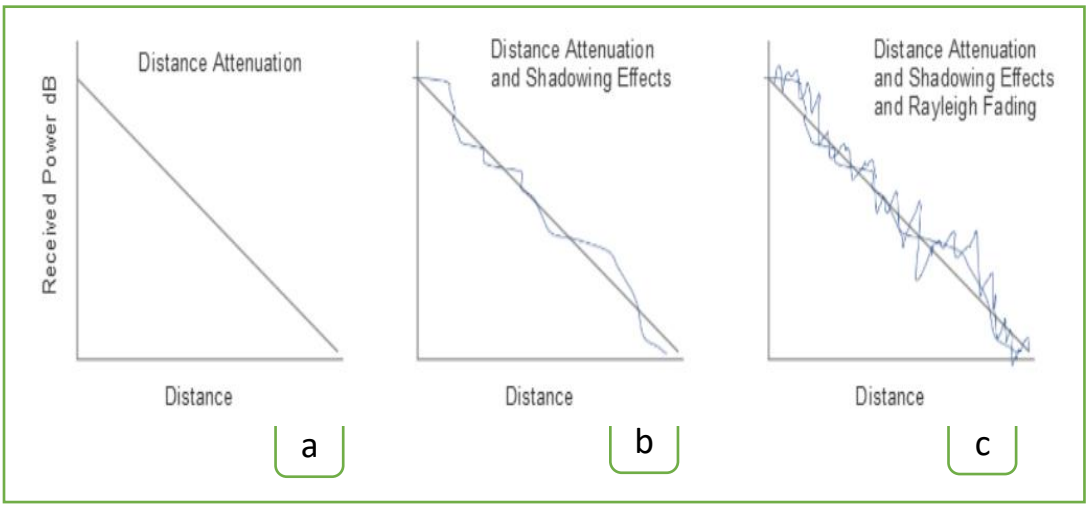

Fig. 2.3: The contrast between slow fading and fast fading: a) path loss of power over distance, b) slow fading effect, c) slow fading effect, fast fading effect, and path loss effect at the same time [38].

As is the case in the time domain, where fading is characterized based on coherence time and Doppler spread. In the frequency domain, channel fading can be described by coherence bandwidth and delay spread, and they can be defined as follows [31]:

- **Coherence bandwidth (B_C):** It is the frequency range over which two or more frequency components maintain a significant amplitude correlation. All multipath pulses within this range are almost of equal phase and attenuation [39].
- **Delay spread (T_s):** it can be defined as the delay time between the first received signal component and the last received signal component for one transmitted pulse [40]. The delay spread is inversely proportional to coherence bandwidth [40]:

$$B_C = \frac{1}{T_s} \tag{2.4}$$

Finally, through the two terms, coherence bandwidth and delay spread, fading can be classified as either a frequency-flat fading (FFF) or frequency-selective fading (FSF). If the bandwidth of the transmitted signal is smaller than

the Coherence Bandwidth, the fading is considered FFF, which means that all paths of the transmitted signal are exposed to the same effects through the channel. On the other hand, if the bandwidth of the transmitted signal is greater than the coherence Bandwidth, then the fading is considered FSF; therefore, we will face the problem of ISI [40].

2.3 Ideal MIMO Channel Model (Narrowband)

In contrast to typical communication systems with one broadcast antenna and one receive antenna, MIMO systems are equipped with several antennas at both ends of the link. Therefore, the MIMO channel must be described regarding its response between all broadcast and receive antenna pairs. In other words, if a MIMO system has N transmit antennas and M receive antennas, as shown in Fig. (2.4), the time-varying MIMO channel of this system can be described by the M × N matrix and as in equation (2.5) [41].

$$\mathbf{H} = \begin{bmatrix} \mathbf{h_{1,1}}(t,\tau) & \mathbf{h_{1,2}}(t,\tau) & \cdots & \mathbf{h_{1,N}}(t,\tau) \\ \mathbf{h_{2,1}}(t,\tau) & \mathbf{h_{2,2}}(t,\tau) & \cdots & \mathbf{h_{2,N}}(t,\tau) \\ \vdots & \vdots & \ddots & \vdots \\ \mathbf{h_{M,1}}(t,\tau) & \mathbf{h_{M,2}}(t,\tau) & \cdots & \mathbf{h_{M,N}}(t,\tau) \end{bmatrix} \tag{2.5}$$

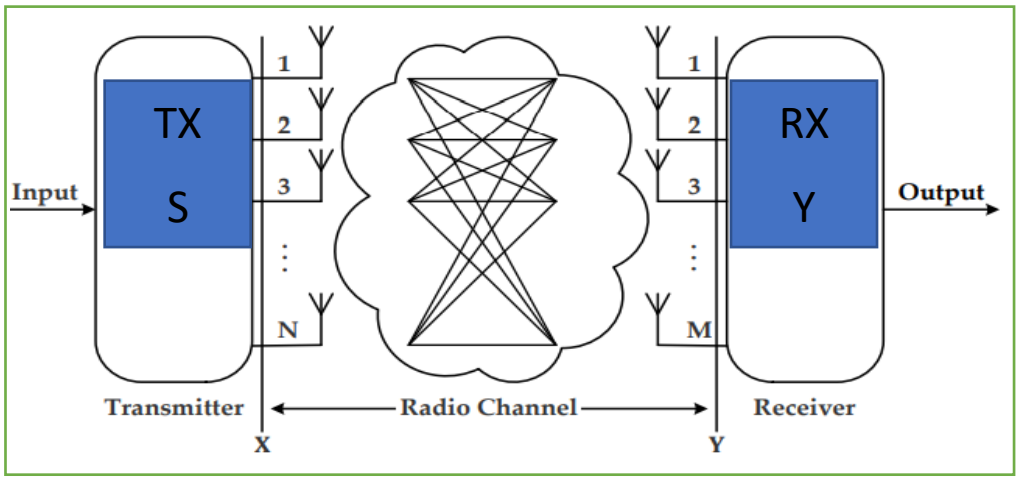

Fig. 2.4: A simplified MIMO channel with N antennas for transmission and M antennas for reception.[42].

where $h_{i,j}(t,\tau)$ represents the time-varying impulse responses from the ith transmit antenna to the jth receive antenna.

Moreover, according to figure (2.4), the relationship between the vector of the input signal (S) and the vector of received signal (Y) can be given in the following equation [41]:

$$\mathbf{Y(t)} = \mathbf{H(t,\tau)}\ \mathbf{S(t,\tau)} + \mathbf{Z(t)} \tag{2.6}$$

Now, suppose the channel suffers from the FFF, which means that the bandwidth of the signal is narrow enough to assume that the channel is nearly constant over frequency. In this case, the input-output relationship represented by equation (2.6) simplifies to the following equation [43]:

$$\mathbf{Y} = \mathbf{H}\ \mathbf{S} + \mathbf{Z} \tag{2.7}$$

Where $\mathbf{Y} \in \mathbf{C^M}$ is the received signal vector, $\mathbf{S} \in \mathbf{C^N}$ is the transmitted signal vector with covariance matrix $\mathbf{Q} = \mathbf{E}(\mathbf{S}\,\mathbf{S^H})$, $\mathbf{H} \in \mathbf{C^{M\times N}}$ is the channel matrix whose entries are assumed random variables all subject to Rayleigh distribution, and $\mathbf{Z}$ is zero-mean circular-symmetric complex Gaussian noise (i.e., $\mathbf{Z} \sim \mathcal{CN}(\mathbf{0},\ \mathbf{I})$**).**

Finally, the MIMO channel model can be represented in another form called the affine MIMO channel model, which means that the SNR becomes seen in the equation of model, as shown in the following equation [44]:

$$\mathbf{Y} = \sqrt{\mathbf{SNR}}\ \mathbf{H}\ \mathbf{S} + \mathbf{Z} \tag{2.8}$$

2.4 Singular Value Decomposition (SVD) Analysis

The channel matrix **H** can be expressed as the product of a unitary matrix **U** with size $\mathbf{M} \times \mathbf{M}$, a Hermitian unitary matrix $\mathbf{V^H}$ with size $\mathbf{N} \times \mathbf{N}$, and a diagonal matrix **Σ** whose diagonal contains only nonnegative singular values, and its size $\mathbf{M} \times \mathbf{N}$. This analysis of the channel matrix **H** can be given in the following equation[45]–[47]:

$$\mathbf{H} = \mathbf{U_{M\times M}} \times \mathbf{\Sigma_{M\times N}} \times \mathbf{V_{N\times N}}^{\mathbf{H}} \tag{2.9}$$

Moreover, the number of the singular values in the matrix **Σ** equals the rank of the MIMO channel matrix **(**Ra_H). Also, the singular values can be found from the square eigenvalues of the $\mathbf{H}\,\mathbf{H}^{\boldsymbol{H}}$ [45]–[47].

2.5 Common MIMO Techniques

The MIMO system is used with two different techniques: one combats fading, which is spatial diversity, and the other exploits fading, which is spatial multiplexing. In the following subsection, these two techniques will be explained.

2.5.1 Spatial Diversity

The concept of diversity in the MIMO system can be explained simply by the following statement: "Do not put all your eggs in one basket". Therefore, if the same information is sent through several independent paths called branches of diversity, the probability of losing this information due to fading will be small because it will require the fading of all paths simultaneously. The probability of branch vanishing is denoted by P_{out}, where If the same data is sent across n branches, the probability of total vanishing is the probability of vanishing all branches (i.e. the probability of total vanishing is denoted by P_{out}^{n} , where n is

the order of diversity). Therefore, the benefit of spatial diversity is to increase the reliability of the link between the transmitter and receiver [48].

In addition, In the MIMO system, if the number of transmitting and receiving antennas approaches infinity, the diversity order will approach infinity. For example, if we assume the Rayleigh environment and there is one antenna in transmitting and an M antenna in receiving, the transmitted signal will pass through M of paths. Therefore, spatial diversity gain is given by the following relationship: $\mathbf{Diversity\ gain = M \times N}$ [49]. For example, the maximum diversity gain of the $\mathbf{3 \times 3}$ MIMO system is **9**.

2.5.2 Spatial Multiplexing

Spatial multiplexing (SM) has been implemented in MIMO systems to give a better transmission rate without assigning more bandwidth or boosting transmit power. In SM technology, the input data streams can be split into multiple separate sub-streams and transmitted concurrently via transmitting antennas [50], [51]. Therefore, utilizing spatial multiplexing methods under specific conditions and assumptions can enhance the capacity linearly with respect to the minimum number of broadcast and receive antennas [51].

2.6 Capacity of the Ideal MIMO Channels

there are two types of MIMO channels, namely, the uncorrelated MIMO channel and the correlated MIMO channel. Therefore, the capacity of the uncorrelated MIMO channel will be offered in the following subsection, and the capacity of the correlated MIMO channel will be explained in another subsection. Also, in the two types of MIMO channels, if the fading is taken into account, it will be considered that the channel suffers from Rayleigh flat fading.

2.6.1 Uncorrelated MIMO Channel Capacity

In general, the MIMO channel is divided into two types, according to fading. The first type is called the deterministic MIMO channel, and the second type is called the random MIMO channel [52], [53]. Thus, the capacity of the deterministic MIMO channel will be clarified firstly in both cases, CSIR and CSIT. Then, it will be offered the capacity of the random MIMO channel for the same cases (CSIR and CSIT).

I. Deterministic Uncorrelated MIMO Channel Capacity

In this type of MIMO channel, the derivation of the general equation of the uncorrelated MIMO channel capacity will be offered. The derivation starts from the definition devoted to the capacity of the wireless channel, which states that the capacity of the wireless channel is the maximum mutual information between the transmitted signal vector and received signal vector [54]. This definition is given in the following equation for the MIMO channel [55], [56]:

$$\mathbf{C_{id}} = \underbrace{\boldsymbol{SUP}}_{\mathbf{tr(Q)=SNR}} \mathbf{max}\ \mathbf{I(S,Y)} \tag{2.10}$$

Where the $\mathbf{C_{id}}$ is the deterministic uncorrelated MIMO channel capacity in ideal model shown in equation (2.7), $\mathbf{I(S,Y)}$ is the mutual information between two vectors of random variables (**S, Y**), and $\mathbf{tr(Q) = SNR}$ is the power contrast of the system. if the relationship of mutual information is written in terms of entropy, equation (2.9) can be rewritten as follows [55], [56]:

$$\mathbf{C_{id}} = \underbrace{\boldsymbol{SUP}}_{\mathbf{tr(Q)=SNR}} \mathbf{max}\ [\boldsymbol{\mathcal{H}}(\mathbf{Y}) - \boldsymbol{\mathcal{H}}(\mathbf{Y/S})] \tag{2.11}$$

Where $\mathcal{H}(\mathbf{Y})$ is the differential entropy of **Y**, and $\mathcal{H}(\mathbf{Y/S})$ is the conditional differential entropy of **Y** when **S** is known. Using the fact that **Z** and **S** are statistically different from each other in Equation (2.7), we can write Equation (2.11) as follows [55], [56]:

$$\mathbf{C_{id}} = \underbrace{\boldsymbol{SUP}}_{\mathbf{tr(Q)=SNR}} \mathbf{max}\,[\mathcal{H}(\mathbf{Y}) - \mathcal{H}(\mathbf{Z})] \tag{2.12}$$

The above equation is maximized when the two terms found in the same equation are maximized. The two terms $\mathcal{H}(\mathbf{Y})$ and $\mathcal{H}(\mathbf{Z})$ are maximized when **S**, **Y**, and **Z** are considered a zero mean circular symmetric complex Gaussian (ZMCSCG) random variables. Therefore, the entropy equations for **Y** and **Z** under this consideration are given as follows [55], [56]:

$$\mathcal{H}(\mathbf{Y}) = \mathbf{log_2}(\mathbf{det}(\boldsymbol{\pi} * \mathbf{e} * \mathbf{Q}_{\boldsymbol{Y}})) \tag{2.13}$$

$$\mathcal{H}(\mathbf{Z}) = \mathbf{log_2}(\mathbf{det}(\boldsymbol{\pi} * \mathbf{e} * \mathbf{Q}_{\boldsymbol{Z}})) \tag{2.14}$$

Where $\mathbf{Q_Y}$ is the covariance matrix of **Y**, and $\mathbf{Q_Z}$ is the covariance matrix of **Z**. Also, the $\mathbf{Q_Y}$ and $\mathbf{Q_Z}$ are called the autocorrelation of the received signal vector and the autocorrelation of the noise vector, respectively [57].

Now, the equations of $\mathbf{Q_Y}$ and $\mathbf{Q_Z}$ must be found. The equation of $\mathbf{Q_Y}$ will be generated first [55], [56]:

$$\mathbf{Q_Y} = \mathbf{E}\{\mathbf{Y} * \mathbf{Y^H}\} = \mathbf{E}\{(\mathbf{H\,S} + \mathbf{Z}) * (\mathbf{H\,S} + +\mathbf{Z})^{\mathbf{H}}\} = \mathbf{H\,Q\,H^H} + \mathbf{I_M} \tag{2.15}$$

Where $\mathbb{E}$ (.) denotes the expectation operator, and $(.)^{H}$ denotes performing the Hermitian operation on the matrix within the bows. After that, the equation of $\mathbf{Q_Z}$ will be created [55], [56]:

$$\mathbf{Q_Z} = \mathbf{E}\{\mathbf{Z} * \mathbf{Z^H}\} = \mathbf{I_M} \quad (2.16)$$

Moreover, after finding the $\mathbf{Q}_{\boldsymbol{Y}}$ and $\mathbf{Q}_{\boldsymbol{Z}}$ equations, it now becomes easy to find $\boldsymbol{\mathcal{H}}(\mathbf{Y})$ and $\boldsymbol{\mathcal{H}}(\mathbf{Z})$ and then insert them in equation (2.12). As a final result, the deterministic uncorrelated MIMO channel capacity is given as follows [55], [56], [58]:

$$\mathbf{C_{id}} = \underbrace{\boldsymbol{SUP}}_{\mathbf{tr(Q)=SNR}} \mathbf{log_2}\left(\mathbf{det}(\mathbf{I_M} + \mathbf{H\ Q\ H^H})\right) \quad \mathbf{B/S/HZ} \quad (2.17)$$

The above equation is found by considering that the channel state information is available at the receiver only. Additionally, the deterministic uncorrelated MIMO channel capacity can be found in two scenarios, namely CSIR and CSIT, and as follows:

A. CSIT Scenario

In this scenario, the channel state information is public at the transmitter and receiver. Therefore, the power allocated to system can be controlled. More clearly, in this case, will be applied a process called the pre-coding process. This process divides the MIMO channel into independent SISO channels. The number of SISO channels generated is equal to the minimum number between the number of transmitting antennas and the number of receiving antennas, which represents the $\mathbf{Ra_H}$; Figure (2.5) shows the block diagram of the pre-coding process in ideal MIMO channel model [55], [59].

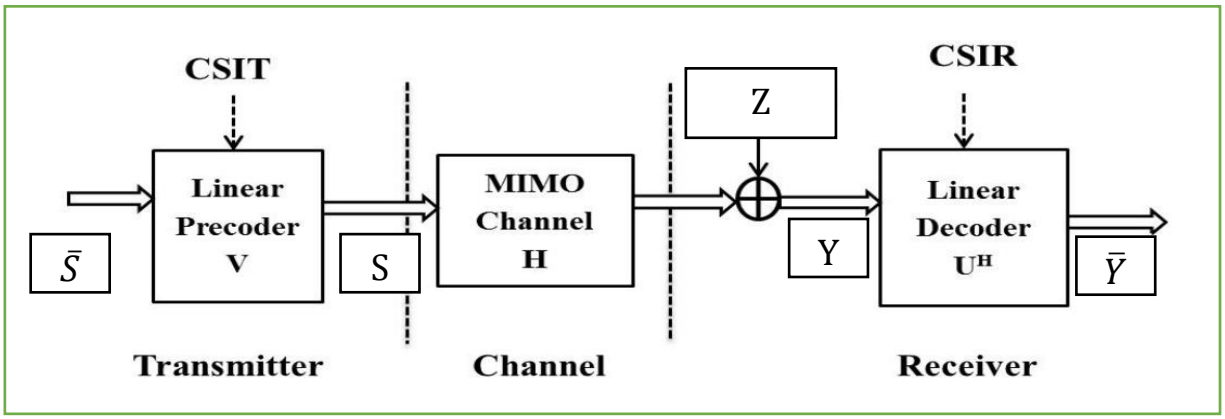

Fig. 2.5: Block diagram of the pre-coding process in ideal MIMO channel model [60].

From the above figure, it can be concluded some points such as, $\mathbf{S} = \mathbf{V}\,\bar{\mathbf{S}}$, $\mathbf{Y} = \mathbf{H}\,\mathbf{S} + \mathbf{Z}$, and $\bar{\mathbf{Y}} = \mathbf{U^H}\,\mathbf{Y}$. Based on the first point, the covariance matrix of the transmitted signal in ideal MIMO model is becomes as follows [61], [62]:

$$\mathbf{Q} = \mathbf{V_{N*M}} * \mathbf{D_{M*M}} * \mathbf{V_{N*M}}^{\mathbf{H}} \tag{2.18}$$

Where $\mathbf{D_{M*M}}$ is a diagonal matrix, its diagonal element values represent the power for the SISO channels (effective channels). The equation (2.18) is inserted into the equation (2.17) to find the deterministic uncorrelated MIMO channel capacity in the CSIT case, which is given in the final form as follows [63]:

$$\mathbf{C_{id}} = \underbrace{\boldsymbol{SUP}}_{\sum_{i=1} \boldsymbol{D_i} \leq \mathbf{SNR}} \left\{\sum_{i=1}^{\mathbf{Ra_H}} \left(\mathbf{log_2}(\mathbf{1} + \boldsymbol{\lambda_i} * \boldsymbol{D_i})\right)\right\} \tag{2.19}$$

Where, $\boldsymbol{D_i}$ is the power of the ith effective channel, and $\boldsymbol{\lambda_i}$ is the channel gain (eigenvalue) of the ith effective channel. All the values of $\boldsymbol{\lambda}$ are the eigenvalues of $\mathbf{H} * \mathbf{H^H}$.

In addition, the power of each effective channel is found by using the water-filling mechanism. This mechanism will show us which effective channel has too much noise in order to be given a little or zero power. Also, this mechanism will show us which channel has too little noise in order to be given much power [64]. For understanding this mechanism, the following example is offered:

Example: Discover the capacity and optimal power assignment for the MIMO channel, considering SNR = 10 dB and the channel matrix is [55]:

$$\mathbf{H} = \begin{bmatrix} .1 & .3 & .7 \\ .5 & .4 & .1 \\ .2 & .6 & .8 \end{bmatrix} \tag{2.20}$$

Solution:

STEP1: Applied the SVD analysis for H [55]:

$$\mathrm{H} = \begin{bmatrix} -.555 & .3764 & -.7418 \\ -.3338 & -.9176 & -.2158 \\ -.7619 & .1278 & .6349 \end{bmatrix} \begin{bmatrix} 1.3333 & 0 & 0 \\ 0 & .5129 & 0 \\ 0 & 0 & .0965 \end{bmatrix} \times \begin{bmatrix} -.2811 & -.7713 & -.5710 \\ -.5679 & -.3459 & .7469 \\ -.7736 & .5342 & -.3408 \end{bmatrix} \tag{2.21}$$

STEP2: Finding the eigenvalues [55]:

$$\lambda = \begin{bmatrix} 1.3333 & 0 & 0 \\ 0 & .5129 & 0 \\ 0 & 0 & .0965 \end{bmatrix}^2 = \begin{bmatrix} 1.7777 & 0 & 0 \\ 0 & 0.2631 & 0 \\ 0 & 0 & 9.312 \times 10^{-3} \end{bmatrix} \tag{2.21}$$

From the above matrix, it can be found the channel gain of each eigenmode (effective channel) and as follows:

$$\lambda_1 = 1.7777,\ \lambda_2 = 0.2631,\ \lambda_3 = 9.312 \times 10^{-3} \tag{2.22}$$

STEP3: Finding the inverse eigenvalues:

$$\frac{1}{\lambda_1} = 0.5625281261,\ \frac{1}{\lambda_2} = 3.801321499,\ \frac{1}{\lambda_3} = 107.3854332 \quad (2.23)$$

STEP4: Finding water level value in the presence of the three effective channels. This value of the water level must be larger than the large inverse eigenvalue shown in the previous step [55]. The water level value is found from following equation [65]:

$$\Omega = \left(\frac{\text{SNR}+\frac{1}{\lambda_1}+\frac{1}{\lambda_2}+\frac{1}{\lambda_3}}{\text{number of channel}}\right)^{+} = \left(\frac{10+0.5625281261+3.801321499+107.3854332}{3}\right) = 40.582 \quad (2.24)$$

From the above equation, it can be seen that the water level's value is smaller than the value of $\frac{1}{\lambda_3}$, which means that channel three has thunderous noises. Therefore this channel will be not allocated any power [55]. In other words, this channel will be cancelled and repeated the calculation of the water level in the presence of two effective channels:

$$\Omega = \left(\frac{\text{SNR}+\frac{1}{\lambda_1}+\frac{1}{\lambda_2}}{\text{number of channel}}\right)^{+} = \left(\frac{10+0.5625281261+3.801321499}{2}\right) = 7.181924813 \quad (2.25)$$

The value of the water level shown in the above equation is larger than the two values of $(\frac{1}{\lambda_1})$ and $(\frac{1}{\lambda_2})$. Therefore, this value of the water level will be adopted to calculate the power of two effective channels to get to the maximum capacity, which will be offered in the next steps.

STEP5: Finding the power of each effective channel. The general low of calculated the power is given in the following equation [65]:

$$D_i = \Omega - \frac{1}{\lambda_i} \tag{2.26}$$

According to the above equation, it can be found the power of each effective channel [55]:

$$\mathrm{D}_1 = 6.619396687 \tag{2.28}$$

$$\mathrm{D}_2 = 3.380603314 \tag{2.29}$$

$$\mathrm{D}_3 = 0 \tag{2.30}$$

STEP5: Finding the capacity of the MIMO channel by applying the equation (2.19) [55].

$$\mathrm{C_{id}} = \sum_{i=1}^{\mathrm{Ra_H}} \left(\log_2(1 + \ \lambda_i * \ D_i\ )\right) = \log_2(1 + (1.7777 * \ 6.619396687)) + \log_2(1 + (0.2631 * \ 3.380603314)) + 0 = 4.59 \ \mathbf{B/S/HZ} \tag{2.31}$$

B. CSIR Scenario

This scenario means that the transmitter do not have any information about the channel, inversely to receiver that has the CSI. In this scenario, the best case to get on the maximum capacity is divided the power in equally between the transmit antennas. In other words, in the equations language, the covariance matrix of the transmitted input becomes equal to SNR/N in the CSIR scenario. Thus the deterministic uncorrelated MIMO channel capacity in the CSIR case is given as follows [66]–[69]:

$$\mathrm{C_{id}} = \ \log_2\left(\det\left(\mathrm{I_M} + \left(\frac{\mathrm{SNR}}{\mathrm{N}}\right)\mathrm{H}\ \mathrm{H^H}\right)\right) \tag{2.32}$$

The equation (2.32) can be rewritten in the term of the eigenvalue to become in the following form [70], [71]:

$$C_{id} = \sum_{i=1}^{Ra_H} \log_2 \left(1 + \frac{SNR}{N} * \lambda_i \right) \quad (2.33)$$

II. Random Uncorrelated MIMO Channel Capacity

In the initial state (I), it is assumed that the MIMO channel is deterministic. Typically, the MIMO channel varies at random. Consequently, H is a random matrix and its channel capacity fluctuates randomly over time. In reality, the MIMO channel capacity formulas for the CSIR and CSIT cases in the random form can be represented in the following table [71]:

Table 2.1: The ergodic capacity formulas of the uncorrelated MIMO channel for the CSIR and CSIT cases in the ideal model

Case	The Formula of Ergodic Capacity (bit/second/hertz)
CSIT	$C_{eid} = \mathbb{E}\left\{ \underbrace{SUP}_{\sum_{i=1} D_i \leq SNR} \sum_{i=1}^{Ra_H} \left(\log_2(1 + \lambda_i * D_i)\right) \right\}$, (2.34)
CSIR	$C_{eid} = \mathbb{E}\left\{ \sum_{i=1}^{Ra_H} \log_2 \left(1 + (SNR/N) * \lambda_i \right) \right\}$ (2.35) OR $C_{eid} = \mathbb{E}\left\{ \log_2 \left(\det \left(I_M + \left(\frac{SNR}{N}\right) H H^H \right) \right) \right\}$, [72] (2.36)

Moreover, it can be necessary to know the difference between the capacity in the CSIT case and the capacity in the CSIR case in the random form. Therefore, figure (2.6) is offered to show the capacities of the 4×4 MIMO channel for the CSIR and CSIT cases in various values of SNR. This figure shows that in the low SNRs, the ergodic capacity in the CSIT case is large than that in the CSIR case. However, this benefit for the capacity in the CSIT

decreases as the value of SNR increases more and more until it disappears in the very high SNRs [71]. This analysis is seen in any antenna configuration, and to prove this, figure (2.7) displays the ergodic capacity for different antennas configuration with CSIT and without CSIT.

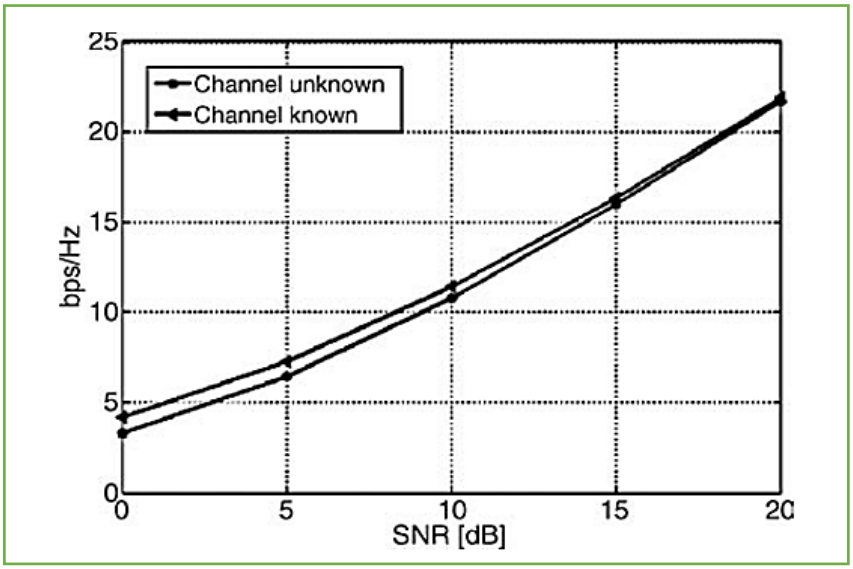

Fig. 2.6: The capacities of the 4×4 MIMO channel for the CSIR and CSIT cases in various values of SNR [71].

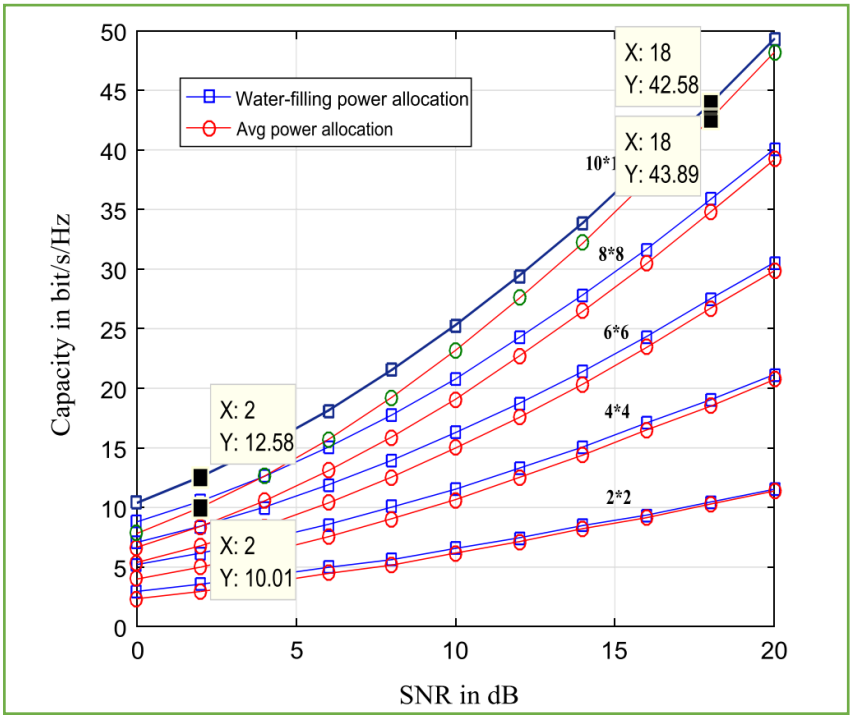

Fig. 2.7: The ergodic capacity for different antennas configuration with CSIT and without CSIT [73]

Finally, it must be noted that the representation of the water-filling mechanism in the MATLAB program will be clarified in an appendix at the end of this work. Also, the equation that generates the realizations of the channel matrix is given as follows [71]:

$$\mathbf{H} = \sqrt{(\mathbf{0.5})} * (\mathbf{randn}(\mathbf{M}, \mathbf{max}(\mathbf{N}), \mathbf{L}) + \mathbf{1i} * \mathbf{randn}(\mathbf{M}, \mathbf{max}(\mathbf{N}), \mathbf{L})) \quad (2.37)$$

The above equation generates L MIMO channels (L is the number of realizations of the channel), each one of these channels whose components are complex random variables subject to a Rayleigh distribution and independent of each other.

2.6.2 Correlated MIMO Channel Capacity

In general, H components are correlated to varying degrees depending on the propagation environment, the polarization of the antenna elements, and their spacing. One alternative model for H that accounts for fading correlation divides the fading correlation into two distinct components called receive correlation and transmit correlation [74]. This amounts to modeling H as follows [74], [75]:

$$\mathbf{H_k} = \mathbf{D_t}^{\mathbf{0.5}} * \mathbf{H} * \mathbf{D_r}^{\mathbf{0.5}} \quad (2.38)$$

where $\mathbf{H_k}$, is the correlated MIMO channel matrix, D_t is the transmit correlation matrix with size $N \times N$, and D_r is the receive correlation matrix with size $M \times M$. The model shown in the above equation is called the Kronecker model. Both matrices D_t and D_r are found as follows [74], [76], [77]:

$$D_t = \begin{bmatrix} 1 & \alpha_t & \alpha_t^4 & \cdots & \alpha_t^{(N-1)^2} \\ \alpha_t & 1 & \alpha_t & \cdots & \vdots \\ \alpha_t^4 & \alpha_t & 1 & \cdots & \alpha_t^4 \\ \vdots & \vdots & \vdots & \ddots & \alpha_t \\ \alpha_t^{(N-1)^2} & \cdots & \alpha_t^4 & \alpha_t & 1 \end{bmatrix}$$

$$D_r = \begin{bmatrix} 1 & \alpha_r & \alpha_r^4 & \cdots & \alpha_r^{(M-1)^2} \\ \alpha_r & 1 & \alpha_r & \cdots & \vdots \\ \alpha_r^4 & \alpha_r & 1 & \cdots & \alpha_r^4 \\ \vdots & \vdots & \vdots & \ddots & \alpha_r \\ \alpha_r^{(M-1)^2} & \cdots & \alpha_r^4 & \alpha_r & 1 \end{bmatrix} \quad (2.39)$$

where α_t is the correlation coefficient on the transmitting side, and α_r is the correlation coefficient on the receiving sides. Generally, in most works, it is considered that the correlation coefficient on the transmitting sides equals the correlation coefficient on the receiving sides (i.e. $\alpha_t = \alpha_r = \alpha$). The value of α is from zero (an uncorrelated MIMO channel) to one (a highly correlated MIMO channel) [74], [76], [77]. For example if $\alpha = 0.4$ and $N = 4, M = 4$, equation (2,39) becomes as follows [74]:

$$D_t = \begin{bmatrix} 1 & 0.4 & 0.0256 & 2.62144 * 10^{-4} \\ 0.4 & 1 & 0.4 & 0.0256 \\ 0.0256 & 0.4 & 1 & 0.4 \\ 2.62144 * 10^{-4} & 0.0256 & 0.4 & 1 \end{bmatrix}$$

$$D_r = \begin{bmatrix} 1 & 0.4 & 0.0256 & 2.62144 * 10^{-4} \\ 0.4 & 1 & 0.4 & 0.0256 \\ 0.0256 & 0.4 & 1 & 0.4 \\ 2.62144 * 10^{-4} & 0.0256 & 0.4 & 1 \end{bmatrix} \quad (2.40)$$

In addition, the formulas of the ergodic capacity for the correlated MIMO channel for the CSIR and CSIT cases are the same those for uncorrelated MIMO channel for the CSIR and CSIT cases, but in the correlated

MIMO channel the channel matrix is H_k. As result, the formulas of the ergodic capacity for the correlated MIMO channel for the CSIR and CSIT cases given as follows [74]:

$$Cc_{eid} = \mathbb{E}\left\{ \underbrace{\sup}_{\sum_{i=1} D_{k\,i} \leq SNR} \sum_{i=1}^{Ra_H} \left(\log_2(1 + \lambda_{k\,i} * D_{k\,i})\right) \right\}, \text{CSIT} \qquad (2.41)$$

$$Cc_{ceid} = \mathbb{E}\left\{ \sum_{i=1}^{Ra_H} \log_2 \left(1 + ({}^{SNR}/_{N}) * \lambda_{k\,i} \right) \right\}, \qquad \text{CSIR} \qquad (2.42)$$

where $\lambda_{k\,i}$ is the channel gain of the ith effective channel in correlated MIMO channel, and $D_{k\,i}$ is the power assigned to ith effective channel in the correlated MIMO channel.

Moreover, it can be necessary to know the difference between the ergodic capacity for the uncorrelated MIMO channel and the ergodic capacity for the correlated MIMO channel. Therefore, figure (2.8) is offered to show the capacity of the 2×2 MIMO channel for the CSIR case in various values of SNR over different correlation coefficients $\alpha \in \{0, 0.8\}$. This figure shows that the correlation between the channel elements degrades the performance of the channel capacity [78].

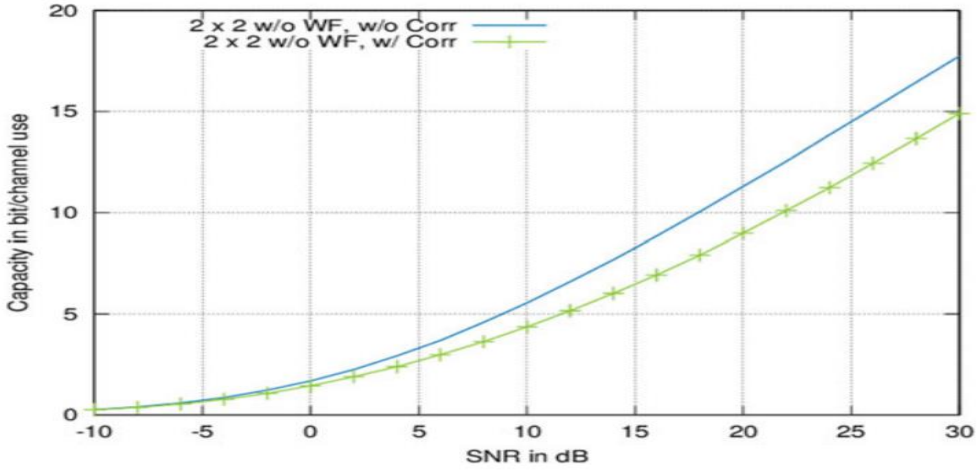

Fig. 2.8: The capacity of the 2×2 MIMO channel for the CSIR case in various values of SNR over different correlation coefficients $\boldsymbol{\alpha} \in \{\mathbf{0}, \mathbf{0.8}\}$ [78].

At the end of the conversation, It should be noted that if the affine MIMO model is used. The equations for channel capacity, whether correlated or uncorrelated, are the same. The only thing that differs is that the power constraint becomes equal to one, and the value of the SNR will be shown in the equations.

2.7 Finite-SNR Multiplexing Gain (F-SNRMG)

As it is known, the multiplexing gain in the MIMO systems is given in the following equation [79]:

$$\lim_{\mathrm{SNR}\to\infty} \frac{\mathrm{R(SNR)}}{\log_2 \mathrm{SNR}} = \mathrm{r} \tag{2.43}$$

where **r** is the multiplexing gain, and **R** is the data rate (bps) per unit hertz. The concept of the multiplexing gain shown in the above equation has become undesirable in systems in which the channel capacity is limited. Therefore, in recent times, most works dealing with the concept of the multiplexing gain as a ratio of the capacity of the MIMO channel to that of the SISO channel, which is shown in equation (2.44). This concept of multiplexing gain is called finite-SNR multiplexing gain [80], and it will be adopted in this work, as will be seen in the next chapter.

$$\mathrm{C_{Seid}} = \mathbb{E}\{\log_2(1 + \mathrm{SNR} * |h|^2)\} \tag{2.44}$$

Moreover, it is necessary to know how the SISO channel h generated in the MATLAB programs. Therefore the following equation is offered to achieve this knowledge:

$$h = \sqrt{(\mathbf{0.5})} * \mathbf{randn}(\mathbf{L}, \mathbf{1}) + \mathbf{1i} * \mathbf{randn}(\mathbf{L}, \mathbf{1})) \tag{2.45}$$

2.8 Defects of the Physical Radio Frequency Transceiver

The non-ideal radio frequency transceiver (RFT) is a critical component that impacts system performance. Where, the physical transceiver suffers from many flaws such as phase noise, quantization noise, IQ imbalance, etc. Numerous of these flaws are avoided or compensated by implementing complex compensation operations in the system. However, some of these flaws remain unaffected by the compensation operations. Thus, these residual flaws, which are also called transceiver distortion, affect the quality of the signal that passes through the RFT [81], [82]. In the following subsection, the most common transceiver flaws will be discussed.

2.8.1 IQ-Imbalance

It is known that the quadrature mixer (IQ mixer) is used in the transmitter and receiver of the wireless system to convert the frequency from the intermediate frequencies or baseband to radio frequencies and vice versa. This mixer deals with the complex signals consisting of the real and imaginary parts. The process of converting the frequency of the baseband signal to the range of the radio frequencies is called the direct up-conversion process, and the process of converting the frequency of the radio signal to the baseband frequency is called the direct down-conversion process [83]. In the direct up-conversion process, which happens in the transmitter, the real part of the input signal goes to a branch called I (In-phase), and it mixes with the cosine wave that has certain amplitude, which prefers to be equal to a unity value. At the same time, the imaginary part of the signal goes to a branch called Q (Quadrature-phase) and then mixes with the sine wave that has amplitude equal to the amplitude of the cosine wave in the I branch. Then, the two signals from the I and Q branches are subtracted from each other and then the resulting signal is transmitted over the channel to represent the radio signal [7]. In contrast, in

the direct down-conversion process in the receiver, both the I and Q branches of the quadrature mixer take the radio signal, where the radio signal in the I branch is multiplied with the cosine wave similarly in the up-conversion, and the radio signal in the Q branch is multiplied with the sine wave similarly in the up-conversion but with a negative sign. The signals from the I and Q branches are summed together and entered into a low pass filter to remove the high frequencies. The local oscillator shares with the phase shifter to generate the sine and cosine waves used in the quadrature mixer [7], [84]. However, in real-world applications, quadrature mixers are hampered by gain and phase mismatches between the I and Q branches that degrade the SNR or generate out-of-band noise. This problem of mismatches the gain and phase between the I and Q branches is called IQ imbalance [85], [86]. In this subsection, the influence of this problem on the broadcast signal, assuming an ideal receiver, will be clarified. Then, the transmitter is deemed ideal, and the impact of IQ imbalance on the received signal is elucidated.

I. Transmitter IQ Mismatch

Here, it will be considered that the IQ mixer in the transmitter suffers from a mismatch in the gain and phase between the I and Q branches and that the mixer in the receiver is ideal; Figure (2.9) displays the transceiver with IQ mismatch in the transmission.

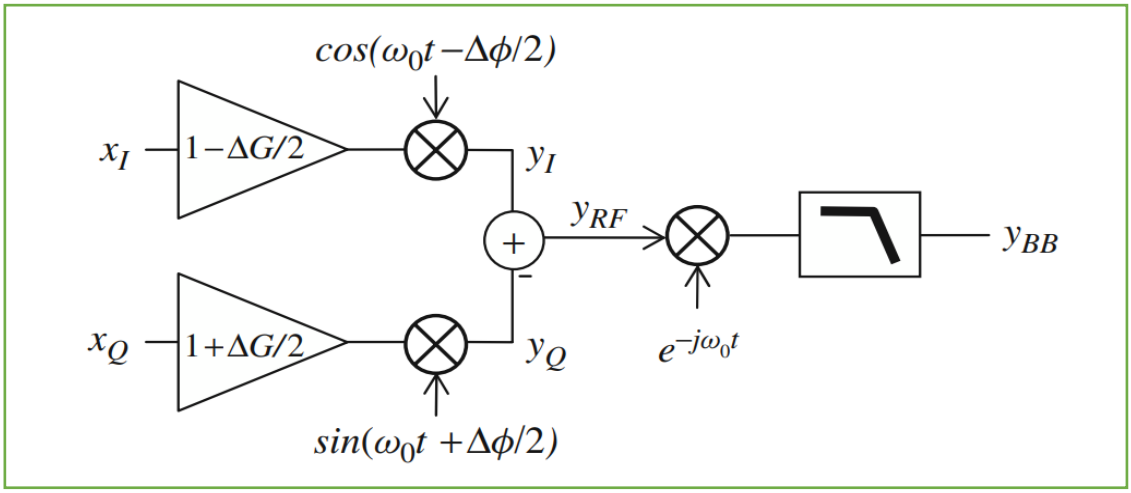

Fig.2.9: Transceiver with IQ mismatch in the transmission [86].

From the above figure it can be seen that the radio frequency signal $y_{RF}(t)$ can be written as follows [86]:

$$y_{RF}(t) = \left(1 - \frac{\Delta G}{2}\right) x_I \cos\left(\omega_0 t - \frac{\Delta\phi}{2}\right) - \left(1 + \frac{\Delta G}{2}\right) x_Q \sin\left(\omega_0 t + \frac{\Delta\phi}{2}\right) \quad (2.46)$$

where x_I and x_Q are the real part and imaginary part of the input signal, respectively. The symbol ΔG is the gain imbalance that represents the difference between the gain of I branch (G_I) and the gain of Q branch (G_Q), and $\Delta\Phi$ is the phase error between I and Q branches. In the ideal case, the value of ΔG is equal to zero, and the value of $\Delta\phi$ is equal to zero. Also, the gain imbalance ΔG can be determined as a percentage from the following equation [86]:

$$\Delta G = \frac{|G_I - G_Q|}{G_Q} \quad (2.47)$$

Moreover, to illustrate the effect of IQ mismatch in the transmitter, it can be assumed that the input signal is as follows [86]:

$$x_I + jx_Q = \cos(2\pi\Delta ft) + j\sin(2\pi\Delta ft) = e^{j2\pi\Delta ft} \quad (2.48)$$

where Δf is the frequency of baseband signal. The equation (2.48) is inserted in equation (2.46) to get the following equation [86]:

$$\text{where } \begin{cases} y_{RF} = \alpha_{TX} e^{j2\pi(f_0+\Delta f)t} + \beta_{TX} e^{j2\pi(f_0-\Delta f)t} \\ \alpha_{TX} = \frac{1}{2}\left[\cos\left(\frac{\Delta\phi}{2}\right) + j\frac{\Delta G}{2}\sin(\Delta\phi/2)\right] \\ \beta_{TX} = \frac{1}{2}\left[-\frac{\Delta G}{2}\cos\left(\frac{\Delta\phi}{2}\right) - j\sin(\Delta\phi/2)\right] \end{cases} \quad (2.49)$$

The above equation indicates that the IQ mismatch in the transmitter leads to generating an image from the original signal. The image signal generated represents the complex conjugate of the original signal. The effect of the image signal is different according to the type of the transceiver; Figure (2.10) shows the effect of the image signal generated due to the IQ mismatch in the transmitter in two different types of transmitters: zero-IF TX and low-IF TX (zero intermediate frequency transmitter and low intermediate frequency transmitter) [86]. Also, the ratio of the image power to the signal power is called the IQ mismatch image suppression ratio (ISR) or Image-to-Signal-Power-Ratio [87]. Thus, the image suppression ratio according to equation (2.49) is represented in the following equation [86]:

$$ISR_{TX} = \frac{|\beta_{TX}|^2}{|\alpha_{TX}|^2} = \frac{\frac{\Delta G^2}{4}\cos^2\left(\frac{\Delta\phi}{2}\right)+\sin^2\left(\frac{\Delta\phi}{2}\right)}{\cos^2\left(\frac{\Delta\phi}{2}\right)+\frac{\Delta G^2}{4}\sin^2\left(\frac{\Delta\phi}{2}\right)} = \frac{\frac{\Delta G^2}{4}+\tan^2\left(\frac{\Delta\phi}{2}\right)}{1+\frac{\Delta G^2}{4}\tan^2\left(\frac{\Delta\phi}{2}\right)} \quad (2.50)$$

By considering that the values of the ΔG and Δϕ are smaller than one, the above equation can be rewritten as follows [86]:

$$ISR_{TX} = \frac{\Delta G^2+\Delta\phi^2}{4} \quad (2.51)$$

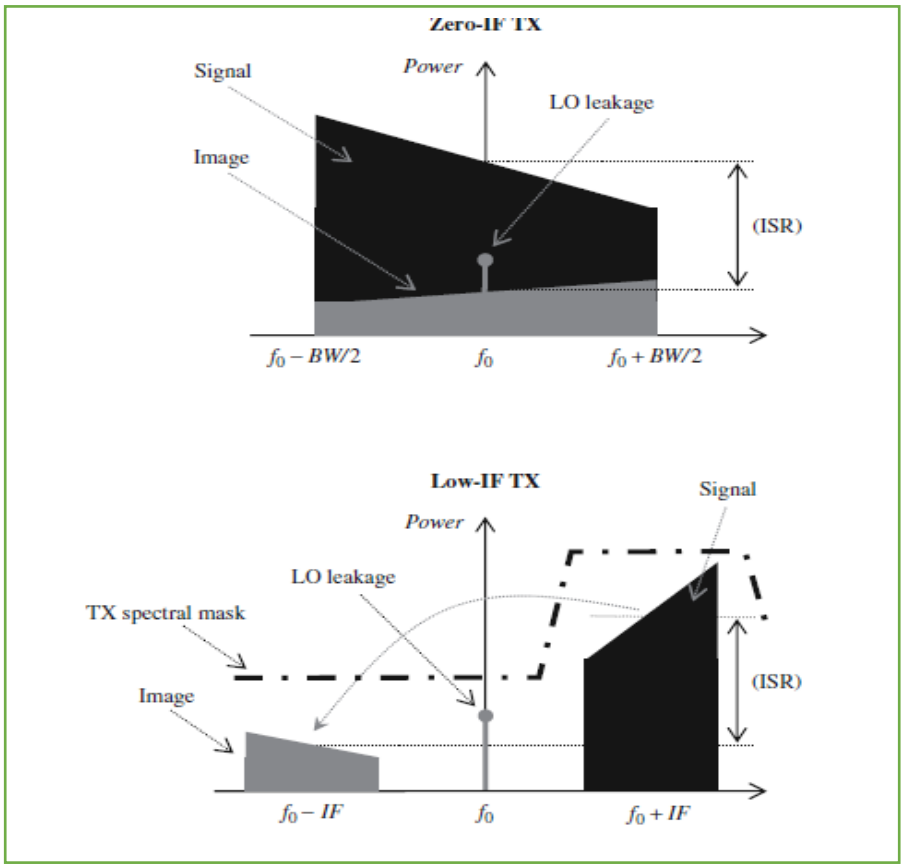

Fig. 2.10: Impact of TX IQ mismatch in zero- and low-IF architectures [86].

The above figure indicates that in the zero-IF transmitter, there is interference between the signal and the image inside the channel range. This interference constrains the value of ISR and reduces the SNR of the desired signal compared to the ideal scenario in which the gain and phase of the signal generated by the local oscillator are perfect [86]. While in the low-IF transmitter, figure (2.9) indicates that the image signal originating in the transmitter is located equally far from the LO frequency (f_o) as the desired signal. As a result, the image signal causes interference with other channels signals located in the frequency range from ($f_o - IF - B_a/2$) to ($f_o - IF + B_a/2$), where B_a is the bandwidth for the desired signal [86], [88].

In addition, in the multichannel scenario in which multiple signals with varying power levels are received as a whole, the image signal for some channels may be 50-100dB greater than the desired signal, and the interference may totally hide the desired signal [89].

II. Receiver IQ Mismatch

Now, the effect of IQ imbalance on received signals will be clarified; Figure (2.11) shows the transceiver device under the influence of IQ mismatch in the mixer located in the receiver and considering that the mixer in the transmitter is ideal.

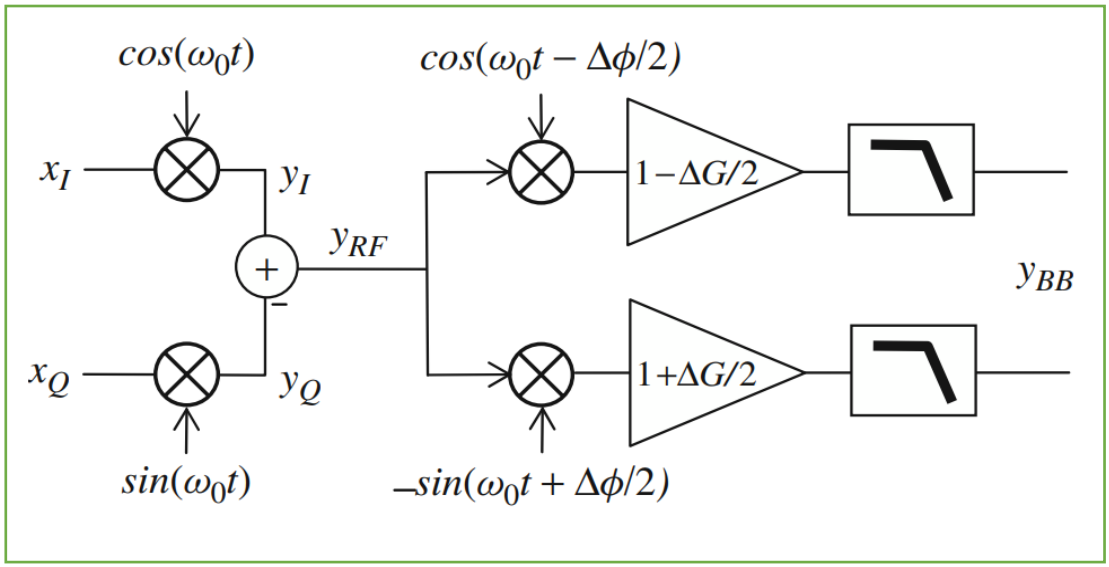

Fig. 2.11: Transceiver with IQ mismatch in the reception [86].

From the above figure it can be seen that the baseband frequency signal $y_{BB}(t)$ can be written as follows [86]:

$$y_{BB}(t) = \left[x_I \cos(\omega_0 t) - x_Q \sin(\omega_0 t)\right] \times \left[\left(1 - \frac{\Delta G}{2}\right)\cos\left(\omega_0 t - \frac{\Delta\phi}{2}\right) - j\left(1 + \frac{\Delta G}{2}\right)\sin\left(\omega_0 t + \frac{\Delta\phi}{2}\right)\right] \quad (2.52)$$

By doing some arithmetic steps and assuming that the low-frequency filter removes the high frequencies around $2\omega_0$, equation (2.52) becomes as follows [86]:

$$y_{BB}(t) = \alpha_{RX}(x_I + jx_Q) + \beta_{RX}(x_I - jx_Q)$$
$$\begin{cases} \alpha_{RX} = \frac{1}{2}\left[\cos\left(\frac{\Delta\phi}{2}\right) - j\frac{\Delta G}{2}\sin(\Delta\phi/2)\right] \\ \beta_{RX} = \frac{1}{2}\left[-\frac{\Delta G}{2}\cos\left(\frac{\Delta\phi}{2}\right) - j\sin(\Delta\phi/2)\right] \end{cases} \quad (2.53)$$

The above equation indicates that the effect of the IQ mismatch in reception is the same as the effect of the IQ mismatch in the transmission, and ISR appears in the same form [86]. Figure (2.12) shows the output spectrum of the down converter frequency in low IF receiver with IQ imbalance.

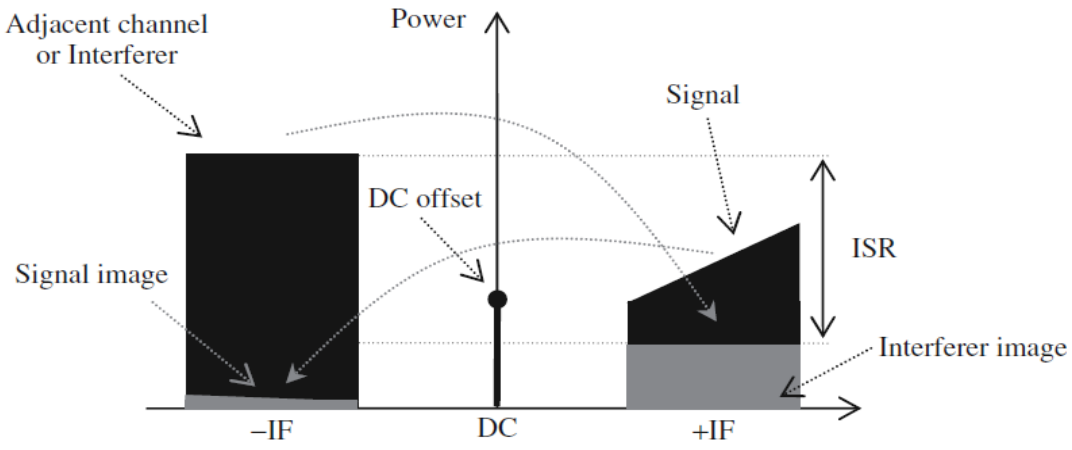

Fig. 2.12: Impact of RX IQ mismatch in low-IF architecture [86].

The above figure shows that in the low-IF architecture with RX IQ mismatch, the image of the interferer or adjacent channel interferes with the desired signal. This interference leads to reduce the SNR of the desired signal [86].

2.8.2 Phase noise

In general, oscillating signals are employed in transceivers to convert signals from and to radio frequencies. In real-world applications, oscillators used to generate such signals are susceptible to several flaws. The most important of these flaws is the so-called phase noise (PN) [90]. PN is defined as the difference in phase between the carrier signal and the local oscillator [91]. In other words, PN happens when an oscillator is unable to produce clean sinusoidal waves that match the Dirac spectrum. This spectrum broadening is a result of fast, short-term, random fluctuations in the carrier wave phase generated by oscillators during up-conversion or down-conversion procedures of the baseband signal and radio frequency chain [92]–[94]. Figure (2.13) depicts an ideal oscillator with the Dirac spectrum in comparison to a real oscillator with PN.

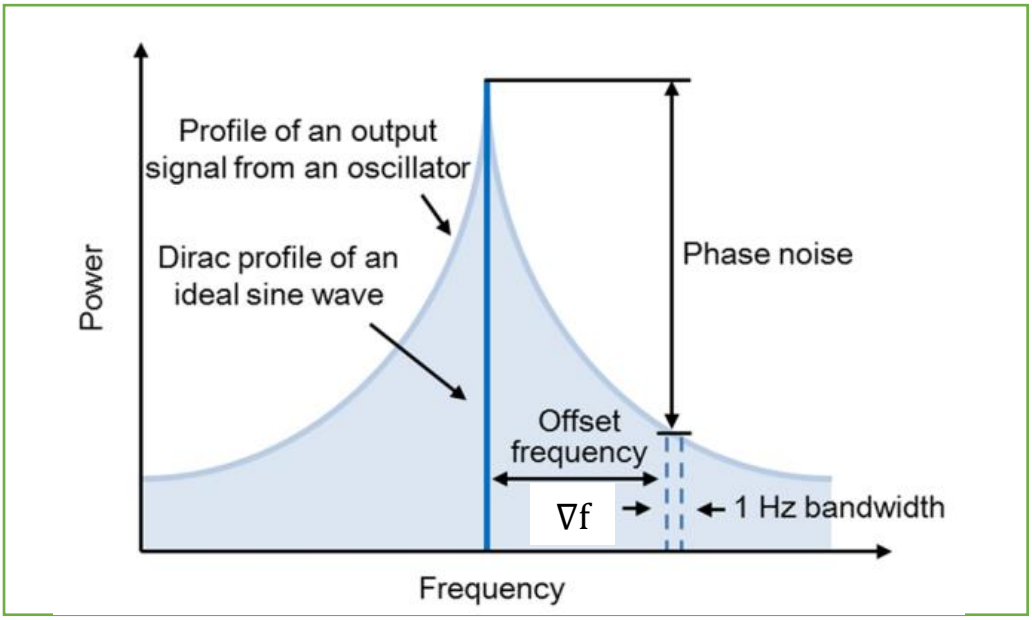

Fig. 2.13: Frequency spectrum of carrier wave with and without PN [95]

Furthermore, scientists commonly describe PN in the frequency domain with a ∇f offset from the carrier over a 1 Hz bandwidth, as shown in above

figure. The PN power over this bandwidth is normalized with respect to the carrier power (− dBc/Hz) [95], [96]. For instance, in GSM applications, the oscillator's PN must be less than -115 dBc/Hz at 600 kHz offset [97].

In addition, PN makes to disperse the signal's spectrum in a manner that may create interference with other channels. For instance, it is known that the spectrum observed by the receiver is the convolution of the passband received signal spectrum and the local oscillator spectrum. The latter, however, spreads due to PN, resulting in spectral spreading. This spreading might introduce interference signals into the signal bandwidth, which degrades the performance of the system. Figure (2.14) depicts this issue [97].

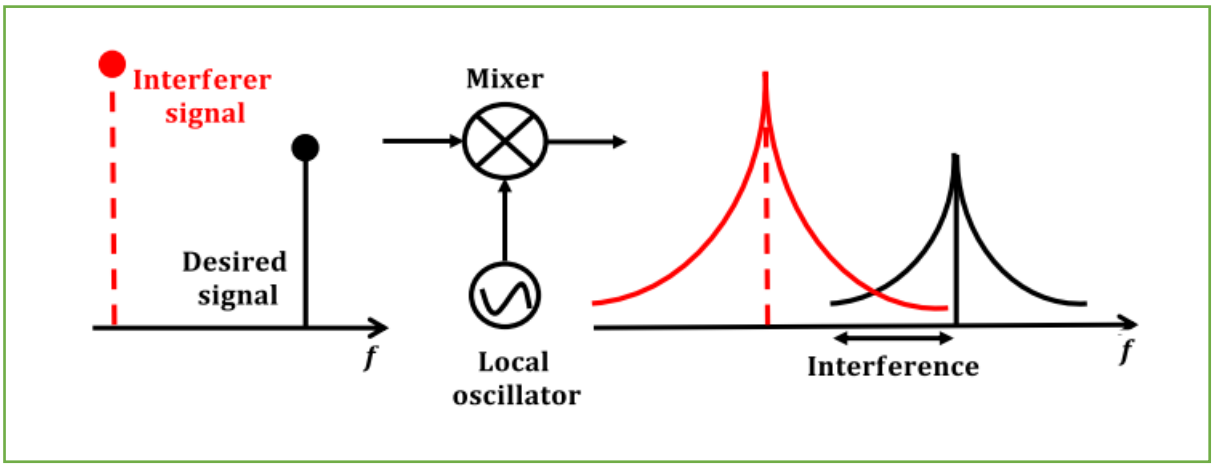

Fig. 2.14: Interference of the desired signal with an adjacent signal due to PN [97]

Finally, the time variation of the channel generated by PN is a crucial consequence. In other words, because of the PN, the effective channel observed by the receiver becomes time-variant, and the transmit signal constellation rotates from symbol to symbol. PN also breaks the coherency between the estimated channel gain and the real channel gain throughout the course of a data frame. In total, these impacts will affect the performance of the wireless system by decreasing the effective SNR, restricting the BER, and decreasing data rates[98], [99].

2.8.3 Transformer effect

In general, all transceivers used in the wireless systems contain the ADC and DAC. The DAC is used to interface the digital portion of a transmitter with its analog circuits, specifically the analog front-end, whereas ADC is used to interface the analog front-end with the digital portion of the transceiver. The low cost of the transceiver makes the quality of these converters is not high. In other words, these converters distort the signal that passes through them. In this section, the focus will be on the ADC, where the effect of the sampling jitter on the SNR will be clarified. Then, the effect of quantizing noise on the SNR of the signal in the presence of a sampling jitter will be clarified.

I. Sampling jitter

The sampling process is considered the first stage in the process of converting the analog signal into a digital signal. In this stage, the analog signal is multiplied by a periodic clock to take samples from it. Usually, the distance between these samples is equal, but sometimes this distance does not remain equal. This inequality in the distance happens due to the jitter when taking samples. This jitter occurs due to instability or phase noise in the clock signal [100], [101].

Moreover, the jitter effect can be measured through signal-to-noise ratio (SNR), and to illustrate this, can be considered the input signal as follows [101]:

$$v(t) = A_a \sin(2\pi ft) \text{ volt} \tag{2.54}$$

where A_a is the signal's amplitude, and f is the frequency. The time derivative of the signal is as follows [101]:

$$\frac{dv(t)}{dt} = 2\pi f A_a \cos 2\pi ft. \tag{2.55}$$

The RMS value of the equation (2.55) is given as follows [101]:

$$\frac{\Delta v_{j\_rms}}{\Delta t_{j\_rms}} = 2\pi f A_a \sqrt{\int_{-1/2f}^{1/2f} \cos^2(2\pi f t)dt} = \sqrt{2}\pi f A \qquad (2.56)$$

where the Δv_{j_rms} is the RMS jitter noise, and the Δt_{j_rms} is the RMS time of jitter. If the jitter is Gaussian distribution with mean equal to zero and variance equal to $\Delta t_{j\_rms}{}^2 = \sigma_{j\_rms}{}^2$, the equation (2.56) becomes as follows [101]:

$$\Delta v_{j\_rms} = \sqrt{2}\pi f A_a \, \sigma_{j\_rms} \qquad (2.57)$$

Now it can be calculated the SNR_{jitter} as follows [101]:

$$\begin{aligned} SNR_{jitter} &= 20\log\left(\frac{A_a/\sqrt{2}}{\Delta v_{j\_rms}}\right) \\ &= 20\log\left(\frac{1}{2\pi f \, \Delta t_{j\_rms}}\right) = 20\log\left(\frac{1}{2\pi f \, \sigma_{j\_rms}}\right) \end{aligned} \qquad (2.58)$$

The above equation indicates that when the jitter variance increases, the SNR value decreases. In other words, The above equation indicates that if the randomness in the sampling process increases, the SNR will decrease [101].

II. Quantization noise

It is the second stage of converting the analog signal into a digital signal. At this stage, a few levels are distributed to the signal on which the sampling process was applied. If the distance between these levels is equal, the quantization process is called the uniform quantizer, where the distance between the levels is symbolized by Δq, which is given in the following equation [101], [102]:

$$\Delta q = \frac{2\,A_a}{L_q} \tag{2.59}$$

Also, Each level is given several bits, and the number of bits for each level depends on the number of levels, according to equation (2.60) [29]:

$$L_q = 2^w \tag{2.60}$$

Where L_q represented the number of quantization levels, and w represented the number of bits for each level.

In addition, each sample taken in the sampling process is rounded to one of the levels to take its digital code. Typically, there is a difference between the value of the quantization level to which the sample is approximated and the true value of the sample. This difference is called quantization noise [101], [103]. The value of SNR in the presence of the quantization noise and jitter noise is given as follows [101]:

$$SNR_{jq} = 10\log\left[\frac{{A_a}^2}{2\left(\frac{\Delta q^2}{12}+2\left(\pi f A_a\,\sigma_j\right)^2\right)}\right] = 10\log\left[\frac{3L_q^2}{2+3\left(2\pi f L_q \sigma_j\right)^2}\right], \tag{2.61}$$

The above equation indicates that the quantization noise and jitter noise affect the signal that passes through the ADC.

2.9 The model of the Physical Radio Frequency Transceiver Defects in the Mobile Communication Systems

In most communication systems, the defects in the transceiver, some of which were explained in the previous section, are modeled as additive complex uncorrelated Gaussian distortion noise with zero mean and variance indicated

by a certain symbol. This variance represented the power distortion of the transceiver [104].

Moreover, to illustrate how to calculate the power distortion of the physical transceiver in the transmission side, the DF Relay System with multi-antenna terminals will be taken as an example to show this. In the DF Relay System with multi-antenna terminals, the power distortion of the transmitter at the nth transmit antenna is proportional to the power of the signal transmitted from the same antenna. This concept for power distortion of the transmitter is applied when the system is an SC. For more precise, the total power distortion of the transmitter in the DF Relay System with multi-antenna terminals and considering the system is SC, is given in the following equation:

$$\Upsilon_{tDF} = \kappa_{tDF}{}^2 * \mathrm{diag}(q_{a1}, \dots\dots\dots, q_{aN}) \qquad (2.62)$$

where Υ_{tDF} is the variance of the distortion of the transmitter in the DF Relay System with multi-antenna terminals, κ_{tDF} is the level of the degradation of the transmitter that is used in the system, and $\mathrm{diag}(q_1, \dots\dots\dots, q_N)$ is a diagonal matrix containing the power allocated of each transmit antenna.

In addition, if the system uses is considered a MC system, there is a distortion leakage between the subcarrier. Therefore equation (2.62) becomes as follows [105]:

$$\Upsilon_{tDF} = \kappa_{tDF}{}^2 * \sum_{i=1}^{N} q_{ai}/N \qquad (2.63)$$

Furthermore, to illustrate how to calculate the power distortion of the physical transceiver on the reception side, the same way mentioned in [22] will be adopted. This way considers that the distortion power of the physical receiver at the nth receive antenna in the SC-MIMO system is proportional to the average signal power received through the mth row of the channel matrix.

Chapter Three

Research Methodology

CHAPTER THREE
RESEARCH METHODOLOGY

3.1 Introduction

In the second chapter, the performance of the random MIMO channel that suffers from Rayleigh flat fading was analyzed. That analysis was limited to channel capacity (ergodic capacity (EC)) and multiplexing gain in two different cases, CSIR and CSIT. However, the analysis mentioned in the second chapter was based on the traditional premise, which assumes the existence of ideal transceivers in the MIMO systems. In other words, the analysis presented in the previous chapter considered that the transceivers used in the MIMO systems do not affect the signal that passes through them. That consideration is in contrast to the truth found in practical reality, in which the practical MIMO system must be contained the physical transceiver, which suffers from many disabilities that generate distortion in the signal that passes through it. Thus, to get results similar to the behavior of practical results, this distortion effect cannot be neglected in the analysis of the performance of the MIMO channel. Therefore, this chapter will be proposed two algorithms to analyze the performance of the random MIMO channel that suffers from Rayleigh flat fading in the presence of the physical transceiver. These two algorithms analyze the performance of the MIMO channel in terms of the channel capacity (ergodic capacity (EC)) and finite-SNR multiplexing gain (F-SNRMG). Also, these two algorithms accept that receiving number antennas smaller than or equivalent to transmitting antennas number. The two algorithms are implemented by the MATLAB software, released in 2018.

For extra clearly, two of the most important things that will be relied upon in this work:

- Modeling the effect of the transmitter in the MIMO system as additive complex uncorrelated Gaussian distortion noise ($\boldsymbol{\sigma_t}$) with a zero mean and variance indicated by the symbol $\boldsymbol{\Upsilon_t}$,
- Modeling the effect of the receiver in the MIMO system also as additive complex uncorrelated Gaussian distortion noise ($\boldsymbol{\sigma_r}$) with a zero mean and variance indicated by the symbol $\boldsymbol{\Upsilon_r}$.

3.2 The First Algorithm

This algorithm considers only the effect of the physical transmitter on both the MIMO channel capacity (EC) and the finite-SNR multiplexing gain, in which it considers the effect of the physical transmitter as additive uncorrelated Gaussian distortion noise ($\boldsymbol{\sigma_t}$) with zero mean and variance indicated by the symbol $\boldsymbol{\Upsilon_t}$. This algorithm is applied to both the uncorrelated MIMO channel and the correlated MIMO in many scenarios: multi-carrier (MC) system with CSIT, multi-carrier (MC) system with CSIR, single-carrier (SC) system with CSIT, and single-carrier (SC) system with CSIR. Figure (3.1) illustrates all cases covered by the first algorithm.

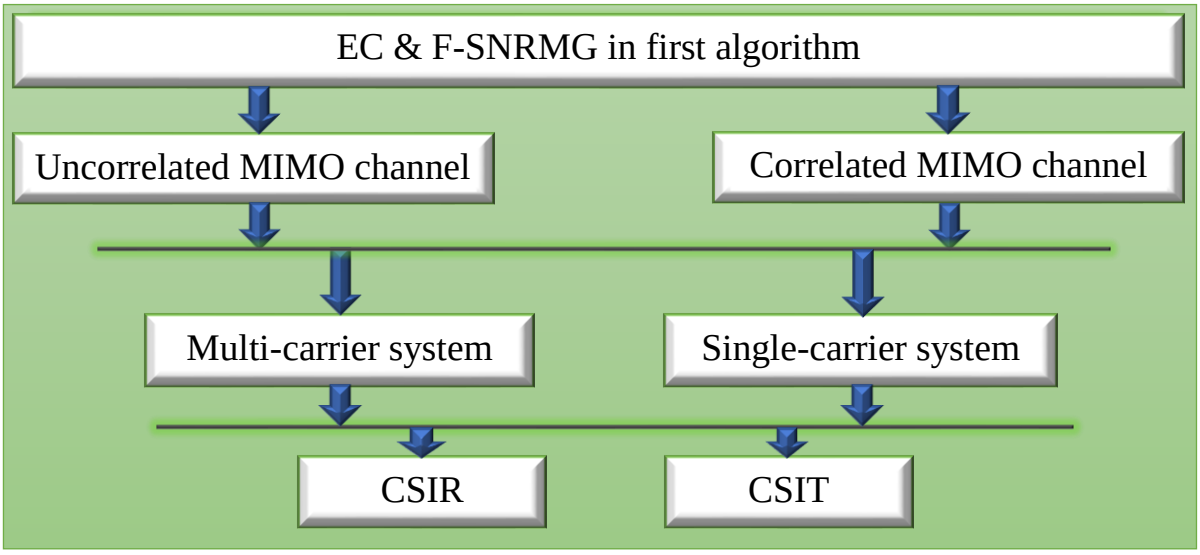

Fig. 3.1: Cases covered by the first algorithm.

Before implementing this algorithm in the MATLAB program, the ergodic capacity equation and the finite-SNR multiplexing gain equation under the influence of the physical transmitter will be clarified in both the uncorrelated MIMO channel and the correlated MIMO channel for all scenarios shown in Fig. (3.1).

3.2.1 Uncorrelated MIMO Channel Model In First Algorithm

In the previous chapter, the traditional affine MIMO channel model was explained in detail, in which the transceiver used in that model is perfect. Thus, the signal that comes out of the transmitter is the same as the signal intended to be sent, and the signal that comes out of the receiver is the same as the received signal. In this subsection, the same model will be clarified, but with the effect of the physical transmitter (effect of the transmitter distortion), so the ousted signal from the transmitter is not the same as the signal planned to be sent. The block diagram of the affine model to the UMIMOC in presence physical transmitter is revealed in Fig. (3.2).

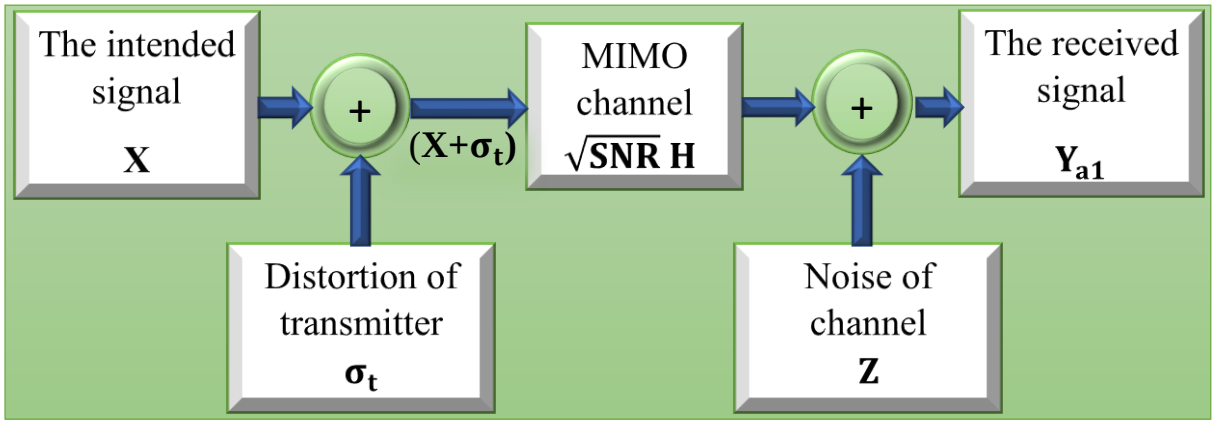

Fig. 3.2: The block diagram of the affine model for the uncorrelated MIMO channel in the first algorithm.

The model clarified in Fig. (3.2) consists of $\mathbf{N}$ antennas to send the signals and $\mathbf{M}$ antennas to receive them. Also, the received signal in this model ($\mathbf{Y_{a1}} \in \mathbf{C^M}$) can be expressed as in equation (3.1).

$$\mathbf{Y_{a1}} = \sqrt{\mathbf{SNR}}\,\mathbf{H} * (\mathbf{X} + \boldsymbol{\sigma_t}) + \mathbf{Z} \qquad (3.1)$$

where **SNR** is the ratio between the power of the transmit signal to the power of the noise that the channel adds to the signal, and $\mathbf{X} \in \mathbf{C^{N_t}}$ is the transmitted signal with covariance matrix $\mathbf{R_{XX}} = \mathbf{E}(\mathbf{x}\,\mathbf{x^H})$. The symbol $\mathbf{H} \in \mathbf{C^{M*N}}$ refers to the channel matrix whose entries are random variables all subject to Rayleigh distribution, and $\mathbf{Z}$ is zero-mean circular-symmetric complex Gaussian noise (i.e., $\mathbf{Z} \sim \boldsymbol{\mathcal{CN}}(\mathbf{0},\ \mathbf{I})$). The term $(\mathbf{X} + \boldsymbol{\sigma_t})$ indicates the signal that will come out of the radio spreader, and the symbol $\boldsymbol{\sigma_t}$ indicates the misalliance between the signal intended to be transmitted and the signal that will be sent from the transmitter "(i.e., the symbol $\boldsymbol{\sigma_t}$ is the transmitter distortion)".

Moreover, it is known that every MIMO system runs with a particular power constraint. Thus, the power constraint of any MIMO system in the first algorithm will be considered equal to one **(i.e., $\mathbf{tr}(\mathbf{R_{XX}}) = \mathbf{1}$)**. Also, it is known that each MIMO system contains an RF chain for each transmitting antenna used in the system, as shown in Fig. (3.3). Thus, the variance of distortion of the transmitter in the MIMO system can be calculated in the same way adopted in equation (2.61), which means the distortion power of each RF chain is proportional to the power assigned to the signal transmitted through the antenna of this chain.

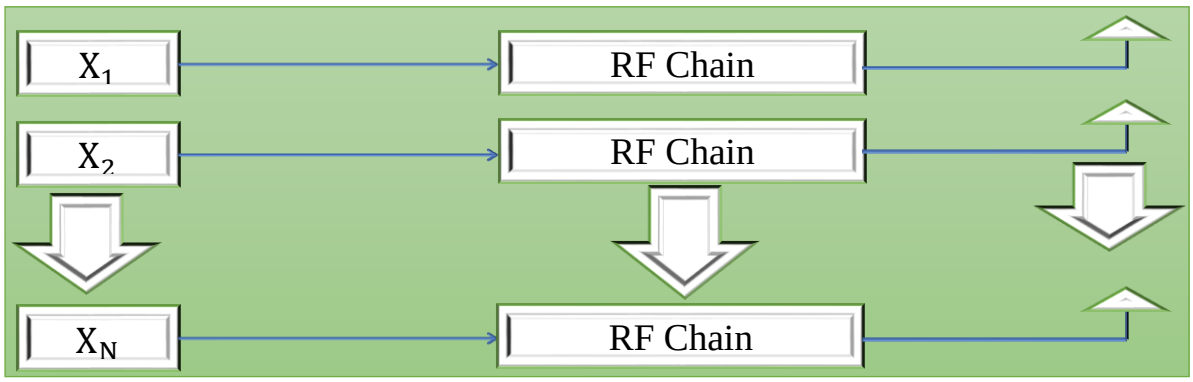

Fig. 3.3: Arrangement of RF chain in the MIMO system (transmitter side).

Based on what was mentioned in the previous paragraph, the variance of distortion of the transmitter ($\boldsymbol{\Upsilon_t}$) in the single-carrier MIMO system (SC-MIMO system) can be expressed as equation (3.2).

$$\Upsilon_t = \kappa_t{}^2 * \mathrm{diag}(q_1, \dots\dots\dots, q_N) \tag{3.2}$$

The parameter $\boldsymbol{\kappa_t}$ indicates the level of the degradation of the transmitter that is used in the MIMO system, the term $(\boldsymbol{q_1}, \dots\dots\dots, \boldsymbol{q_{N_t}})$ indicates the diagonal components of the matrix $\mathbf{R_{XX}}$, and the term $\mathbf{diag}(\boldsymbol{q_1}, \dots\dots\dots, \boldsymbol{q_N})$ indicates to work a diagonal matrix from elements $(\boldsymbol{q_1}, \dots\dots\dots, \boldsymbol{q_N})$. The degradation level of the transceivers is given in the range of 0.08 to 0.175 in the long-term evolution (LTE) systems.

In the multi-carrier MIMO system (MC-MIMO system), in which equation (3.1) can express each sub-carrier, there is a distortion leaked between the sub-carriers. Thus, equation (3.2) cannot be applied. Therefore, the same way in equation (2.62) is adopted to calculate the transmitter distortion power in the MC-MIMO system. Hence, if the system is MC, the transmitter's distortion variance can be expressed as equation (3.3).

$$\boldsymbol{\Upsilon_t = \kappa_t{}^2 * \sum_{i=1}^{N} q_i / N} \tag{3.3}$$

where $\boldsymbol{q_i}$ is the power of the ith transmit antenna.

After knowing how to find the variance of distortion of the transmitter depending on the type of the system used, equations (3.2) and (3.3) can be summed up in one equation as follows:

$$\boldsymbol{\Upsilon_t = \kappa_t{}^2 \left((1-\beta) * \mathrm{diag}[q_1, \dots\dots\dots, q_{N_t}] + \beta * \frac{\sum_{i=1}^{N} q_i}{N} \right)} \tag{3.4}$$

where the parameter **β** has a value of zero or one. In other words, if **β** equals zero (**β = 0**), the system used is the single carrier system, and if **β** equals one (**β = 1**), the system used is the multi-carrier system.

I. EC of Uncorrelated MIMO channel in First Algorithm

The basic equation of the EC in the first algorithm will be derived in this subsection. This derivation is based on the basis that considers the channel state information available at the receiver. Also, the same steps used to derive the deterministic MIMO channel capacity in the presence of the ideal transceiver will be relied upon here. Therefore, the derivation will be started from the basic definition of the wireless channel capacity and as follows:

$$\mathbf{C_{a1}} = \underbrace{SUP}_{\mathrm{tr}(\mathrm{R}_{XX})=1} \max \mathbf{I}(\mathrm{X}, \mathrm{Y}_{\mathbf{a1}}) \tag{3.5}$$

where $\mathbf{C_{a1}}$ is the deterministic MIMO channel capacity in the first algorithm, and $\mathbf{I}(\mathbf{X}, \mathbf{Y_{a1}})$ is the mutual information between two vectors of random variables ($\mathbf{X}$, $\mathbf{Y_{a1}}$). The mutual information rapport between two vectors of random variables is given as follows:

$$\mathrm{I}(\mathrm{X}, \mathrm{Y}_{\mathrm{a1}}) = \mathcal{H}(\mathrm{Y}_{\mathrm{a1}}) \ - \mathcal{H}(\mathrm{Y}_{\mathrm{a1}}/\mathrm{X}) \tag{3.6}$$

where $\boldsymbol{\mathcal{H}}(\mathbf{Y_{a1}})$ is the entropy of the received signal vector ($\mathbf{Y_{a1}}$), and $\boldsymbol{\mathcal{H}}(\mathbf{Y_{a1}/X})$ is the entropy of the received signal vector ($\mathbf{Y_{a1}}$) given the transmitted signal vector ($\mathbf{X}$). Equation (3.1) is inserted into equation (3.6) to obtain the following equation:

$$\begin{aligned} \mathrm{I}(\mathrm{X}, \mathrm{Y}_{\mathrm{a1}}) \ &= \mathcal{H}\left(\sqrt{\mathrm{SNR}}\,\mathrm{H} * (\mathrm{X} + \sigma_{\mathrm{t}}) + \mathrm{Z}\right) - \mathcal{H}\left(\left(\sqrt{\mathrm{SNR}}\,\mathrm{H} * (\mathrm{X} + \sigma_{\mathrm{t}}) + \mathrm{Z}\right)/\mathrm{X}\right) \\ &= \mathcal{H}\left(\sqrt{\mathrm{SNR}}\,\mathrm{H} * (\mathrm{X} + \sigma_{\mathrm{t}}) + \mathrm{Z}\right) - \mathcal{H}\left(\sqrt{\mathrm{SNR}}\,\mathrm{H}\,\sigma_{\mathrm{t}} + \mathrm{Z}\right) \end{aligned} \tag{3.7}$$

The mutual information $\mathbf{I(X, Y_{a1})}$ in equation (3.7) is maximized when the two terms found in the same equation are maximized. The two terms $\boldsymbol{\mathcal{H}}(\sqrt{\mathbf{SNR}}\,\mathbf{H} * (\mathbf{X} + \boldsymbol{\sigma_t}) + \mathbf{Z})$ and $\boldsymbol{\mathcal{H}}(\sqrt{\mathbf{SNR}}\,\mathbf{H}\,\boldsymbol{\sigma_t} + \mathbf{Z})$ are maximized when **X**, $\mathbf{Y_{a1}}$, and $\boldsymbol{\sigma_t}$ are considered a zero mean circular symmetric complex Gaussian random variables. Therefore, the entropy equations for $\mathbf{Y_{a1}}$ and $\mathbf{Y_{a1}\,/\,X}$ under this consideration are given as follows:

$$\mathcal{H}(\mathrm{Y_{a1}}) = \mathcal{H}\left(\sqrt{\mathrm{SNR}}\,\mathrm{H} * (\mathrm{X} + \sigma_t) + \mathrm{Z}\right) = \log_2\left(\det\left(\pi * \mathrm{e} * \mathrm{R_{Y_{a1}}}\right)\right) \quad (3.8)$$

$$\mathcal{H}(\mathbf{Y_{a1}}/\mathrm{X}) = \mathcal{H}\left(\sqrt{\mathrm{SNR}}\,\mathrm{H}\,\sigma_t + \mathrm{Z}\right) = \log_2\left(\det\left(\pi * \mathrm{e} * \mathrm{R_{Y_{a1}/X}}\right)\right) \quad (3.9)$$

where $\mathbf{R_{Y_{a1}}}$ is the autocorrelation of the received signal ($\mathbf{Y_{a1}}$), and $\mathbf{R_{Y_{a1}/X}}$ is the autocorrelation of the received signal given the transmitted signal ($\mathbf{Y_{a1}\,/\,X}$).

Now, the equations of $\mathbf{R_{Y_{a1}}}$ and $\mathbf{R_{Y_{a1}/X}}$ must be found. The equation of $\mathbf{R_{Y_{a1}}}$ will be created first:

$$\mathrm{R_{Y_{a1}}} = \mathrm{E}\{\mathbf{Y_{a1}} * \mathrm{Y_{a1}}^{\mathrm{H}}\}$$

$$= \mathrm{E}\left\{\left(\sqrt{\mathrm{SNR}}\,\mathrm{H}\,\mathrm{X} + \sqrt{\mathrm{SNR}}\,\mathrm{H}\,\sigma_t + \mathrm{Z}\right) * \left(\sqrt{\mathrm{SNR}}\,\mathrm{H}\,\mathrm{X} + \sqrt{\mathrm{SNR}}\,\mathrm{H}\,\sigma_t + \mathrm{Z}\right)^{\mathrm{H}}\right\}$$

$$= \mathbb{E}\left\{\left(\sqrt{\mathrm{SNR}}\,\mathrm{H}\,\mathrm{X} + \sqrt{\mathrm{SNR}}\,\mathrm{H}\,\sigma_t + \mathrm{Z}\right) * \left(\sqrt{\mathrm{SNR}}\,\mathrm{X}^{\mathrm{H}}\,\mathrm{H}^{\mathrm{H}} + \sqrt{\mathrm{SNR}}\,\sigma_t{}^{\mathrm{H}}\,\mathrm{H}^{\mathrm{H}} + \mathrm{Z}^{\mathrm{H}}\right)\right\}$$

$$= \mathbb{E}\left\{\left(\mathrm{SNR}\,\mathrm{H}\,\mathrm{X}\,\mathrm{X}^{\mathrm{H}}\,\mathrm{H}^{\mathrm{H}} + \mathrm{SNR}\,\mathrm{H}\,\mathrm{X}\,\sigma_t{}^{\mathrm{H}}\,\mathrm{H}^{\mathrm{H}} + \sqrt{\mathrm{SNR}}\,\mathrm{H}\,\mathrm{X}\,\mathrm{Z}^{\mathrm{H}} + \mathrm{SNR}\,\mathrm{H}\,\sigma_t\,\mathrm{X}^{\mathrm{H}}\,\mathrm{H}^{\mathrm{H}} + \right.\right.$$
$$\left.\left.\mathrm{SNR}\,\mathrm{H}\,\sigma_t\,\sigma_t{}^{\mathrm{H}}\,\mathrm{H}^{\mathrm{H}} + \sqrt{\mathrm{SNR}}\,\mathrm{H}\,\sigma_t\,\mathrm{Z}^{\mathrm{H}} + \sqrt{\mathrm{SNR}}\,\mathrm{Z}\,\mathrm{X}^{\mathrm{H}}\,\mathrm{H}^{\mathrm{H}} + \sqrt{\mathrm{SNR}}\,\mathrm{Z}\,\sigma_t{}^{\mathrm{H}}\,\mathrm{H}^{\mathrm{H}} + \mathrm{Z}\,\mathrm{Z}^{\mathrm{H}}\right)\right\} \quad (3.10)$$

where $\mathbb{E}$ (.) refers to the expectation operator, and $(.)^{\mathrm{H}}$ Indicates applying the Hermitian operation on the matrix inside the bows.

Because **X**, **Z**, and $\boldsymbol{\sigma_t}$ are independent of each other, the equation of the autocorrelation of the received signal ($\mathrm{R_{Y_{a1}}}$) becomes as follows:

$$\mathrm{R_{Y_{a1}}} = \mathbb{E}\{(\mathrm{SNR}\,\mathrm{H}\,\mathrm{X}\,\mathrm{X}^{\mathrm{H}}\,\mathrm{H}^{\mathrm{H}} + \mathrm{SNR}\,\mathrm{H}\,\sigma_t\,\sigma_t{}^{\mathrm{H}}\,\mathrm{H}^{\mathrm{H}} + \mathrm{Z}\,\mathrm{Z}^{\mathrm{H}})\}$$

$$= \text{SNR H } \mathbb{E}(X X^H) \text{ H}^H + \text{SNR H } \mathbb{E}(\sigma_t \sigma_t^H) \text{ H}^H + \mathbb{E}(Z Z^H)$$
$$= \text{SNR H } R_{XX} \text{ H}^H + \text{SNR H } \Upsilon_t \text{ H}^H + I_M \quad (3.11)$$

After deriving the equation of autocorrelation of the received signal vector ($\mathbf{R_{Y_{a1}}}$), the equation of the autocorrelation of the received signal given the transmitted signal ($\mathbf{R_{Y_{a1}/X}}$) will be found now in the same way:

$$R_{Y_{a1}/X} = E\{(Y_{a1}/X) * (Y_{a1}/X)^H\}$$
$$= E\{\left(\sqrt{SNR}\, H\, \sigma_t + Z\right) * (\sqrt{SNR}\, H\, \sigma_t + Z)^H\}$$
$$= \mathbb{E}\{\left(\sqrt{SNR}\, H\, \sigma_t + Z\right) * \left(\sqrt{SNR}\, \sigma_t^H\, H^H + Z^H\right)\}$$
$$= \mathbb{E}\{\left(SNR\, H\, \sigma_t\, \sigma_t^H\, H^H + \sqrt{SNR}\, H\, \sigma_t\, Z^H + \sqrt{SNR}\, Z\, \sigma_t^H\, H^H + Z\, Z^H\right)\}$$
$$= \mathbb{E}\{(SNR\ H\ \sigma_t\, \sigma_t^H\, H^H + Z\, Z^H)\} = SNR\ H\ \mathbb{E}(\sigma_t\, \sigma_t^H)\ H^H + \mathbb{E}(Z\, Z^H)$$
$$= \text{SNR H } \Upsilon_t \text{ H}^H + I_M \quad (3.12)$$

After that, equation (3.11) will be inserted into equation (3.8), and equation (3.12) into equation (3.9) to get the following equations:

$$\mathcal{H}(Y_{a1}) = \log_2 \det\left(\pi * e * (\text{SNR H } R_{XX} \text{ H}^H + \text{SNR H } \Upsilon_t \text{ H}^H + I_M)\right) \quad (3.13)$$

$$\mathcal{H}(Y_{a1}/X) = \log_2 \det\left(\pi * e * (\text{SNR H } \Upsilon_t \text{ H}^H + I_M)\right) \quad (3.14)$$

The two equations (3.13) and (3.14) show the maximum entropies of $\mathbf{Y_{a1}}$ and $\mathbf{Y_{a1}/X}$, respectively. These two equations are entered into equation (3.6) to obtain the maximum mutual information between the received signal vector ($\mathbf{Y_{a1}}$) and the transmitted signal vector (**X**), as apparent in equation (3.15).

$$\mathbf{I}(X, Y_{a1}) = \log_2\left(\det\left(\pi * e * (\text{SNR H } R_{XX} \text{ H}^H + \text{SNR H } \Upsilon_t \text{ H}^H + I_M)\right)\right) - \log_2\left(\det\left(\pi * e * (\text{SNR H } \Upsilon_t \text{ H}^H + I_M)\right)\right) \quad (3.15)$$

To continuity in derivation, equation (3.15) will be inserted into equation (3.4) to get the deterministic uncorrelated MIMO channel capacity in the first algorithm, which is represented in equation (3.16).

$$C_{a1} = \underbrace{SUP}_{tr(R_{XX})=1} \log_2\left(\frac{\det(SNR\ H\ R_{XX}\ H^H + SNR\ H\ \Upsilon_t\ H^H + I_M)}{\det(SNR\ H\ \Upsilon_t\ H^H + I_M)}\right)$$

$$= \underbrace{SUP}_{tr(R_{XX})=1} \log_2\left(\det\left(\frac{SNR\ H\ R_{XX}\ H^H + SNR\ H\ \Upsilon_t\ H^H + I_M}{SNR\ H\ \Upsilon_t\ H^H + I_M}\right)\right)$$

$$= \log_2\left(\det\left(I_M + \frac{SNR\ H\ R_{XX}\ H^H}{SNR\ H\ \Upsilon_t\ H^H + I_M}\right)\right) \quad \text{bit/second/hertz} \quad (3.16)$$

Moreover, it is known that the random MIMO channel has **L** number of realizations. Thus, the capacity of the uncorrelated random MIMO channel in the first algorithm can be computing by applying equation (3.16) for each realization of the channel. Then, the mean of the calculated values is taken. Therefore, the EC (random capacity) of the UMIMOC in the first algorithm can be expressed by equation (3.17).

$$C_{ea1} = \mathbb{E}\left\{\log_2\left(\det\left(I_M + \frac{SNR\ H\ R_{XX}\ H^H}{SNR\ H\ \Upsilon_t\ H^H + I_M}\right)\right)\right\} \quad \text{bit/second/hertz} \quad (3.17)$$

where $\mathbf{C_{ea1}}$ is the EC for UMIMOC in the first algorithm.

Now, the EC of the UMIMOC shown in equation (3.17) will be studied in two systems:

A. Multi-carrier MIMO system (for one sub-carrier)
B. Single-carrier MIMO system

In the above systems, the EC of the uncorrelated MIMO channel with the presence of the physical transmitter will be clarified in two different cases, namely CSIT and CSIR.

A. Multi-Carrier MIMO System

Here, the system used will be considered the multi-carrier MIMO system. Therefore, the variance of the transmitter distortion ($\boldsymbol{\Upsilon_t}$) is computing by applying the equation (3.3) or equation (3.4) with $\boldsymbol{\beta = 1}$. These two equations can be rewritten to become like the form shown in equation (3.18), in which the term $\sum_{\mathbf{i=1}}^{\mathbf{N}} \mathbf{q_i}$ is equaled to one (i.e. $\sum_{\mathbf{i=1}}^{\mathbf{N}} \mathbf{q_i} = \mathbf{1}$) because the power constraint of any MIMO system in the first algorithm is $\mathbf{tr}(\mathbf{R_{XX}}) = \mathbf{1}$.

$$\Upsilon_t = \kappa_t{}^2 * \sum_{i=1}^{N} q_i/N = \kappa_t{}^2 * 1/N = \kappa_t{}^2/N \qquad (3.18)$$

Furthermore, equation (3.18) is inserted into equation (3.17) to get the following equation:

$$C_{ea1} = \mathbb{E}\left\{\log_2\left(\det\left(I_M + \frac{SNR\ H\ R_{XX}\ H^H}{(SNR*\kappa_t{}^2/N))\ H\ H^H + I_M}\right)\right)\right\} \qquad (3.19)$$

Now, the ergodic capacity shown in equation (3.19) will be clarified in two different cases:

1) Information of channel is known at transmitter(i.e. CSIT)
2) Information of channel is known at receiver Only(i.e. CSIR)

1) Information of Channel is Known at Transmitter (i.e. CSIT)

This event means that the channel state information is available at the receiver and transmitter. Therefore, the pre-coding process can be applied,

which works with the help of the analysis technique SVD to divide the MIMO network into similar SISO networks. The number of these SISO channels (effective channels) is equal to the rank of the channel matrix H, which is equivalent for minimum (M,N). Also, power allocated to each channel of these effective channels will be computed by applying the WATER-FILLING mechanism. As a result, equation (3.19) can be simplified as follows:

$$C_{ea1} = \mathbb{E}\left\{\log_2\left(\det\left(I_M + \frac{SNR\ H\ R_{XX}\ H^H}{(SNR*\kappa_t{}^2/N)\ H\ H^H + I_M}\right)\right)\right\}$$

$$=$$

$$\mathbb{E}\left\{\log_2\left(\det\left(I_M + \frac{SNR * U_{M*M} * \Sigma_{M*N} * V_{N*N}{}^H * V_{N*M} * D_{M*M} * V_{N*M}{}^H * V_{N*N} * \Sigma_{M*N}{}^H * U_{M*M}{}^H}{(SNR*\kappa_t{}^2/N) * U_{M*M} * \Sigma_{M*N} * V_{N*N}{}^H * V_{N*N} * \Sigma_{M*N}{}^H * U_{M*M}{}^H + I_M}\right)\right)\right\}$$

$$= \mathbb{E}\left\{\log_2\left(\det\left(I_M + \frac{SNR * U_{M*M} * \Sigma_{M*M} * D_{M*M} * \Sigma_{M*M} * U_{M*M}{}^H}{(SNR*\kappa_t{}^2/N) * U_{M*M} * \Sigma_{M*N} * \Sigma_{M*N}{}^H * U_{M*M}{}^H + I_M}\right)\right)\right\} \quad (3.20)$$

where **D** is a square diagonal matrix containing the power assigned to each effective channel, the size of the matrix **D** is **M*M (D_{M*M})** because the number of effective channels is equal to the rank of matrix **H**, which considers equivalent for receiving antennas **(M)**number at this chapter. Also, sum for power of the effective channels must be equal to the power constraint of the system (i.e. $\mathbf{tr}(\mathbf{D}) = \mathbf{1}$).

Moreover, equation (3.20) can be simplified more by getting help from the mathematical property shown in equation (3.21).

$$\det\left(I + \frac{A\ C\ A^H}{A\ F\ A^H + I}\right) = \det\left(I + \frac{A^H\ A\ C}{A^H\ A\ F + I}\right) \quad (3.21)$$

where **A** is a square matrix with any size, **C** is a diagonal matrix with a size similar to the size of **A,** and **F** is a diagonal matrix with a size similar to the size of **C**. By applying this property, equation (3.20) can be rewritten as follows:

$$C_{ea1} = \mathbb{E}\left\{\log_2\left(\det\left(I_M + \frac{SNR * U_{M*M}{}^H * U_{M*M} * \Sigma_{M*M} * D_{M*M} * \Sigma_{M*M}}{(SNR*\kappa_t{}^2/N) * U_{M*M}{}^H * U_{M*M} * \Sigma_{M*N} * \Sigma_{M*N}{}^H + I_M}\right)\right)\right\}$$

$$= \mathbb{E}\left\{\log_2\left(\det\left(I_M + \frac{SNR * \Sigma_{M*M} * D_{M*M} * \Sigma_{M*M}}{(SNR*\kappa_t{}^2/N) * \Sigma_{M*N} * \Sigma_{M*N}{}^H + I_M}\right)\right)\right\}$$

$$= \mathbb{E}\left\{\log_2\left(\det\left(I_M + \frac{SNR * \Sigma_{M*M} * \Sigma_{M*M} * D_{M*M}}{(SNR*\kappa_t{}^2/N) * \Sigma_{M*N} * \Sigma_{M*N}{}^H + I_M}\right)\right)\right\}$$

$$= \mathbb{E}\left\{\log_2\left(\det\left(I_M + \frac{SNR * \lambda * D_{M*M}}{(SNR*\kappa_t{}^2/N) * \lambda + I_M}\right)\right)\right\} \quad \text{bit/second/hertz} \quad (3.22)$$

where $\boldsymbol{\lambda}$ is a square diagonal matrix with size M*M, which is equal to $\{\boldsymbol{\Sigma_{M*N}} * \boldsymbol{\Sigma_{M*N}{}^H}\}$ or $\{\boldsymbol{\Sigma_{M*M}} * \boldsymbol{\Sigma_{M*M}}\}$. Also, the values of matrix $\boldsymbol{\lambda}$ are the same as the eigenvalues of the matrix that result from multiplying the matrix **H** with the matrix $\mathbf{H^H}$. This matrix ($\boldsymbol{\lambda}$) contains the channel gain of each effective channel.

In addition, the equation (3.22) can be abridged more by using some mathematical properties and as follows:

$$C_{ea1} = \mathbb{E}\left\{\log_2\left(\det\left(I_M + \frac{SNR * \lambda * D_{M*M}}{(SNR * \kappa_t{}^2/N) * \lambda + I_M}\right)\right)\right\}$$

$$= \mathbb{E}\left\{\log_2\left(\prod_{i=1}^{\text{rank (H)=M}}\left(1 + \frac{SNR * \lambda_i * D_i}{(SNR * \kappa_t{}^2/N) * \lambda_i + 1}\right)\right)\right\}$$

$$= \mathbb{E}\left\{\sum_{i=1}^{M}\left(\log_2\left(1 + \frac{SNR * \lambda_i * D_i}{(SNR * \kappa_t{}^2/N) * \lambda_i + 1}\right)\right)\right\} \quad \text{bit/second/hertz} \quad (3.23)$$

where λ_i is the channel gain of the ith effective channel in the uncorrelated MIMO channel, and D_i is the power assigned to the ith effective channel in the

uncorrelated MIMO channel. Also, the sum of values of **D** is equal to one (**i.e** $\sum_{i=1}^{m} D_i = 1$**),** according to the power constraint allocated to the system.

The equation (3.23) computes the EC for UMIMOC to the CSIT case in the multi-carrier system with the physical transmitter. The value result from equation (3.23) needs to multiply by the number of sub-carriers to get the total capacity.

Furthermore, in the very high SNRs, the maximum capacity of the UMIMOC for the CSIT case in the multi-carrier system with the physical transmitter can be found by putting the SNR is approaching infinity in equation (3.23). Also, the values of D in the same equation must be equal and as follows:

$$C_{ea1}(SNR\sim\infty) = \lim_{SNR\sim\infty} \mathbb{E}\left\{\sum_{i=1}^{M}\left(\log_2\left(1+\frac{SNR*\lambda_i*D_i}{(SNR*{\kappa_t}^2/N)*\lambda_i+1}\right)\right)\right\}$$

$$= \mathbb{E}\left\{\sum_{i=1}^{M}\left(\log_2\left(1+\frac{D_i}{({\kappa_t}^2/N)}\right)\right)\right\}$$

$$= M*\log_2\left(1+\frac{1}{M*({\kappa_t}^2/N)}\right) \quad \text{bit/second/hertz} \qquad (3.24)$$

The result in equation (3.24) represents the capacity limit, which is the value that the channel capacity **(EC)** stops growing in the high SNRs.

2) Channel Information is Known at the Receiver Only (i.e.CSIR)

This case means the information of channel is obtainable at receiver only. Thus, equal power will be allocated to each transmitting antenna (i.e. $\mathbf{R_{XX}} = \frac{\mathbf{I_N}}{\mathbf{N}}$). Therefore, equation (3.19) can be rewritten as follows:

$$C_{ea1} = \mathbb{E}\left\{\log_2\left(\det\left(I_M + \frac{\frac{SNR}{N} H * H^H}{(SNR * \kappa_t{}^2/N) * H * H^H + I_M}\right)\right)\right\}$$

$$= \mathbb{E}\left\{\sum_{i=1}^{M} \log_2\left(1 + \frac{\frac{SNR}{N} * \lambda_i}{(SNR * \kappa_t{}^2/N) * \lambda_i + 1}\right)\right\} \quad \text{bit/second/hertz} \quad (3.25)$$

The result from equation (3.25) represents the EC of the UMIMOC for the CSIR case in the multi-carrier system with the physical transmitter.

Moreover, in this case (CSIR case), the capacity limit of the uncorrelated MIMO channel in the multi-carrier system having a physical transmitter becomes as in equation (3.26).

$$C_{ea1}(SNR \sim \infty) = \lim_{SNR \sim \infty} \mathbb{E}\left\{\sum_{i=1}^{M} \log_2\left(1 + \frac{\frac{SNR}{N} * \lambda_i}{(SNR * \kappa_t{}^2/N) * \lambda_i + 1}\right)\right\}$$

$$= M * \log_2\left(1 + \frac{1}{\kappa_t{}^2}\right) \quad \text{bit/second/hertz} \quad (3.26)$$

Finally, it can be seen that equation (3.26) becomes similar to equation (3.24) when the amount of transferring antennas is equivalent to the amount of receipting antennas. Thus, it can be said that if the numeral of transferring antennas is equivalent to the numeral of accepting antennas, the capacity limit of the UMIMOC in the multi-carrier system holding a physical transmitter is equal in both cases, CSIT and CSIR.

B. Single-Carrier MIMO System

Here, the variance of the transmitter distortion is computed by applying the equation (3.2) or applying equation (3.4) with **β = 0**. Thus, the EC of the UMIMO in the first algorithm, which is shown in equation (3.17), becomes as follows:

$$C_{ea1} = \mathbb{E}\left\{\log_2\left(\det\left(I_M + \frac{SNR * H * R_{XX} * H^H}{(SNR * \kappa_t{}^2) * H * diag(diag(R_{XX})) * H^H + I_M}\right)\right)\right\} \quad (3.27)$$

The equation (3.27) will be presented in two different cases, CSIR and CSIT. Therefore, Table (3.1) is developed to show the forms of the equation (3.27) for the CSIR case and the CSIT case.

Table 3.1: The EC formulas of the UMIMOC for the CSIR & CSIT cases in the SC system containing a physical transmitter

Case	The formula of ergodic capacity (bit/second/hertz)
CSIT	$C_{ea1} = \mathbb{E}\left\{\log_2\left(\det\left(I_M + \frac{SNR * H * R_{XX} * H^H}{(SNR * \kappa_t{}^2) * H * diag(diag(R_{XX})) * H^H + I_M}\right)\right)\right\}$, **where** $\mathbf{R_{XX} = V_{N*M} * D_{M*M} * V_{N*M}{}^H}$
CSIR	$C_{ea1} = \mathbb{E}\left\{\sum_{i=1}^{M} \log_2\left(1 + \frac{(SNR/N) * \lambda_i}{(SNR * \kappa_t{}^2/N) * \lambda_i + 1}\right)\right\}$, Note: This equation results from simplifying the equation (3.27) when putting the R_{XX} equals to $\frac{I_N}{N}$ ($R_{XX} = \frac{I_N}{N}$). Also, this equation is the same equation (3.25).

After that, It can be seen that if the information of the channel state is present at the receiver only (i.e. CSIR), the random uncorrelated MIMO channel capacity with the presence of the physical transmitter is equal in both systems, the multi-carrier system (for one sub-carrier) and the single-carrier system.

In addition, Table (3.2) is presented to show the capacity limit formulas of the uncorrelated MIMO channel for the CSIR case and CSIT case in the single-carrier system with the physical transmitter.

Table 3.2: The capacity limit formulas of the uncorrelated MIMO channel for the CSIR and CSIT cases in the SC system with the physical transmitter.

Case	The formula of capacity limit (bit/second/hertz)
CSIT	$\mathrm{C_{ea1}}\left(\mathrm{SNR}\sim\infty_{\text{in Eq.(3.27)}}\right) = \mathbb{E}\left\{\log_2\left(\det\left(\mathrm{I_M} + \frac{\mathrm{H} * \mathrm{R_{XX}} * \mathrm{H^H}}{{\kappa_t}^2 * \mathrm{H} * \mathrm{diag}(\mathrm{diag}(\mathrm{R_{XX}})) * \mathrm{H^H}}\right)\right)\right\}$. (3.28)
CSIR	$\mathrm{C_{ea1}}\left(\mathrm{SNR}\sim\infty_{\text{in Eq.(3.25)}}\right) = \mathrm{M} * \log_2\left(1 + \frac{1}{{\kappa_t}^2}\right)$, same equation (3.26)

II. F-SNRMG of Uncorrelated MIMO Channel in First Algorithm

In this subsection, the same concept of the MG of the MIMO network explained in section (2.7) will be trusted. That concept considers that the MG of the MIMO network can be calculated by dividing the capacity of the MIMO network by the capacity of the SISO network. That concept is called the F-SNRMG. Therefore, the F-SNRMG of the UMIMOC in the first algorithm can be given as in equation (3.30).

$$\mu_{a1} = \frac{\mathrm{C_{ea1}}}{\mathrm{C_{Sea1}}} \tag{3.29}$$

where μ_{a1} is the F-SNRMG of the UMIMOC in the first algorithm, and $\mathrm{C_{Sea1}}$ is the channel capacity of the SISO system in the first algorithm, which is given as in equation (3.30).

$$\mathrm{C_{Sea1}} = \mathbb{E}\left\{\log_2\left(1 + \frac{\mathrm{SNR} * |h|^2}{(\mathrm{SNR} * {\kappa_t}^2) * |h|^2 + 1}\right)\right\}, \text{ derived from Eq. (3.17).} \tag{3.30}$$

where $|h|^2$ is the channel gain of the SISO system.

In addition, here, the focus will be on the F-SNRMG of the UMIMOC in multi-carrier system containing a physical transmitter. Therefore, the finite-SNR multiplexing gain formulas of the uncorrelated MIMO channel for the CSIR and CSIT cases in the multi-carrier system containing a physical transmitter will be found at both the high and low SNRs.

A. Case of CSIT

In this case, the limit of the finite-SNR multiplexing gain in the low SNRs can be found from equation (3.31):

$$\mu_{a1}(\mathrm{SNR}\sim 0) = \lim_{\mathrm{SNR}\sim 0} \frac{\mathbb{E}\left\{\sum_{i=1}^{\mathrm{M}}\left(\log_2\left(1+\frac{\mathrm{SNR}*\lambda_i*D_i}{(\mathrm{SNR}*{\kappa_t}^2/\mathrm{N})*\ \lambda_i+1}\right)\right)\right\}}{\mathbb{E}\left\{\log_2\left(1+\frac{\mathrm{SNR}*|h|^2}{(\mathrm{SNR}*{\kappa_t}^2)*|h|^2+1}\right)\right\}} \tag{3.31}$$

In the CSIT case, it is known that if the value of SNR is minimal, the power of the system will be allocated to the channel owning the highest gain (highest value of λ). Therefore, equation (3.31) can be rewritten as follows:

$$\mu_{a1}(\mathrm{SNR}\sim 0) = \lim_{\mathrm{SNR}\sim 0} \frac{\mathbb{E}\left\{\log_2\left(1+\frac{\mathrm{SNR}*\lambda_{max}*D_i}{(\mathrm{SNR}*{\kappa_t}^2/\mathrm{N})*\ \lambda_{max}+1}\right)\right\}}{\mathbb{E}\left\{\log_2\left(1+\frac{\mathrm{SNR}*|h|^2}{(\mathrm{SNR}*{\kappa_t}^2)*|h|^2+1}\right)\right\}} \tag{3.32}$$

The equation (3.32) can be solved with L'Hôpital's method and get the following result:

$$\mu_{a1}(\mathrm{SNR}\sim 0) = \frac{\mathbb{E}\{\lambda_{max}\}}{\mathbb{E}\{|h|^2\}} \tag{3.33}$$

The above equation computes the finite-SNR multiplexing gain limit in the low SNRs for the uncorrelated MIMO channel for the CSIT case in the multi-carrier system with the physical transmitter.

Moreover, in the high SNRs, the F-SNRMG limit of the UMIMOC for CSIT case in the multi-carrier system with the physical transmitter can be given as in equation (3.34):

$$\mu_{a1}(\mathrm{SNR}\sim\infty) = \lim_{\mathrm{SNR}\sim\infty} \frac{\mathbb{E}\left\{\sum_{i=1}^{\mathrm{M}}\left(\log_2\left(1+\frac{\mathrm{SNR}*\lambda_i*D_i}{(\mathrm{SNR}*{\kappa_t}^2/\mathrm{N})*\ \lambda_i+1}\right)\right)\right\}}{\mathbb{E}\left\{\log_2\left(1+\frac{\mathrm{SNR}*|h|^2}{(\mathrm{SNR}*{\kappa_t}^2)*|h|^2+1}\right)\right\}}$$

$$= \frac{\mathrm{M}*\log_2\left(1+\frac{1}{\mathrm{M}*({\kappa_t}^2/\mathrm{N})}\right)}{\log_2\left(1+\frac{1}{{\kappa_t}^2}\right)} \qquad (3.34)$$

B. Case of CSIR

Here, the same scenario followed in the case of CSIT will be adopted. Therefore, Table (3.3) is developed to show the finite-SNR multiplexing gain formulas at the low and high SNRs for the uncorrelated MIMO channel for the CSIR case in the multi-carrier system carrying a physical transmitter.

Table 3.3: The F-SNRMG formulas at low and high SNRs for the uncorrelated MIMO channel for the CSIR case in the MC system carrying a physical transmitter

Rates of SNR	F-SNRMG Formula
Low SNRs	$\mu_{a1}(\mathrm{SNR}\sim0) = \lim_{\mathrm{SNR}\sim0} \frac{\mathbb{E}\left\{\sum_{\mathrm{i}=1}^{\mathrm{M}}\log_2\left(1+\frac{({\mathrm{SNR}}/{\mathrm{N}})*\lambda_\mathrm{i}}{(\mathrm{SNR}*{\kappa_t}^2/\mathrm{N})*\ \lambda_\mathrm{i}+1}\right)\right\}}{\mathbb{E}\left\{\log_2\left(1+\frac{\mathrm{SNR}*|h|^2}{(\mathrm{SNR}*{\kappa_t}^2)*|h|^2+1}\right)\right\}} = \frac{\mathbb{E}\{\sum_{i=1}^{M}\lambda_i\ \}}{\mathrm{N}*\mathbb{E}\{|h|^2\}}$$ (3.35)
High SNRs	$\mu_{a1}(\mathrm{SNR}\sim\infty) = \lim_{\mathrm{SNR}\sim\infty} \frac{\mathbb{E}\left\{\sum_{\mathrm{i}=1}^{\mathrm{M}}\log_2\left(1+\frac{({\mathrm{SNR}}/{\mathrm{N}})*\lambda_\mathrm{i}}{(\mathrm{SNR}*{\kappa_t}^2/\mathrm{N})*\ \lambda_\mathrm{i}+1}\right)\right\}}{\mathbb{E}\left\{\log_2\left(1+\frac{\mathrm{SNR}*|h|^2}{(\mathrm{SNR}*{\kappa_t}^2)*|h|^2+1}\right)\right\}} = \mathrm{M}$. (3.36)

3.2.2 Correlated MIMO Channel Model In First Algorithm

In this subsection, the affine correlated MIMO channel model with the presence of the physical transmitter is being presented, in which the Kronecker model is applied to consider the effect of the correlation between the channel elements. Figure (3.4) shows the block diagram of the affine correlated MIMO channel model with the presence of the physical transmitter.

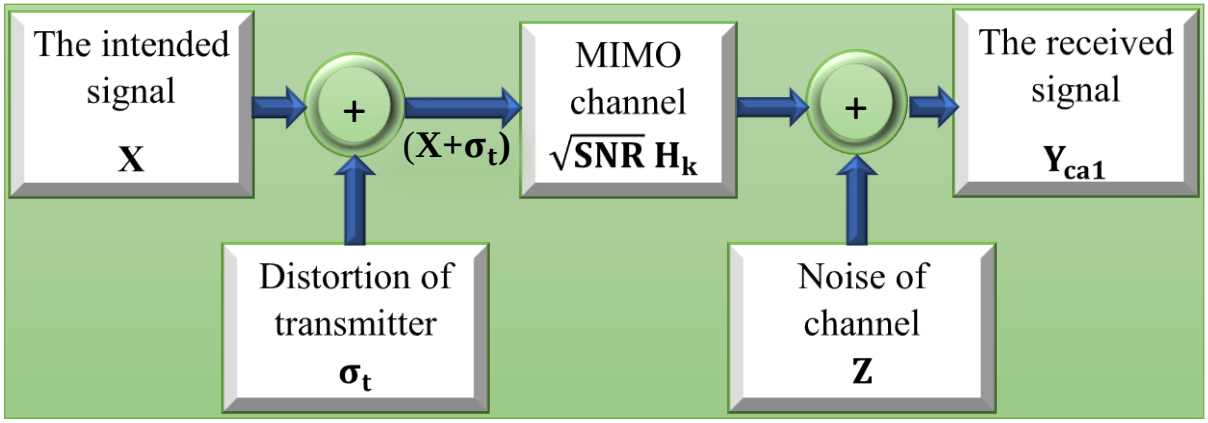

Fig. 3.4: Block diagram of the affine correlated MIMO channel model in the first algorithm

The above model consists of **N** antennas to send the signals and **M** antennas to receive them. Also, the received signal in this model ($\mathbf{Y_{ca1}} \in \mathbf{C^M}$) can be expressed as in equation (3.37).

$$\mathbf{Y_{ca1}} = \sqrt{\mathrm{SNR}}\,\mathbf{H_k} * (\mathrm{X} + \sigma_t) + \mathrm{Z} \qquad (3.37)$$

where symbol $\mathbf{H_k} \in \mathbf{C^{M*N}}$ refers to the channel matrix whose entries are random variables not independent, which is computed by equation (2.38). Also, the interconnection matrix on receiving side&interconnection matrix on transferring side, which are mentioned in equation (2.38), are computed by equation (2.39).

I. EC and Capacity limit of Correlated MIMO channel in First Algorithm

In the first algorithm, the EC equations and capacity limit equations of the correlated MIMO channel are the same as those of the uncorrelated MIMO channel, but in the correlated MIMO channel, the channel matrix used is $\mathbf{H_k}$. Therefore, table (3.4) is developed to clarify the EC and capacity limit equations for the correlated MIMO channel in all scenarios covered by the first algorithm.

Table 3.4: The ergodic capacity formulas and capacity limit formulas for the correlated MIMO channel in the first algorithm.

Name of equation, and system used	Case	The formula in (bit/second/hertz)
EC, MC	CSIT	$C_{ca1} = \mathbb{E}\left\{\sum_{i=1}^{M}\left(\log_2\left(1+\frac{SNR*\lambda_{k\,i}*D_{ki}}{(SNR*\kappa_t{}^2/N)*\ \lambda_{k\,i}+1}\right)\right)\right\}$, (3.38) where, C_{ca1} is the EC of the CMIMOC in the first algorithm, $\lambda_{k\,i}$ is the channel improvement of the ith effective channel in CMIMOC, and $D_{k\,i}$ is the power assigned to ith effective channel in the CMIMOC.
	CSIR	$C_{ca1} = \mathbb{E}\left\{\sum_{i=1}^{M}\log_2\left(1+\frac{\frac{SNR}{N}*\lambda_{k\,i}}{(SNR*\kappa_t{}^2/N)*\ \lambda_{k\,i}+1}\right)\right\}$, (3.39)
Capacity limit, MC	CSIT	$C_{ca1}\left(SNR\sim\infty_{\text{in Eq.(3.38)}}\right) = M*\log_2\left(1+\frac{1}{M*(\kappa_t{}^2/N)}\right)$, . . , (3.40)
	CSIR	$C_{ca1}\left(SNR\sim\infty_{\text{in Eq.(3.39)}}\right) = M*\log_2\left(1+\frac{1}{\kappa_t{}^2}\right)$, (3.41)

EC, SC	CSIT	$C_{ca1} = \mathbb{E}\left\{\log_2\left(\det\left(I_M + \frac{SNR * H_k * R_{XX} * H_k{}^H}{(SNR * \kappa_t{}^2) * H_k * diag(diag(R_{XX})) * H_k{}^H + I_M}\right)\right)\right\}$. (3.42) Note: The covariance matrix (R_{XX}) in the correlated MIMO channel is equal to ($\mathbf{V_k}_{N*M} * \mathbf{D_k}_{M*M} * \mathbf{V_k}_{N*M}{}^{\mathbf{H}}$).
	CSIR	Same equation (3.39).
Capacity limit, SC	CSIT	$C_{ca1}(SNR \sim \infty_{\text{in Eq.(3.42)}}) =$ $\mathbb{E}\left\{\log_2\left(\det\left(I_M + \frac{H_k * R_{XX} * H_k{}^H}{\kappa_t{}^2 * H_k * diag(diag(R_{XX})) * H_k{}^H}\right)\right)\right\}$ (3.43)
	CSIR	Same equation (3.41).

Moreover, the above Table shows that the capacity limit formulations of the CMIMOC for the CSIT case and CSIR case in the multi-carrier system are not dependent on the correlation between channel elements. Also, it shows that the capacity limit of the CMIMOC for the CSIR case in the single-carrier system is not dependent on the correlation between channel elements. In contrast, it shows that the capacity limit of the CMIMOC for the case of CSIT case in the single-carrier system may be dependent on the correlation between channel elements. Therefore, it can be said that in the multi-carrier system owning a physical transmitter, the capacity limit formulas of the correlated MIMO channel for the CSIR and CSIT cases are the same capacity limit formulas of the uncorrelated MIMO channel for the CSIR and CSIT cases.

II. F-SNRMG of Correlated MIMO channel in First Algorithm

The same concept of the F-SNRMG shown in the uncorrelated MIMO channel owning a physical transmitter will be dependent here. Thus, in the first algorithm, the F-SNRMG equation for the CMIMOC will be the same as that

for the UMIMOC, but the MIMO channel capacity engaged in the equation of the F-SNRMG for the correlated MIMO channel is $\mathbf{C_{ca1}}$ not $\mathbf{C_{ea1}}$.

In addition, the focus here also will be on the multi-carrier system as in the uncorrelated MIMO channel. Therefore, the F-SNRMG formulas of the correlated MIMO channel for the CSIR and CSIT cases in the first algorithm will be presented at the low and high SNRs in the multi-carrier system, as shown in the Table (3.5).

Table 3.5: The F-SNRMG formulas at low and high SNRs for the correlated MIMO channel for the CSIR and CSIT cases in the MC system with the physical transmitter

Name, and system used	Case	F-SNRMG Formula
F-SNRMG limit in Low SNRs, Multi-carrier	CSIT	$\mu_{ca1}(\text{SNR}\sim 0) = \lim_{\text{SNR}\sim 0} \frac{C_{ca1}}{C_{Sea1}} = \frac{\mathbb{E}\{\lambda_{k\,max}\}}{\mathbb{E}\{\lvert h\rvert^2\}}$ (3.44) where μ_{ca1} is the F-SNRMG of the correlated MIMO channel in the first algorithm.
	CSIR	$\mu_{ca1}(\text{SNR}\sim 0) = \lim_{\text{SNR}\sim 0} \frac{C_{ca1}}{C_{Sea1}} = \frac{\mathbb{E}\{\sum_{i=1}^{M} \lambda_{k\,i}\}}{N * \mathbb{E}\{\lvert h\rvert^2\}}$ (3.45)
F-SNRMG limit in high SNRs, Multi-carrier	CSIT	$\mu_{ca1}(\text{SNR}\sim \infty) = \lim_{\text{SNR}\sim \infty} \frac{C_{ca1}}{C_{Sea1}} = \frac{M * \log_2\left(1+\frac{1}{M*(\kappa_t{}^2/N)}\right)}{\log_2\left(1+\frac{1}{\kappa_t{}^2}\right)}$. (3.46)
	CSIR	$\mu_{ca1}(\text{SNR}\sim \infty) = \lim_{\text{SNR}\sim \infty} \frac{C_{ca1}}{C_{Sea1}} = M$ (3.47)

After that, it can be seen that in the multi-carrier systems owning a physical transmitter and for the CSIT and CSIR cases, the F-SNRMG formulas of the correlated MIMO channel in the high SNRs are the same as those of the uncorrelated MIMO channel in the high SNRs, which means that the F-SNRMG

formulas of the MIMO channel for the CSIR and the CSIT cases in the multi-carrier systems owning a physical transmitter are not dependent on the correlation between the channel elements in the high SNRs.

Finally, all equations of the correlated MIMO channel and uncorrelated MIMO channel mentioned in the first algorithm can be allocated to the traditional MIMO system by putting the value of κ_t equal to zero.

3.2.3 Implementing of First Algorithm in MATLAB Program

This subsection presents the steps of implementing the first algorithm in the MATLAB program. These steps provide all the necessary needs to calculate the random MIMO channel capacity in any case of t3he cases that the first algorithm covers. Before presenting these steps, there are some considerations must be taken into account:

1. The number of transmitting antennas in the system must be larger or equivalent to amount of receipt antennas.
2. The correlation coefficients must be greater or equal to zero and smaller than one (i.e. $0 \leq \alpha_t < 1$ and $0 \leq \alpha_r < 1$). Also, if the α_t is equal to α_r, the correlation coefficients are represented by the parameter α (i.e. $\alpha_t = \alpha_r = \alpha$).
3. The required cases must be selected in which the channel capacity & F-SNRMG are calculated under the transmitter distortion effect. All cases ready for selection are shown in Fig. (3.1).

After taking into account the matters mentioned above, the algorithm is implemented by the MATLAB program, and the implementation steps are as follows:

Step 1: Entering all required inputs (number of transmitting antennas (N), number of receiving antennas (M), the correlation coefficient of the antennas on the transmitting side (α_t), the correlation coefficient of the antennas on the receiving side (α_r), number of realizations of the channel (**L**), transmitter impairments level (κ_t), and a range of SNR values in decibel).

Step 2: Converting the range of SNR from decibel to linear scale by using the following equation:

$$\text{SNR} = 10.^{\frac{\text{SNRdB}}{10}} \tag{3.48}$$

Step 3: This step includes the following points:

- Generating the MIMO channel matrix (H), whose components are complex random variables subject to the Rayleigh distribution and are independent of each other. The generating of the H matrix is done by using equation (2.37).

- Generating the SISO channel by using the equation (2.45).

Step 4: Creating zero matrices for each selected case from Fig. (3.1). The size of each one of these matrices is (length (SNR) * L). Also, the number of these zero matrices in each selected case is equal to the length of the impairment level vector (e.g., if the impairments level entering consists of two values, the number of zero matrices generated in each selected case will be two matrices). Each matrix of these zero matrices in each selected case is devoted to saving the value of the EC of the MIMO channel at first algorithm for each value of SNR values at each realization of the channel.

For example, suppose the ergodic capacity of the uncorrelated MIMO channel in the multi-carrier system having a physical transmitter is required in two cases, CSIR and CSIT, and with two values of the transmitter impairment level (κ_t). In this case, the total number of zero matrices generated is four matrices. Each two of these matrices are devoted to one case.

Step 5: Finding the D_t and D_r matrices by using equation (2.39).

Step 6: Creating the first loop to encompass all MIMO channel matrix realizations. This loop determines the matrix $\mathbf{H_k}$ at each channel realization. The equation (2.38) is used to determine the $\mathbf{H_k}$ matrix at each realization of the MIMO channel (**H**). Additionally, this loop does an SVD analysis on each of the $\mathbf{H_k}$ and **H** matrices at each realization of the MIMO channel. Thus, at each realization of the channel, the channel gain of each effective channel in the UMIMOC and the channel gain of each effective channel in the CMIMOC can be determined.

Step 7: Creating the second loop inside the first loop to cover all the values of the SNR at each realization of the channel. This loop includes applying the WATER-FILLING mechanism on each MIMO channel (the correlated and uncorrelated MIMO channels). In other words, the power assigned to each effective channel in each of the correlated and uncorrelated MIMO channels will be computed for each value of SNR at each realization of the channel, assuming the channel state information is available at the transmitter (i.e., the D and D_k matrixes will be computed for each value of SNR at each realization of the channel, both matrices D and D_k resulting from the WATER-FILLING mechanism in the MATLAB program will be with the size M * 1).

Step 8: Creating the third loop inside the second loop to cover all values of the impairment level when the impairment level is entered with more than one value. This loop includes the following points:

- Finding the covariance matrix of the transmitted signal (R_{xx}) in the uncorrelated MIMO channel, which is equal $\mathbf{V_{N*M}} * \mathbf{D_{M*M}} * \mathbf{V_{N*M}}^{\mathbf{H}}$ in the case of CSIT
- Finding the covariance matrix of the transmitted signal (R_{xx}) in the correlated MIMO channel, which is equal $\mathbf{V_{k\ N*M}} * \mathbf{D_{k\ M*M}} * \mathbf{V_{k\ N*M}}^{\mathbf{H}}$ in the case of CSIT
- Apply the ergodic capacity equation of each selected case to compute the random MIMO channel capacity in the first algorithm. Then, saving the calculated value of the ergodic capacity of each selected case in the matrix defined for it in the fourth step with location (b, a, c), where a is the counter of the first loop, b is the counter of the second loop, and c is the counter of the third loop.

Step 9: Finding the SISO channel capacity at each value of impairment level (κ_t). The SISO channel capacity in the first algorithm is shown in equation (3.30). The result from applying this equation at each time is a matrix with size (length (SNR) * L). Also, the mean is taken for the result matrix to produce a matrix with size (length (SNR) * 1). The final matrix holds the SISO channel capacity value (random capacity) in the first algorithm for each SNR value.

Step 10: Taking the mean for each matrix which was filled in step 8. The result from taking the mean for one matrix of these matrices is a matrix with the size (length (SNR) * 1). The resulting matrix has the ergodic capacity value of the MIMO channel at each SNR value for one case of the selected cases in the first

algorithm. Also, the values in the resulting matrix were computed at one value of impairment level (κ_t).

Step 11: Computing the finite-SNR multiplexing gain for each value of impairment level (κ_t) at each selected case. This is done by dividing the matrix containing the ergodic capacity values of the MIMO channel by the matrix containing the values of the SISO channel capacity. The matrix containing the ergodic capacity values of the MIMO channel is the matrix resulting from step 10. Also, the matrix containing the capacity values of the SISO channel is the matrix resulting from step 9.

Step 12: Drawing the values of the random MIMO channel capacity calculated in each selected case as a function of SNR and showing the result as a curve.

Step 13: Drawing the values of finite-SNR multiplexing gain calculated in each selected case as a function of SNR and showing the result in a new curve.

In addition, the above steps can be simplified by a flowchart. Therefore, Fig.(3.5) shows the flowchart of implementing the first algorithm in the MATLAB software with two values of the impairment level. This flowchart is devoted to showing the ergodic capacity and F-SNRMG in two cases selected from Fig. (3.1):

- Uncorrelated MIMO channel, Multi-carrier, CSIT.
- Correlated MIMO channel, Multi-carrier, CSIT.

Furthermore, this flowchart is designed to provide all the required needs to calculate the random MIMO channel capacity in the first algorithm for any case of the cases shown in Fig. (3.1).

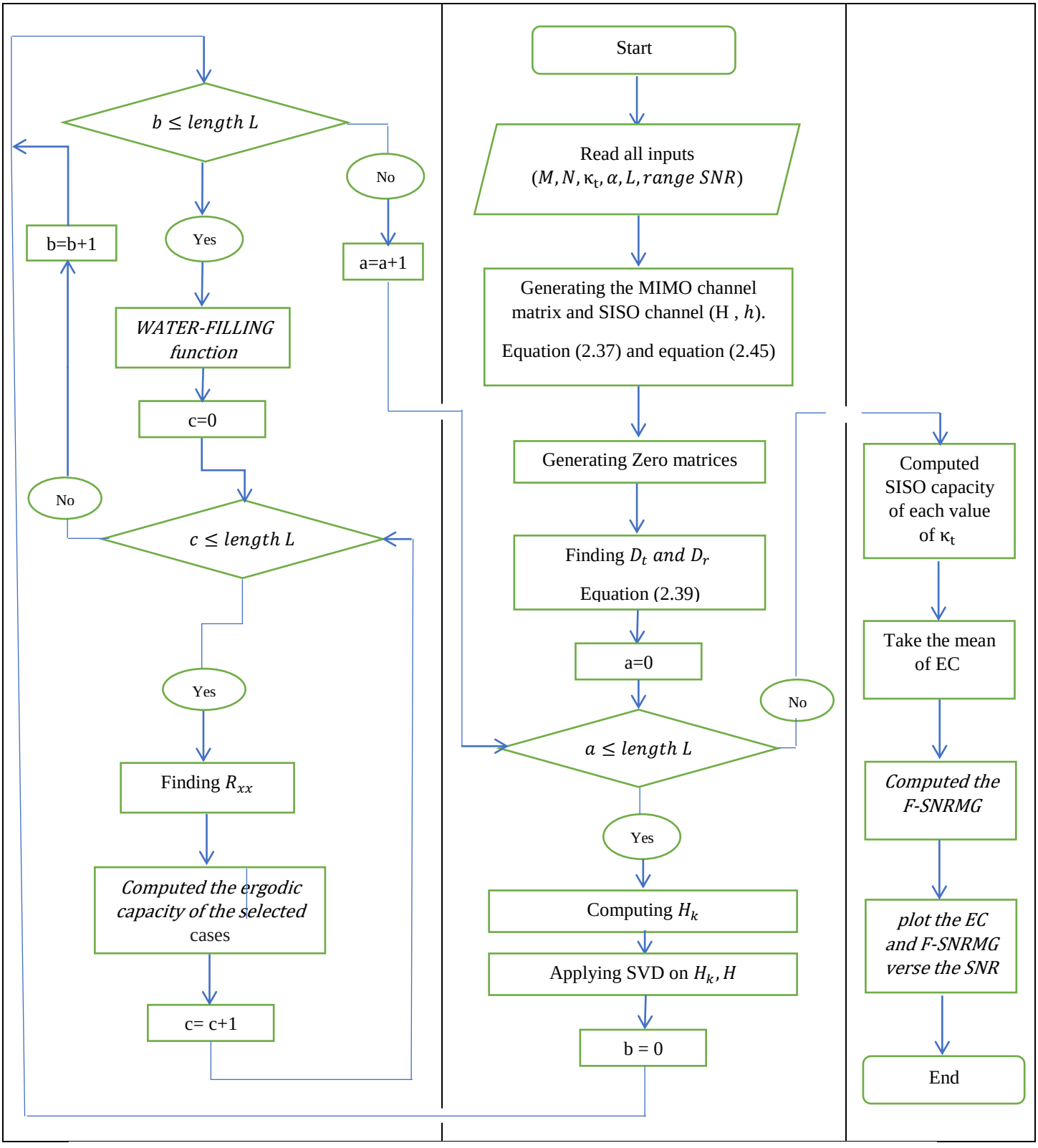

Fig 3.5: The flowchart for implementing the first algorithm in the MATLAB software, (Selected cases: the uncorrelated MIMO channel, and correlated channel, both for the case of CSIT in the MC system).

Moreover, the same steps shown in the above flowchart can be applied to show the ergodic capacity and F-SNRMG for any case shown in Fig. (3.1). Also, the WATER-FILLING function MATLAB code can be watched in the appendix.

3.3 The Second Algorithm

This algorithm evaluates the effects of the physical transmitter and physical receiver on both the MIMO c

hannel capacity (EC) and the finite-SNR multiplexing gain, in which this algorithm considers the effect of the physical transmitter as the same method followed in the first algorithm. Also, it considers the effect of the physical receiver as additive uncorrelated Gaussian distortion noise ($\boldsymbol{\sigma_r}$) with zero mean and variance indicated by the symbol $\boldsymbol{\Upsilon_r}$. Additionally, the second algorithm's topics are shown in Fig. (3.6).

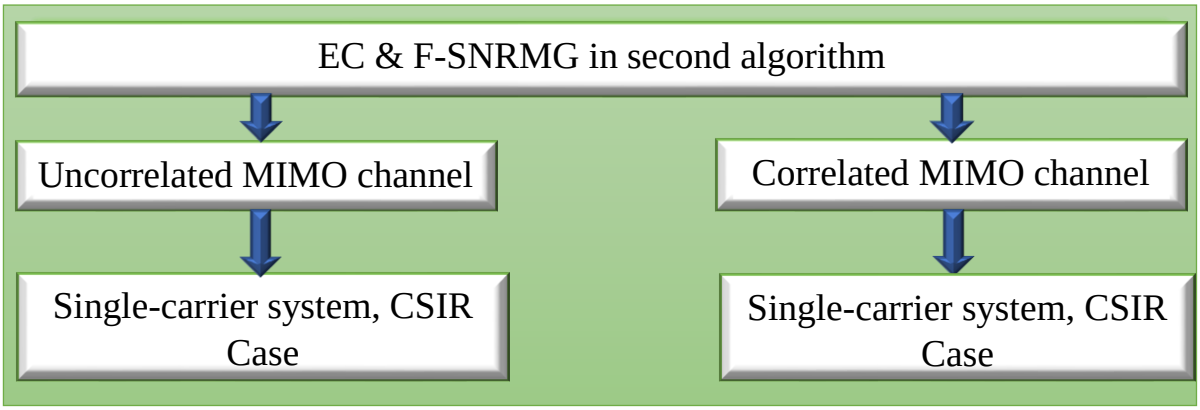

Fig. 3.6: Cases Covered By the Second Algorithm.

Before implementing this algorithm in the MATLAB program, the correlated MIMO channel model and the uncorrelated MIMO channel model will be presented under the second algorithm. Then, the ergodic capacity equation and finite-SNR multiplexing gain equation will be presented in both these models, assuming the system used is a single-carrier system containing a

physical receiver knowing the channel information and a physical transmitter not knowing the channel information.

3.3.1 The Affine Model for MIMO Channels in Second Algorithm

In this subsection, the affine models for the correlated MIMO channel and uncorrelated MIMO channel will be presented with the presence of the physical transmitter and physical receiver. The block diagrams of the affine models for the CMIMOC and the UMIMOC in the second algorithm are not different from those in the first algorithm, but in the second algorithm, both the receiver distortion and transmitter distortion will be taken into account. Thus, the block diagrams of the affine models for the correlated MIMO channel and uncorrelated MIMO channel under the second algorithm can be given in Fig. (3.7).

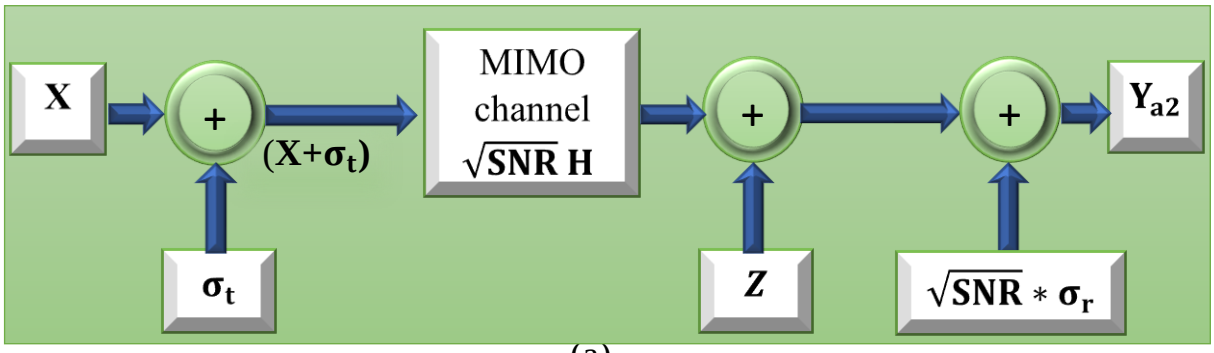

(a)

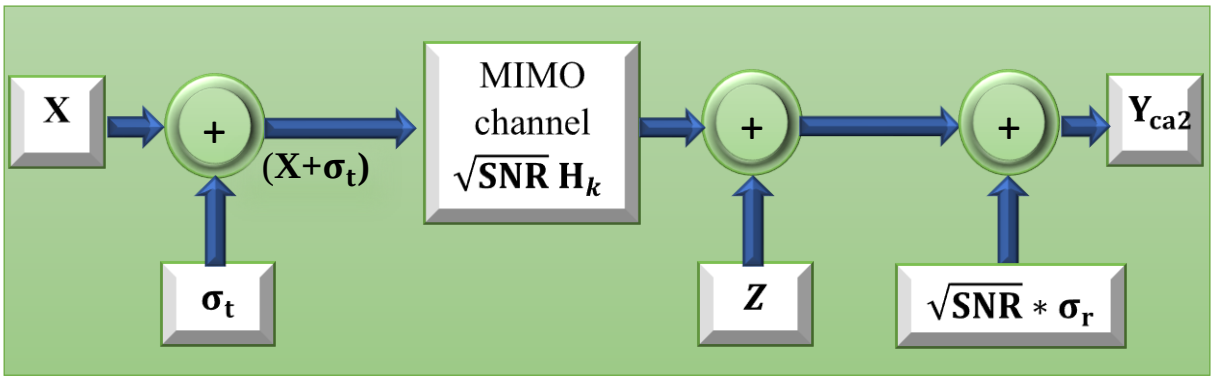

(b)

Fig. 3.7: Block Diagrams of the Affine Models in the second algorithm: a) Uncorrelated MIMO Channel, b) Correlated MIMO Channel

The above models consist of N antennas to send the signals and M antennas to receive them. Also, the received signals for the uncorrelated and correlated models can be represented in equations (3.49) and (3.50), respectively.

$$\mathbf{Y_{a2}} = \sqrt{\mathbf{SNR}}\,\mathbf{H} * (\mathbf{X} + \boldsymbol{\sigma_t}) + \sqrt{\mathbf{SNR}} * \boldsymbol{\sigma_r} + \mathbf{Z} \qquad (3.49)$$

$$\mathbf{Y_{ca2}} = \sqrt{\mathbf{SNR}}\,\mathbf{H_k} * (\mathbf{X} + \boldsymbol{\sigma_t}) + \sqrt{\mathbf{SNR}} * \boldsymbol{\sigma_r} + \mathbf{Z} \qquad (3.50)$$

where, Y_{a2} and Y_{ca2} represent the received signals of the UMIMOC and the CMIMOC in the second algorithm, respectively.

Moreover, the variance of the receiver distortion ($\boldsymbol{\Upsilon_r}$) in the MIMO system will be computed as the same method shown in section (2.9). Thus, the receiver distortion variance in the MIMO system can be given as equation (3.51).

$$\boldsymbol{\Upsilon_r} = \boldsymbol{\kappa_r}^2 * \mathbf{tr}(\mathbf{R_{xx}}) * \mathbf{I} \qquad (3.51)$$

where $\boldsymbol{\kappa_r}$ is the receiver impairment level**.**

Furthermore, in the second algorithm, the MIMO system's power constraint will be considered equal to one (i.e. $\mathbf{tr}(\mathbf{R_{xx}}) = 1$). Thus, equation (3.52) can be rewritten as follows:

$$\boldsymbol{\Upsilon_r} = \boldsymbol{\kappa_r}^2 * \mathbf{I} \qquad \mathbf{(3.52)}$$

In addition, the variance of the transmitter distortion ($\boldsymbol{\Upsilon_t}$) in the second algorithm will be computed from equation (3.4) by putting $\boldsymbol{\beta} = \mathbf{1}$ because the system-dependent here is the single-carrier system. Also, the term $\mathbf{diag}(\mathbf{q_1}, \dots\dots\dots, \mathbf{q_N})$ that appears in the equation (3.4) after putting $\boldsymbol{\beta} = \mathbf{1}$ is equal to $\frac{\mathbf{I_N}}{\mathbf{N}}$ because the case depended here is the CSIR case, which means that the covariance matrices of the transmitted signals in the MIMO channels

(correlated MIMO channel and uncorrelated MIMO channel) are equal to $\frac{\mathbf{I_N}}{\mathbf{N}}$ as mentioned earlier. Thus, the variance of the transmitter distortion in the second algorithm is given as the following equation:

$$\boldsymbol{\Upsilon_t = \kappa_t^2 * \frac{I_N}{N}} \quad \textbf{(3.53)}$$

Finally, in the second algorithm, the impairment level of the transmitter distortion will be considered equal to the impairment level of the receiver distortion (i.e. $\boldsymbol{\kappa_r = \kappa_t = \kappa}$).

3.3.2 EC and F-SNRMG of MIMO channels in Second Algorithm

In this subsection, the EC equations and F-SNRMG equations of the UMIMOC and CMIMOC will be presented with the presence of the physical transmitter and physical receiver. The steps for finding the EC equations and F-SNRMG equations of the uncorrelated MIMO channel and correlated MIMO channel for the CSIR case in the second algorithm are the same as those mentioned in the first algorithm. Therefore, Table (3.6) is developed to clarify the EC equations and F-SNRMG equations for the UMIMOC and CMIMOC in the second algorithm.

Table (3.6): The Ergodic capacity equations and F-SNRMG equations for the UMIMOC and CMIMOC in the second algorithm

Name	Channel type	Equation
Ergodic capacity	Uncorrelated MIMO channel	$C_{ea2} = \mathbb{E}\left\{\sum_{i=1}^{M} \log_2\left(1 + \frac{\frac{SNR}{N} * \lambda_i}{(SNR*\kappa^2/N) * \lambda_i + SNR*\kappa^2+1}\right)\right\}$, bit/second/hertz (3.54) where C_{ea2} is the EC of the uncorrelated MIMO channel in the second algorithm.

Ergodic capacity	Correlated MIMO channel	$C_{ca2} = \mathbb{E}\left\{\sum_{i=1}^{M} \log_2\left(1 + \frac{\frac{SNR}{N} * \lambda_{k\,i}}{(SNR*\kappa^2/N) * \lambda_{k\,i} + SNR*\kappa^2*1}\right)\right\}$ bit/second/hertz (3.55) where C_{ca2} is the EC of the uncorrelated MIMO channel in the second algorithm.
F-SNRMG	Uncorrelated MIMO channel	$\mu_{a2} = \frac{C_{ea2}}{C_{Sea2}} = \frac{\mathbb{E}\left\{\sum_{i=1}^{M} \log_2\left(1+\frac{\frac{SNR}{N}*\lambda_i}{(SNR*\kappa^2/N)*\lambda_i + SNR*\kappa^2*1}\right)\right\}}{\mathbb{E}\left\{\log_2\left(1+\frac{SNR*\lvert h\rvert^2}{(SNR*\kappa^2)*\lvert h\rvert^2 + SNR*\kappa^2+1}\right)\right\}}$ (3.56) where μ_{a2} is the F-SNRMG of the uncorrelated MIMO channel in the second algorithm, and C_{Sea2} is the capacity of the SISO channel in the second algorithm. The capacity equation of the SISO channel is derived from Eq.(3.54).
F-SNRMG	Correlated MIMO channel	$\mu_{ca2} = \frac{C_{ca2}}{C_{Sea2}} = \frac{\mathbb{E}\left\{\sum_{i=1}^{M} \log_2\left(1+\frac{\frac{SNR}{N}*\lambda_{k\,i}}{(SNR*\kappa^2/N)*\lambda_{k\,i} + SNR*\kappa^2*1}\right)\right\}}{\mathbb{E}\left\{\log_2\left(1+\frac{SNR*\lvert h\rvert^2}{(SNR*\kappa^2)*\lvert h\rvert^2 + SNR*\kappa^2+1}\right)\right\}}$ (3.57) where μ_{ca2} is the F-SNRMG of the correlated MIMO channel in the second algorithm.

3.3.3 Implementing of Second Algorithm in MATLAB program

This subsection presents the steps of implementing the second algorithm in the MATLAB program. These steps allow computing the ergodic capacity and F-SNRMG of the uncorrelated MIMO channel under the influences of the physical transmitter and physical receiver. Also, these steps allow computing the ergodic capacity and F-SNRMG of the correlated MIMO channel under the impact of the physical transmitter and the impact of the physical receiver. However, there are some considerations that must be taken into account before applying these steps:

1. The number of transmitting antennas in the system must be bigger or equivalent for amount of acceptance antennas.
2. The correlation coefficients must be greater or equal to zero and smaller than one (i.e. $0 \leq \alpha_t < 1$ and $0 \leq \alpha_r < 1$). Also, if the α_t is equal to α_r, the correlation coefficients are represented by the parameter α (i.e. $\alpha_t = \alpha_r = \alpha$).
3. The required cases must be selected in which the channel capacity & the F-SNRMG are calculated under transmitter distortion & receiver distortion effects. All cases ready for selection are shown in Fig. (3.6).

After taking into account the points described previously, the algorithm is implemented using the MATLAB software in the following manner:

Step 1: Entering all required inputs (number of transmitting antennas (N), number of receiving antennas (M), the correlation coefficient of the antennas on the transmitting side (α_t), the correlation coefficient of the antennas on the receiving side (α_r), number of realizations of the channel (**L**), impairments level (κ), and a range of SNR values in decibel).

Step 2: Converting the range of SNR from decibel to linear scale by using the equation (3.48).

Step 3: This step includes the following points:

- Generating the MIMO channel matrix H, whose components are complex random variables subject to a Rayleigh distribution and are independent of each other. The generating of the H matrix is done by using equation (2.37).
- Generating the SISO channel by using equation (2.45):

Step 4: Creating zero matrices for each selected case from Fig. (3.6). The detail about this step was explained in step four in the implementation steps of the first algorithm, which was displayed in subsection 3.2.3.

Step 5: Finding the D_t and D_r matrices by using equation (2.39).

Step 6: Creating the first loop to cover all the realizations of the MIMO channel matrix (**H**). This loop includes finding the matrix $\mathbf{H_k}$ at each realization of the channel. The finding of the $\mathbf{H_k}$ matrix is done by applying the equation (2.38) at each realization of the MIMO channel (**H**). Also, this loop includes applying the SVD analysis to each of the $\mathbf{H_k}$ and **H** matrices at each realization of the MIMO channel. Thus, the channel gain of each effective channel in the UMIMOC and the channel gain of each effective channel in the CMIMOC can be found in each realization of the channel.

Step 7: Creating the second loop inside the first loop to cover all the values of the SNR at each realization of the channel.

Step 8: Creating the third loop inside the second loop to cover all values of the impairment level when the impairment level is entered with more than one value. This loop includes applying the ergodic capacity equation of each selected case to compute the random MIMO channel capacity in the second algorithm. Then, saving the calculated value of the ergodic capacity of each selected case in the matrix defined for it in the fourth step with location (e, d, f), where d is the counter of the first loop, e is the counter of the second loop, and f is the counter of the third loop.

Step 9: Finding the SISO channel capacity under the second algorithm at each value of impairment level (κ). The SISO channel capacity equation in the second algorithm was shown in the denominator of equation (3.56). The result

from applying this equation at each time is a matrix with size (length (SNR) * L). Then, the mean is taken for the result matrix to produce a matrix with size (length (SNR) * 1). The final matrix contains the value of the SISO channel capacity (random capacity) under the second algorithm at each SNR value for one value of impairment level (κ).

Step 10: Taking the mean for each matrix that was filled in step 8. The result from taking the mean for one matrix of these matrices is a matrix with the size (length (SNR) * 1). The resulting matrix has the EC value of the MIMO network in the second algorithm at each SNR value for one case of the selected cases. Also, the values in the resulting matrix were computed at one value of impairment level (κ_t).

Step 11: Computing the F-SNRMG of the MIMO network for each value of (κ) in each selected case. This is done by dividing the matrix containing the ergodic capacity values of the MIMO channel by the matrix containing the values of the SISO channel capacity. The matrix containing the ergodic capacity values of the MIMO channel is the matrix resulting from step 10. Also, the matrix containing the capacity values of the SISO channel is the matrix resulting from step 9.

Step 12: Drawing the values of the random MIMO channel capacity calculated in each selected case as a function of SNR and showing the result as a curve.

Step 13: Drawing the values of finite-SNR multiplexing gain calculated in each selected case as a function of SNR and showing the result in a new curve.

Additionally, the flowchart can be used to simplify the above processes. As a result, Fig. (3.8) depicts the flowchart for implementing the second algorithm in the MATLAB program with two values of impairment level (κ).

This flowchart illustrates the ergodic capacity and F-SNRMG in each instance presented in Fig. (3.6).

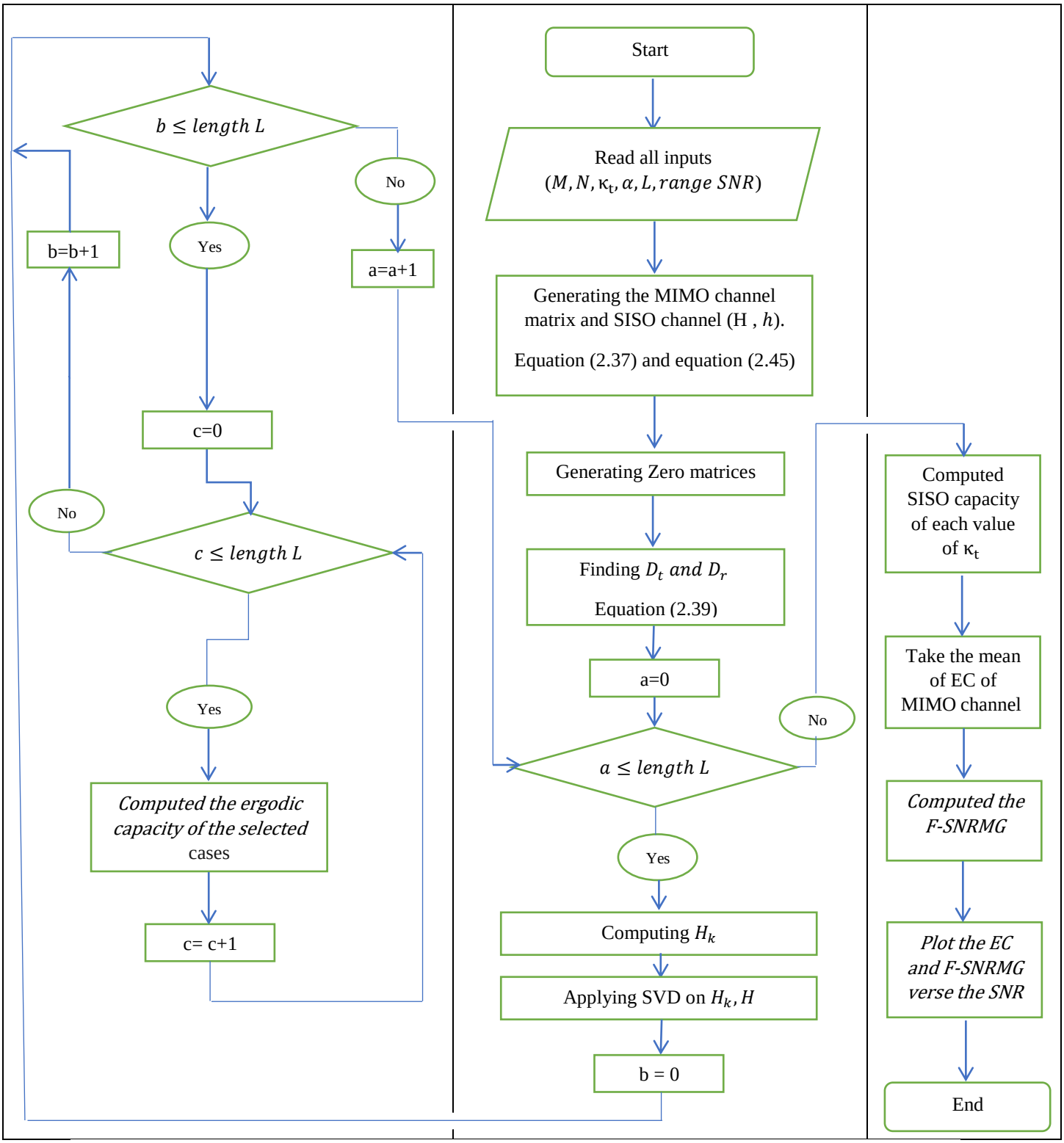

Fig 3.8: The flowchart for implementing the second algorithm in the MATLAB software.

Chapter Four

Result and Discussion

CHAPTER FOUR

RESULTS AND DISCUSSION

4.1 Introduction

The previous chapter displays two algorithms to analyze the performance of the MIMO channels in the presence of the physical transceiver. The previous chapter mentioned that the first algorithm analyzes the performance of the MIMO channels in the presence of the physical transmitter, while the second algorithm analyzes the performance of the MIMO channels in the presence of the physical transmitter and physical receiver. Also, it indicates that those algorithms analyze the performance of the MIMO channels in terms of the ergodic capacity and the finite-SNR multiplexing gain. Furthermore, it shows that the first algorithm can be applied to the uncorrelated MIMO channel and the correlated MIMO channel in many scenarios shown in Fig. (3.1), and the second algorithm can be applied to the uncorrelated MIMO channel and the correlated MIMO channel in one scenario shown in figure (3.1). This chapter presents the simulation results of those algorithms and discusses these results. All simulation processes are run in MATLAB 2018. The number of channel realizations used in each simulation is 10000. Also, the impairment level for the physical transceiver used in each simulation is 0.08, 0.175, or both.

This chapter consists of four main sections. The first section is presented under the name Introduction, which contains a summary of the algorithms proposed in the third chapter, what will present in this chapter, and the value of some main criteria used in each simulation process. The second part presents the simulation results of the first algorithm, while the third section presents the simulation results of the second algorithm. Finally, the last section compares the results of this work with some related work that is very near to the work presented in this letter.

4.2 Results of First Algorithm

The third chapter mentioned that the first algorithm analyzes the performance of the UMIMOC and the performance of the CMIMOC under the influence of the physical transmitter in many scenarios. Thus, the uncorrelated MIMO channel analysis results under the first algorithm will be presented in the following subsection. Then the correlated MIMO channel analysis results according to the same algorithm will be given in another subsection.

4.2.1 Uncorrelated MIMO Channel Analysis Results in the First Algorithm

As mentioned in the previous chapter, the first algorithm analyzes the performance of the MIMO channel under the influence of the physical transmitter in terms of the ergodic capacity and finite-SNR multiplexing gain. Therefore, the uncorrelated MIMO channel analysis results in the first algorithm include two main parts: I. EC Results of the Uncorrelated MIMO Channel in the First Algorithm, II. F-SNRMG Results of the uncorrelated MIMO Channel in the First Algorithm.

I. EC Results of the Uncorrelated MIMO Channel in the First Algorithm

In the previous chapter, the EC (Average capacity) of the UMIMOC in first algorithm is clarified in many scenarios: **Multi-carrier MIMO system with CSIT case**, **Multi-carrier MIMO system with CSIR case** (which is the same as the SC- MIMO system with CSIR case), **and Single-carrier MIMO system with CSIT case**. Here, the ergodic capacity simulation results of the uncorrelated MIMO channel for these scenarios under the influence of the physical transmitter will be presented. Also, the discussion of these results and the comparison between them will be given.

A. Multi-carrier MIMO system with CSIT case

In this scenario, the EC behavior of the UMIMOC with the ideal transmitter will be compared with the EC behavior of the UMIMOC with the physical transmitter, assuming that the information of the channel is obtainable at the receiver and the transmitter. Then, effect of increase in the number of transmitting antennas on the EC of the UMIMOC in MC system with the physical transmitter will be clarified.

Initially, it can be considered the existence of an uncorrelated MIMO channel with $M = 4$, $N = 4$, $\beta = 1$, and varying SNR values. Figure (4.1) shows the ergodic capacity of this model over different impairment levels $\kappa_t \in \{0, 0.08, 0.175\}$, assuming that the information of the channel is obtainable at the receiver and transmitter.

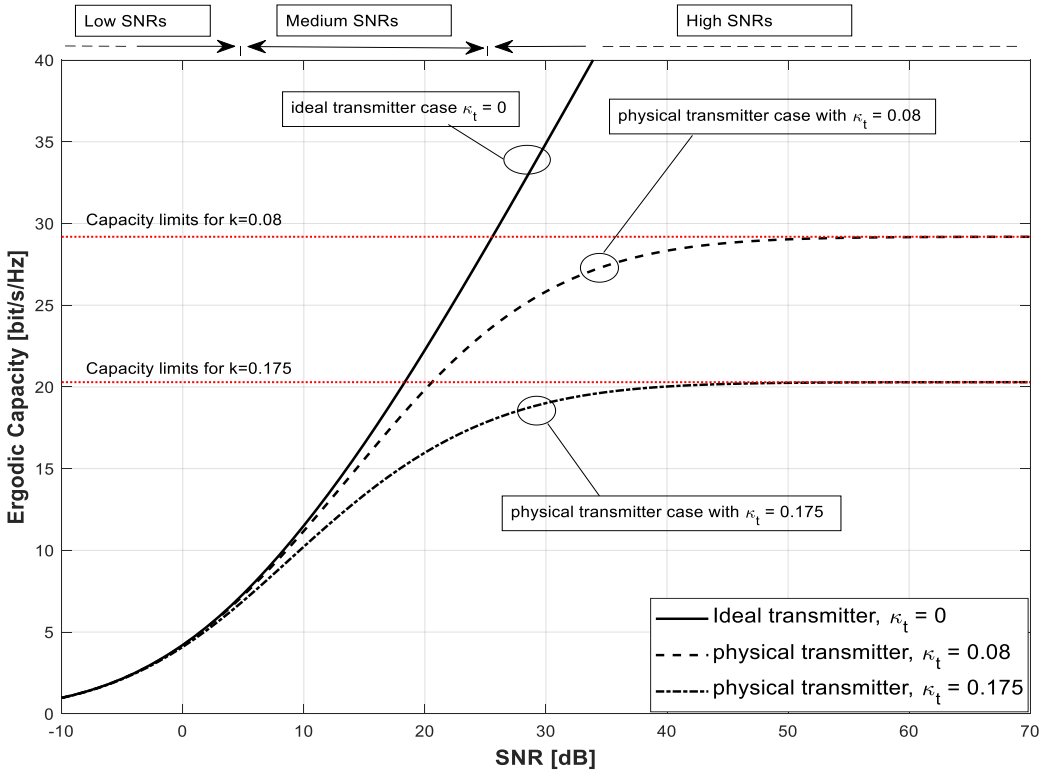

Fig. 4.1: EC of the 4*4 UMIMOC for the CSIT case in the MC system with different impairment levels $\kappa_t \in \{0, 0.08, 0.175\}$.

The above figure illustrates that in low and medium SNRs, the ergodic capacity behavior with the ideal transmitter ($\kappa_t = 0$) is the same as the ergodic capacity behavior with the physical transmitter for any level of impairment ($\kappa_t \in \{0.08, 0.175\}$). While in the high SNRs, the above figure shows that the ergodic capacity behavior with the ideal transmitter is fundamentally different from the ergodic capacity behavior with the physical transmitter for any level of impairment. In other words, figure (4.1) shows that the ergodic capacity with the ideal transmitter grows unboundedly in the high SNRs, while the ergodic capacity with the physical transmitter for any level of impairment ($\kappa_t \in \{0.08, 0.175\}$) approaches the capacity limit $C_{ea1}(\text{SNR}\sim\infty) = 4 * \log_2\left(1 + \frac{1}{4*(\kappa_t{}^2/4)}\right)$ in the high SNRs. Also, figure (4.1) presents that the value of the capacity limit is inversely proportional to the impairment level for the transmitter, which means that the capacity limit's value decreases as the impairment level for the transmitter increases. Table (4.1) shows the capacity limit value of the 4*4 uncorrelated MIMO channel for the CSIT case in the MC system with $\kappa_t \in \{0, 0.08, 0.175\}$.

Table 4.1: The capacity limit value of 4*4 uncorrelated MIMO channel for the CSIT case in the MC system with different impairment levels $\kappa_t \in \{0, 0.08, 0.175\}$

Value of κ_t	Capacity limit value
0	**Unboundedly**
0.08	**29.19 bit/second/hertz**
0.175	**20.29 bit/second/hertz**

In addition, the above figure shows that both values of the SNR at which the effect of the physical transmitter on the ergodic capacity starts to appear and at which the channel capacity arrives at its limit decrease as the impairment level of the transmitter increases.

Next, the effect of increment the amount of transferring antennas on the EC of the UMIMOC for the CSIT case in the MC system with the physical transmitter will be clarified. Figure (4.2) presents the EC of the UMIMOC for the CSIT case in the MC system with $M = 2$, different N, varying SNR values, and different impairment levels for the transmitter $\kappa_t \in \{0.08, 0.175\}$.

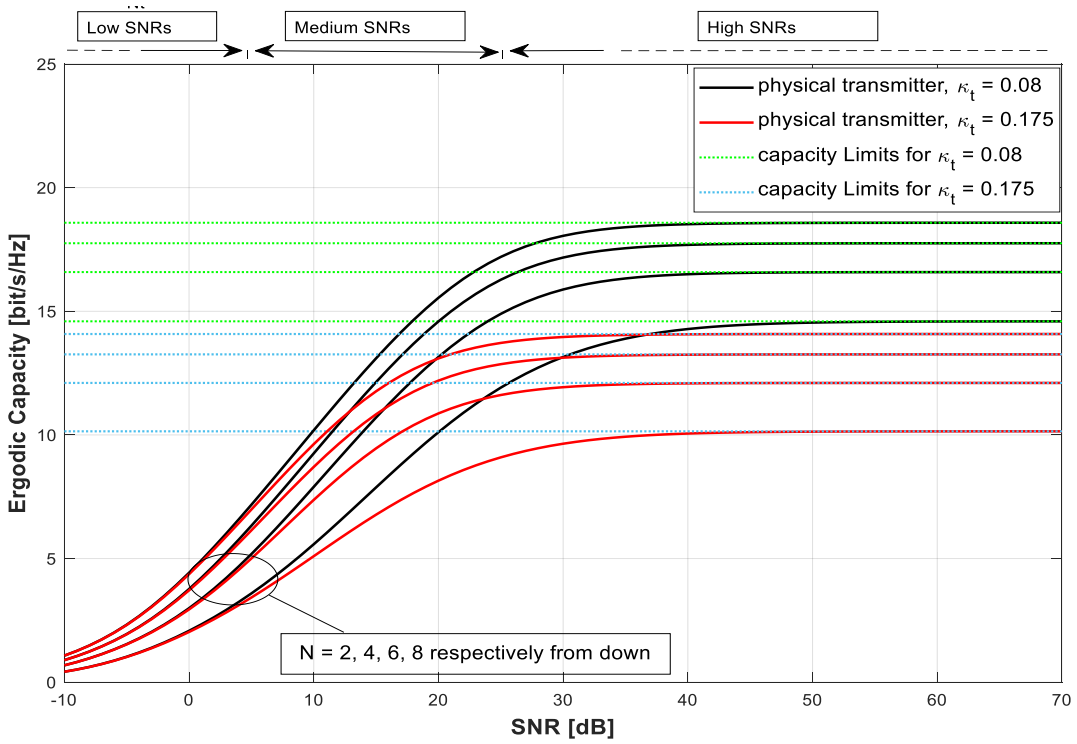

Fig. 4.2: EC of the UMIMOC for the CSIT case in the MC system with $M = 2$, $N \in \{2, 4, 6, 8\}$, and different impairment levels $\kappa_t \in \{0.08, 0.175\}$.

The above figure illustrates that the capacity limit of the uncorrelated MIMO channel for the CSIT case in the MC system for any impairment level ($\kappa_t \in \{0.08, 0.175\}$) increases as the number of the transmitting antennas increases. Also, it shows that the EC of UMIMOC for the CSIT case in the MC system for any impairment level ($\kappa_t \in \{0.08, 0.175\}$) at any SNR value also increases as the number of transmitting antennas increases. However, figure (4.2) shows that the amounts of increase in the ergodic capacity and capacity

limit, which happen due to adding several antennas to the transmitting antennas, reduce when the same number of the antennas is added to the transmitting antennas again. Thus, it can be concluded that the incensement in amount of transferring antennas to a large quantity without increasing the number of receiving antennas may not give many benefits.

Moreover, Table (4.2) offers the capacity limit value of the uncorrelated MIMO channel for the CSIT case in the MC system with $M = 2$, $N \in \{2, 4, 6, 8\}$, and different impairment levels $\kappa_t \in \{ 0.08, 0.175\}$.

Table 4.2: The capacity limit value of the uncorrelated MIMO channel for the CSIT case in the MC system with $M = 2$, different N, and different impairment levels $\kappa_t \in \{ 0.08, 0.175\}$.

Value of κ_t	Number of transmitting antennas (N)	Capacity limit value in bit/second/hertz
0.08	**2**	**14.59**
	4	**16.58**
	6	**17.75**
	8	**18.58**
0.175	**2**	**10.15**
	4	**12.1**
	6	**13.26**
	8	**14.08**

After that, it can be seen that the value of the capacity limit with $M = 2$, $N = 4$, and $\kappa_t = 0.08$ is equal to 16.58 bit/second/hertz, as shown in Table (4.2), while the capacity limit value with the same criteria, but $M = 4$, is equal to 29.19 bit/second/hertz, as illustrated in Table (4.1). Therefore, it can be concluded that the ergodic capacity and the capacity limit of the uncorrelated MIMO channel for the CSIT case in the MC system with the physical transmitter are directly proportional to the number of receiving antennas.

B. Multi-carrier MIMO system with CSIR case

Here, the EC of the UMIMOC for the CSIR case in the MC system with the actual transmitter (physical transmitter) will be presented. Also, it will be compared with the EC of the UMIMOC for the CSIT case in the MC system with the actual transmitter. Therefore, it can be assumed the existence of an uncorrelated MIMO channel with M = 4, different N, $\beta = 1$, and varying SNR values. Figure (4.3) shows the ergodic capacity of this model over different impairment levels $\kappa_t \in \{0.08, 0.175\}$ in two different cases, CSIR and CSIT.

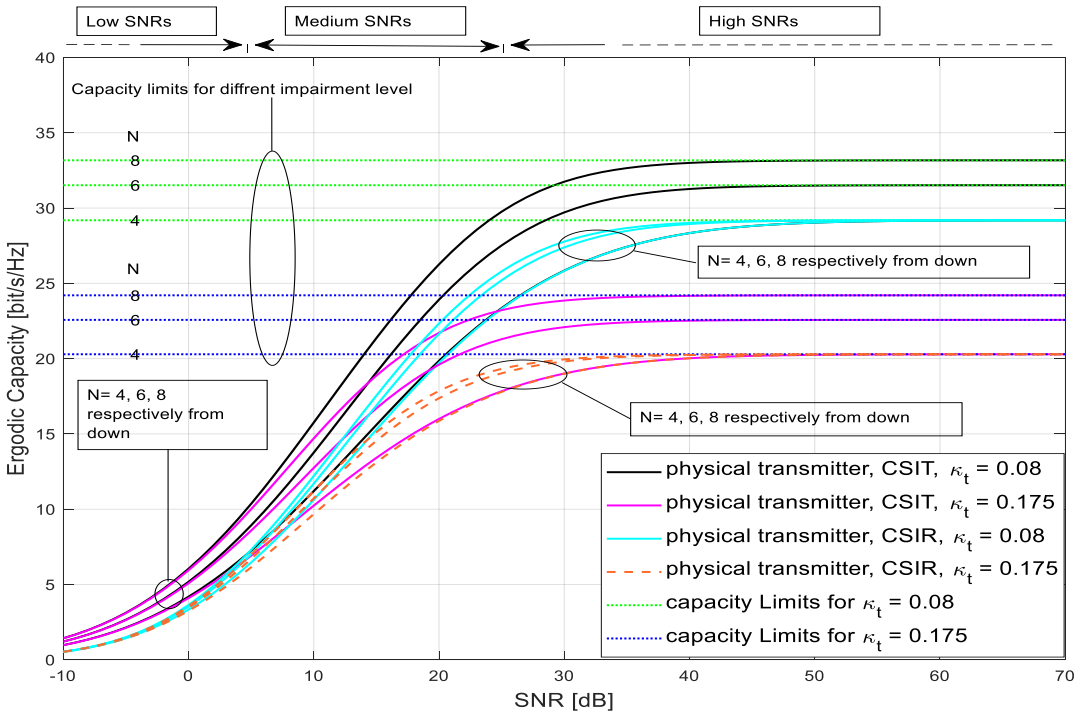

Fig. 4.3: Ergodic capacities of the uncorrelated MIMO channel for the CSIT and CSIR cases in the MC system with $M = 4$, $N \in \{4, 6, 8\}$, and different impairment levels $\kappa_t \in \{0.08, 0.175\}$.

The above figure shows that the ergodic capacities of the uncorrelated MIMO channel for the CSIR and CSIT cases in the MC system for any impairment level ($\kappa_t \in \{0.08, 0.175\}$) and any number of the transmitting antennas ($N \in \{4, 6, 8\}$) have the same behavior in the low, medium, and high

SNRs. Also, it shows that at any value of the SNR (from the beginning of the SNR range to the value at which the capacity limit begins), the EC of the UMIMOC for the CSIR case in the MC system for any impairment level ($\kappa_t \in \{0.08, 0.175\}$) increases as the number of transmitting antennas increases. However, figure (4.3) indicates that in the CSIR case, for any impairment level ($\kappa_t \in \{0.08, 0.175\}$), the improvement in channel capacity that results from adding several antennas to the transmitting antennas reduces when the same number of antennas is added to the transmitting antennas again.

Furthermore, the above figure illustrates that the incensement in amount of transferring antennas does not affect capacity limit for the UMIMOC for the CSIR case in the MC system with the actual transmitter, which is in contrast to the CSIT case. Therefore, it can be said that the capacity limit of the uncorrelated MIMO channel for the CSIR case in the MC system with the physical transmitter does not depend on the number of transmitting antennas. Table (4.3) displays the capacity limit values of the uncorrelated MIMO channel for the CSIR and CSIT cases in the MC system with $M = 4$, $N \in \{4, 6, 8\}$, and different impairment levels ($\kappa_t \in \{ 0.08, 0.175\}$).

Moreover, figure (4.3) shows that when the number of transmitting antennas is equal to the number of receiving antennas, the ergodic capacities of the uncorrelated MIMO channel for the CSIR and CSIT cases in the MC system for any impairment level get closer to congruence as the SNR value increases.

In addition, it can be seen from Fig. (4.3) that in the MC system with any impairment level, when $N > M$, the EC of the UMIMOC for the CSIT case at any value of the SNR is greater than the EC of the UMIMOC for the CSIR case.

Table 4.3: The capacity limit values of the uncorrelated MIMO channel for the CSIT and CSIR cases in the MC system with $M = 4$, $N \in \{4, 6, 8\}$, and different impairment levels $\kappa_t \in \{0.08, 0.175\}$.

Value of κ_t	Number of transmitting antennas (N)	Capacity limit value in bit/second/hertz CSIT	Capacity limit value in bit/second/hertz CSIR
0.08	4	29.19	29.19
	6	31.52	29.19
	8	33.17	29.19
0.175	4	20.29	20.29
	6	22.57	20.29
	8	24.2	20.29

The above table indicates that the capacity limit values of the uncorrelated MIMO channel for the CSIR and CSIT cases in the MC system are inversely proportional to the impairment level of the transmitter. Also, the values of the capacity limit of the CSIR case found in the above table are taken from Fig. (4.3). These values can also be found from the formulation of the capacity limit of the UMIMOC for the CSIR case in the MC system. That formula was shown in equation (3.26). Thus, depending on that formula, it can be said that the capacity limit of the uncorrelated MIMO channel for the CSIR case in the MC system with the physical transmitter is directly proportional to the number of receiving antennas.

C. Single-carrier MIMO system with CSIT case

Here, the EC of the UMIMOC for the CSIT case in the SC system with the physical transmitter will be discussed. In addition, it will be compared to the EC of the UMIMOC for the CSIT case in the MC system with the physical transmitter. Therefore, it can be assumed the existence of an uncorrelated MIMO channel with M = 4, different N, and varying SNR values. Figure (4.4)

shows the ergodic capacity of this model for the CSIT case over different impairment levels $\kappa_t \in \{0.08, 0.175\}$ in two different systems, MC and SC.

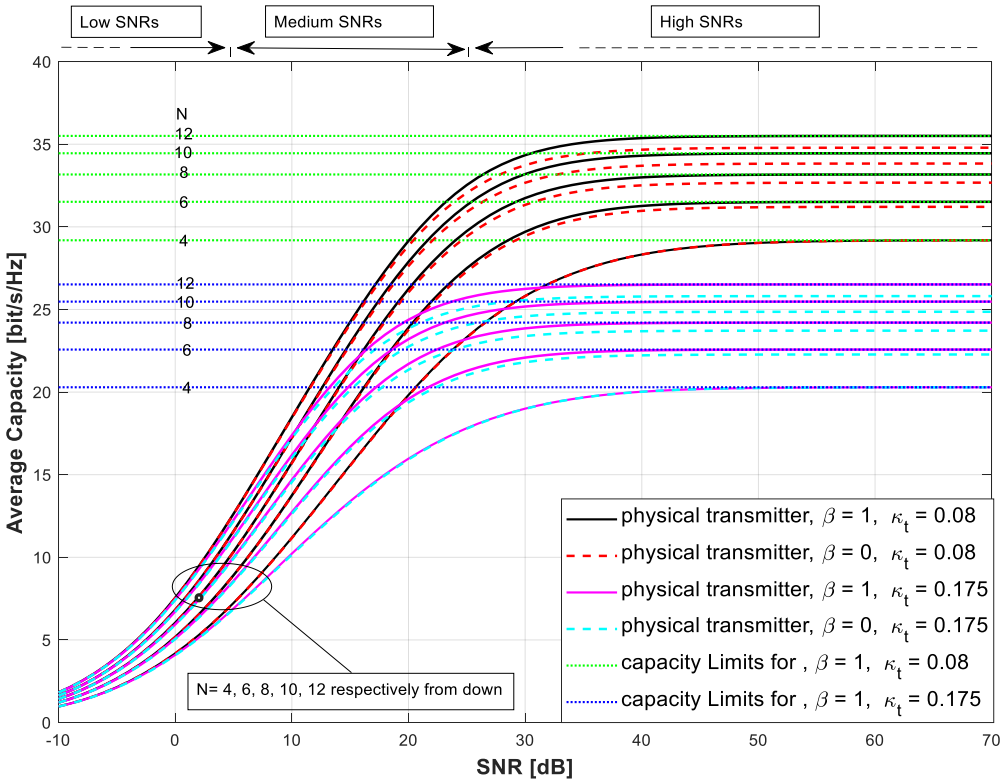

Fig. 4.4: EC of the UMIMOC for the CSIT case in the MC and SC systems with $M = 4$, $N \in \{4, 6, 8, 10, 12\}$, and different impairment levels $\kappa_t \in \{0.08, 0.175\}$.

The above figure shows that all mentioned in the discussion of the EC of the UMIMOC for the CSIT case in the MC system with the physical transmitter applies to the EC of the UMIMOC for the CSIT case in the SC system containing a physical transmitter. However, the above figure indicates that in the CSIT case, for any impairment level ($\kappa_t \in \{0.08, 0.175\}$) and when $N > M$, the capacity limit of the uncorrelated MIMO channel in the MC system is greater than the capacity limit for the uncorrelated MIMO channel in the SC system. In contrast, Fig. (4.4) indicates that in the CSIT case, for any impairment level ($\kappa_t \in \{0.08, 0.175\}$) and when $N = M$, the capacity limit of the uncorrelated MIMO channel in the MC system is identical to the capacity

limit for the uncorrelated MIMO channel in the SC system. Also, it can be seen from Fig. (4.4) that in the CSIT case, for any impairment level ($\kappa_t \in \{0.08, 0.175\}$) and when $N = M$, the EC value of the UMIMOC in the MC system at any value of SNR is almost identical to the EC for the UMIMOC in the SC system.

Furthermore, Table (4.4) displays the value of the capacity limit of the uncorrelated MIMO channel for the CSIT case in the SC system with $M = 4$, $N \in \{4, 6, 8, 10, 12\}$, and different impairment levels $\kappa_t \in \{0.08, 0.175\}$.

Table 4.4: The value of capacity bound of UMIMOC for the CSIT case in the SC system with $M = 4$, $N \in \{4, 6, 8, 10, 12\}$, and different impairment levels $\kappa_t \in \{0.08, 0.175\}$.

Value of κ_t	Number of transmitting antennas (N)	Capacity limit value in bit/second/hertz
0.08	**4**	**29.19**
	6	**31.21**
	8	**32.68**
	10	**33.83**
	12	**34.79**
0.175	**4**	**20.29**
	6	**22.27**
	8	**23.72**
	10	**24.86**
	12	**25.81**

Moreover, it can be presented a new figure to prove that the capacity limit of the uncorrelated MIMO channel for the CSIT case in the SC system with the physical transmitter is directly proportional to the number of receiving antennas. Thus, Fig. (4.5) illustrates the average capacity of the 2*4 uncorrelated MIMO channel for the CSIT case in the SC system over different impairment levels $\kappa_t \in \{0.08, 0.175\}$.

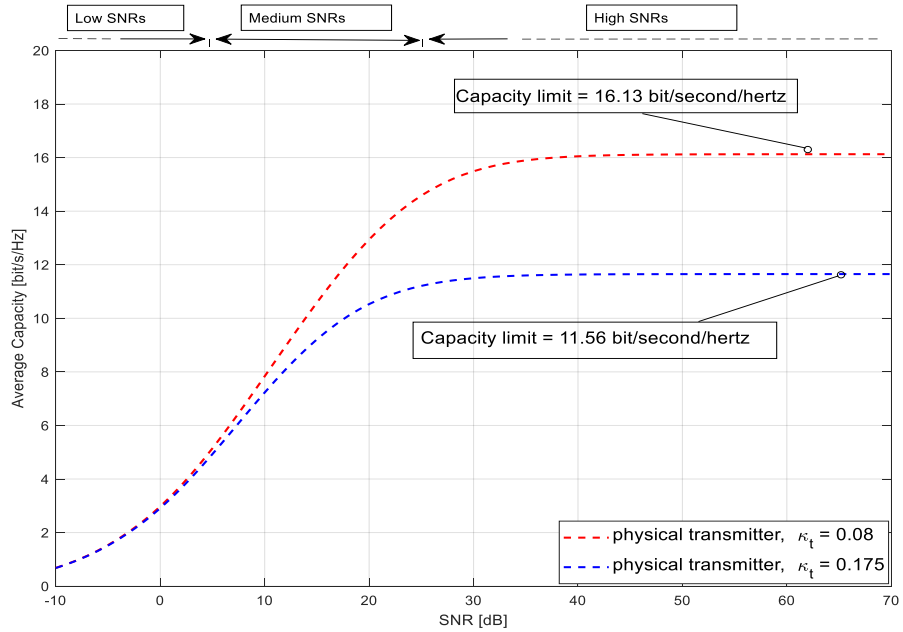

Fig. 4.5: EC of the 2*4 UMIMOC for the CSIT case in the SC system over different impairment levels $\kappa_t \in \{0.08, 0.175\}$.

The above figure shows that the capacity limit value of the uncorrelated MIMO channel for the CSIT case in the SC system with M = 2, N = 4 is equal to 16.13 bit/second/hertz if the impairment level is equal to 0.08, and it is equal to 11.65 bit/second/hertz if the impairment level is equal to 0.175. While the capacity limit value of the uncorrelated MIMO channel for the CSIT case in the SC system with the same criteria but M =4 is equal to 29.19 bit/second/hertz if the impairment level is equal to 0.08, and it is equal to 20.29 bit/second/hertz if the impairment level is equal to 0.175, according to table (4.4). Therefore, it can be concluded that the ergodic capacity and the capacity limit of the uncorrelated MIMO channel for the CSIT case in the SC system with the physical transmitter are directly proportional to the number of receiving antennas.

II. F-SNRMG Results of the Uncorrelated MIMO Channel in the First Algorithm

The previous chapter focused on clarifying the F-SNEMG of the uncorrelated MIMO channel in the first algorithm in the MC system, in which it clarified the F-SNEMG in the MC-MIMO system with the physical transmitter in two different cases, CSIR and CSIT. Therefore, this subsection presents the F-SNEMG simulation results of the uncorrelated MIMO channel for CSIR and CSIT cases in the MC system with the physical transmitter.

A. CSIT case

In this case, the F-SNRMG of the UMIMOC in the MC system with the physical transmitter will be compared with the F-SNRMG of the UMIMOC in the MC system with the ideal transmitter. Therefore, it can be considered the presence of an uncorrelated MIMO channel with $M = 4$, $N \in \{4, 8, 12\}$, $\beta = 1$, and varying SNR. Figure (4.6a) displays the simulation result of the F-SNRMG for this channel with impairment levels $\kappa_t \in \{0, 0.08\}$. At the same time, Figure (4.6b) displays the simulation result of the F-SNRMG for the same channel but with impairment levels $\kappa_t \in \{0, 0.175\}$.

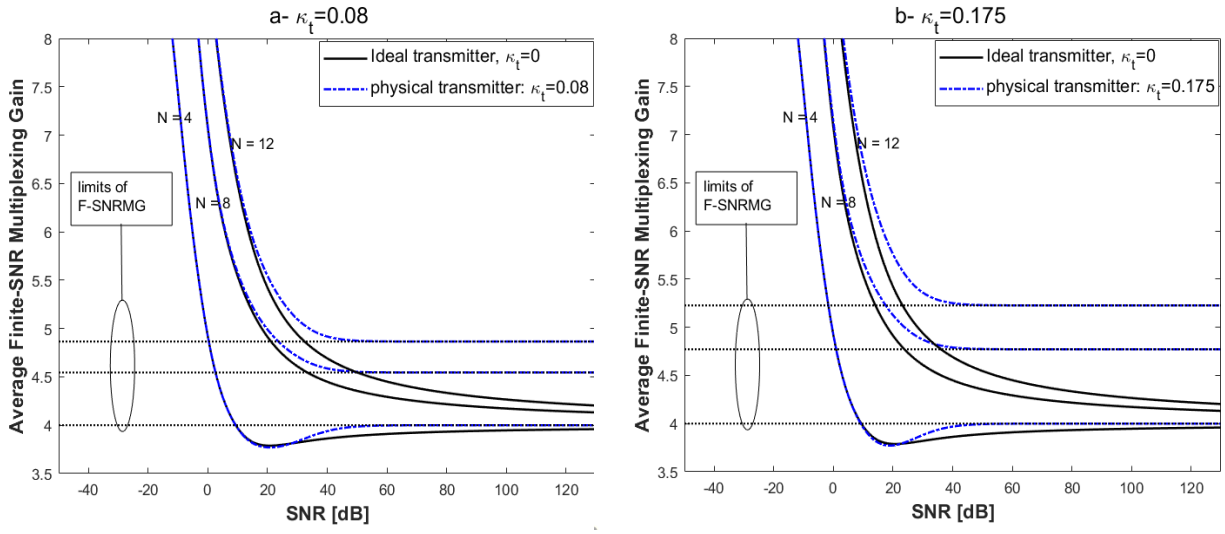

Fig. 4.6: F-SNRMG of the uncorrelated MIMO channel for the CSIT case in the MC system with $M = 4$, $N \in \{4, 8, 12\}$, and different impairment levels: (a) $\kappa_t \in \{0, 0.08\}$, (b) $\kappa_t \in \{0, 0.175\}$

The above figure illustrates that the F-SNRMG of the uncorrelated MIMO channel for the CSIT case in the MC system with the ideal transmitter for any number of the transmitting antennas ($N \in \{4, 8, 12\}$) approaches the value M in the high SNRs. At the same time, it illustrates that the F-SNRMG of the uncorrelated MIMO channel for the CSIT case in the MC system with the physical transmitter for any impairment level ($\kappa_t \in \{0.08, 0.175\}$) and any number of the transmitting antennas ($N \in \{4, 8, 12\}$) approaches the limit $\frac{M*\log_2\left(1+\frac{1}{M*(\kappa_t{}^2/N)}\right)}{\log_2\left(1+\frac{1}{\kappa_t{}^2}\right)}$ in the high SNRs.

Moreover, Table (4.5) displays the value of the F-SNRMG limit in the high SNRs for the uncorrelated MIMO channel for the CSIT case in the MC system with $M = 4$, $N \in \{4, 8, 12\}$, and different impairment levels $\kappa_t \in \{0.08, 0.175\}$.

Table 4.5: The F-SNRMG limit in the high SNRs for the uncorrelated MIMO channel for the CSIT case in the MC system with $M = 4$, $N \in \{4, 8, 12\}$, and different impairment levels $\kappa_t \in \{0.08, 0.175\}$.

Number of transmitting antennas (N)	**F-SNRMG limit value,** $\kappa_t = 0.08$	**F-SNRMG limit value,** $\kappa_t = 0.175$
4	**4**	**4**
8	**4.546**	**4.772**
12	**4.865**	**5.227**

The above table indicates that in the MC system with the physical transmitter, for any impairment levels ($\kappa_t \in \{0.08, 0.175\}$), the F-SNRMG limit in the high SNRs for the uncorrelated MIMO channel for the CSIT case is equal to M when $N = M$, and it is greater than M when $N > M$.

B. CSIR case

Here, the F-SNRMG of the uncorrelated MIMO channel for the CSIR case in the MC system with the physical transmitter is discussed. Also, it will be compared to the F-SNRMG of the uncorrelated MIMO channel for the CSIR case in the MC system with the perfect transmitter. Therefore, it can be regarded as the presence of an uncorrelated MIMO channel with $M = 4$, $N \in \{4, 8, 12\}$, $\beta = 1$, and variable SNR. Figure (4.7a) depicts the simulation result of the F-SNRMG for this channel for the CSIR example in the MC system with impairment levels $\kappa_t \in \{0, 0.08\}$. Similarly, Fig. (4.7b) depicts the simulation result of the F-SNRMG for the same channel for the CSIR example in the MC system but with impairment levels $\kappa_t \in \{0, 0.175\}$.

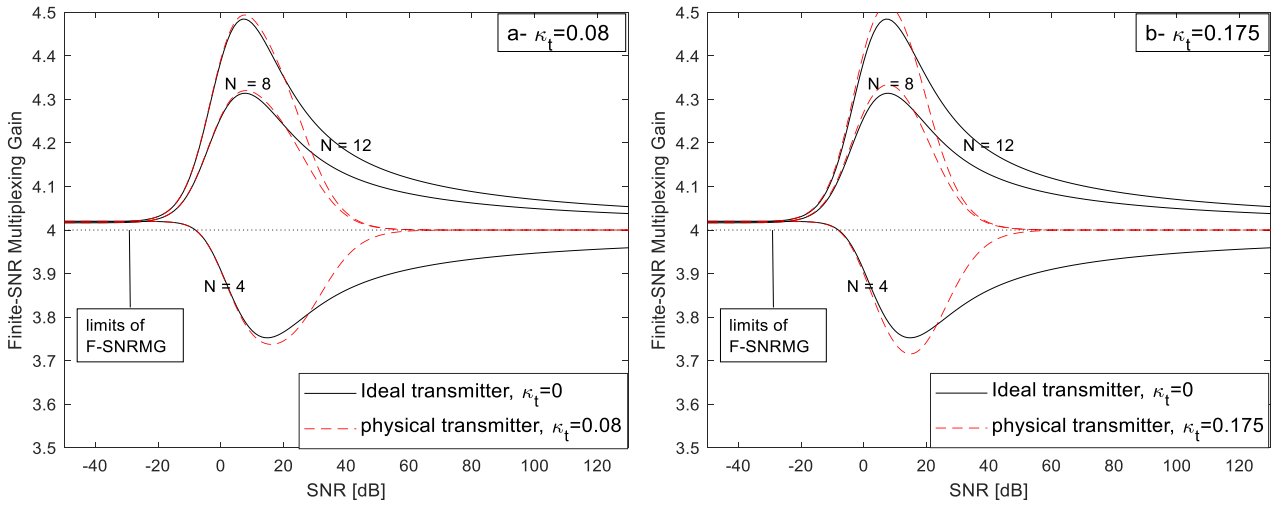

Fig. 4.7: F-SNRMG of the uncorrelated MIMO channel for the CSIR case in the MC system with $M = 4$, $N \in \{4, 8, 12\}$, and different impairment levels: (a) $\kappa_t \in \{0, 0.08\}$, (b) $\kappa_t \in \{0, 0.175\}$

The above figure directs that the F-SNRMG for the uncorrelated MIMO channel for the CSIR case in the MC system for any impairment level ($\kappa_t \in \{0, 0.08, 0.175\}$) and any number of the transmitting antennas approaches the value M in the high SNRs (i.e., the F-SNRMG limit in the high SNRs depends on the number of receiving antennas only, whatever the system's criteria other).

Finally, from Fig. (4.6) and Fig. (4.7), it can be seen that the F-SNRMG with the physical transmitter arrives at its limit faster than the F-SNRMG with the ideal transmitter.

4.2.2 Correlated MIMO Channel Analysis Results in the First Algorithm

The correlated MIMO channel analysis results in the first algorithm include two parts. The first part is devoted to displaying the simulation results of the EC of the CMIMOC under the effect of the physical transmitter in different scenarios: MC-MIMO system with CSIT case, MC-MIMO system with CSIR case, and SC-MIMO system with CSIT case. The second part is devoted to showing the simulation result of the F-SNRMG of the CMIMOC in the MC scheme having the physical transmitter in two cases, CSIR and CSIT.

I. EC Results of the Correlated MIMO Channel in the First Algorithm

In this subsection, the emulation results of the EC of the CMIMOC for the scenarios mentioned in the previous subsection will be offered under the effect of the physical transmitter:

A. MC-MIMO system with CSIT case

In this scenario, the EC of the CMIMOC will be presented under the influence of the physical transmitter. Also, it will be compared with the EC of the UMIMOC in the presence physical transmitter. Thus, it can be assumed the presence of the 4*4 MIMO channel with $\beta = 1$ and varying SNR values. Figure (4.8) shows the ergodic capacity of this model for the CSIT case over different impairment levels $\kappa_t \in \{0.08, 0.175\}$ and different correlation coefficients $\alpha \in \{0, 0.4\}$.

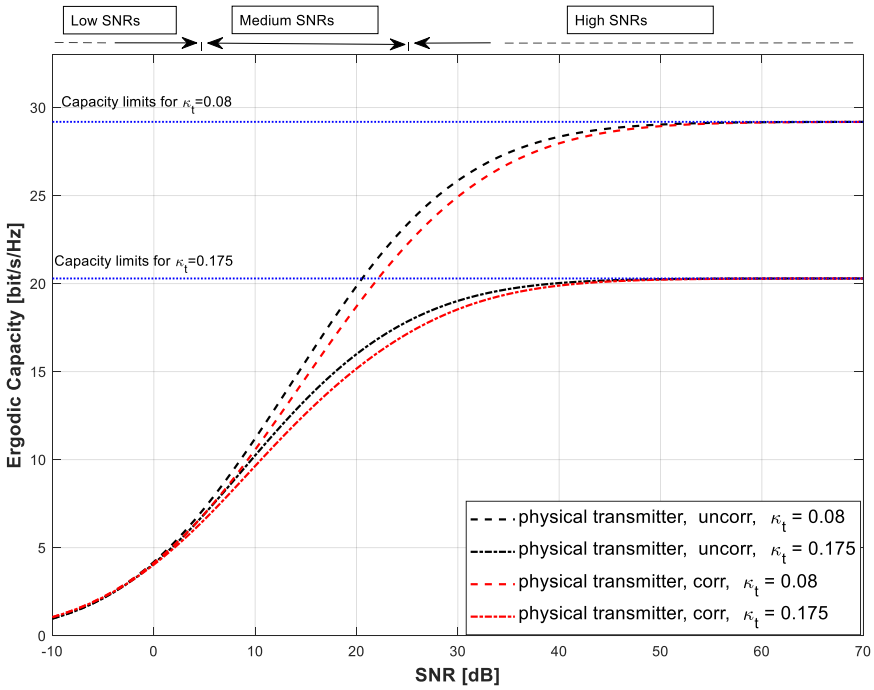

Fig. 4.8: Ergodic capacity of the 4*4 MIMO channel for the CSIT case in the MC system over different impairment levels $\kappa_t \in \{0.08, 0.175\}$ and different correlation coefficients $\alpha \in \{0, 0.4\}$.

The above figure indicates that in the MC system for the CSIT case with any impairment level ($\kappa_t \in \{0.08, 0.175\}$), there is a spacing between the ergodic capacity of the uncorrelated MIMO channel ($\alpha = 0$) and EC of the CMIMOC ($\alpha = 0.4$). The above figure shows that at any impairment level ($\kappa_t \in \{0.08, 0.175\}$), this spacing started to grow in the low SNRs, and then it started to decrease in the medium SNRs until it completely disappeared in the very high SNRs. Thus, according to the above figure, it can be said that the capacity limit of the MIMO channel for the CSIT case in the MC system with the physical transmitter is not influenced by the connection between the channel components.

Moreover, it can be presented a table to show the EC value of the 4*4 MIMO network for CSIT case in the MC system over different impairment

levels $\kappa_t \in \{0.08, 0.175\}$, different SNR values, and different correlation coefficients $\alpha \in \{0, 0.4\}$, according to Fig. (4.8).

Table 4.6: The ergodic capacity value for the 4*4 MIMO channel for the CSIT case in the MC system over different impairment levels $\kappa_t \in \{0.08, 0.175\}$, different SNR values, and different correlation coefficients $\alpha \in \{0, 0.4\}$.

Value of κ_t	SNR value in dB	Ergodic capacity value in bit/second/hertz $\alpha = 0$	Ergodic capacity value in bit/second/hertz $\alpha = 0.4$	The difference
0.08	0	4.187	4.133	0.054
	5	7.247	6.927	0.32
	10	11.2	10.56	0.64
	20	19.85	18.7	1.15
	22	21.37	20.2	1.17
	23	22.055	20.89	1.165
	30	25.85	24.93	0.92
	40	28.34	27.97	0.37
	70	29.19 (capacity limit)	29.19 (capacity limit)	0
0.175	0	4.093	4.034	0.059
	5	6.914	6.594	0.32
	10	10.24	9.638	0.602
	18	15.05	14.21	0.84
	19	15.52	14.69	0.83
	20	15.99	15.17	0.82
	30	19.02	18.54	0.48
	40	20.03	19.89	0.14
	70	20.29 (capacity limit)	20.29 (capacity limit)	0

The above table shows that in the low SNRs, medium SNRs, and high SNRs, the EC of the MIMO channel for the CSIT case in the MC system with the physical transmitter is inversely proportional to the correlation coefficient. In contrast, the above table shows that this inverse proportion disappears in the very high SNRs. Also, according to the above table, it can be seen that the maximum value of the difference between the uncorrelated MIMO channel

capacity and correlated MIMO channel capacity decreases as the impairment level increases. Therefore, it can be concluded that the effect of the correlation is almost ignored when the impairment level value is very large.

B. MC-MIMO system with CSIR case

Here, the EC of the CMIMOC for the CSIR case in the MC system having the physical transmitter will be offered. Also, it will be compared with the EC of the UMIMOC for the CSIR case in the MC system holding a physical transmitter. Then, the effect of the increase in the correlation coefficient on the EC of the MIMO channel for the CSIR case in the MC system containing the physical transmitter will be discussed. Finally, the effect of the incensement in amount of transferring antennas on the EC of the CMIMOC for the CSIR case in the MC system with the physical transmitter will be clarified.

Initially, it can be considered the existence of a MIMO channel with $M = 4$, $N = 4$, $\beta = 1$, and varying SNR values. Figure (4.9) shows the ergodic capacity of this model over different impairment levels $\kappa_t \in \{0.08, 0.175\}$ and different correlation coefficient $\alpha \in \{0, 0.4\}$, assuming the information of channel state are obtainable at receiver only.

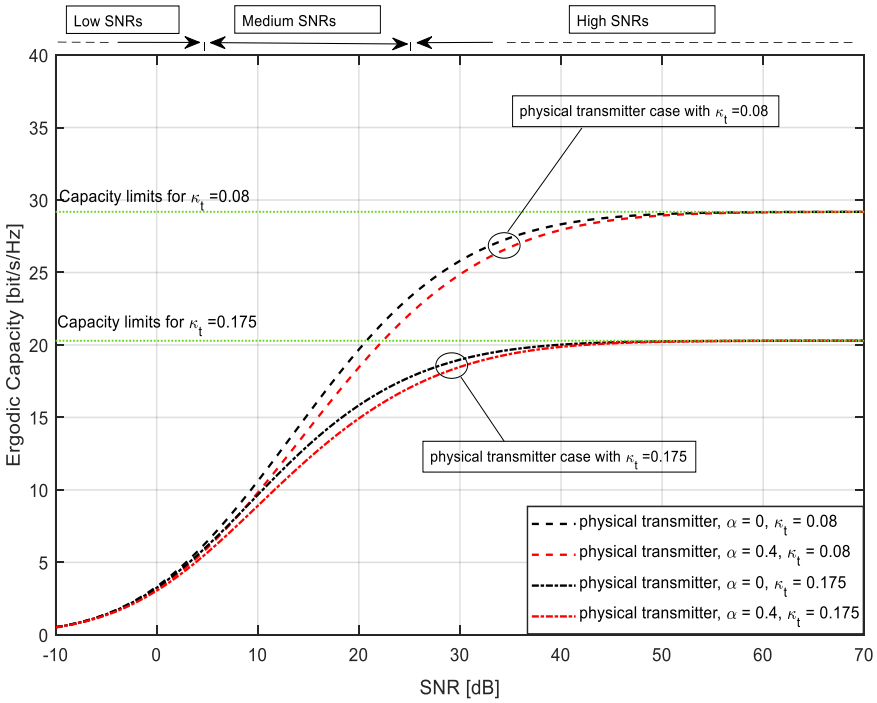

Fig. 4.9: EC of the 4*4 MIMO network for CSIR case in the MC system over different impairment levels $\kappa_t \in \{0.08, 0.175\}$ and different correlation coefficients $\alpha \in \{0, 0.4\}$.

The above figure is almost similar to Fig. (4.8). Therefore, everything mentioned in the discussion for Fig. (4.8) can be adopted as a discussion for this figure. The one difference is that Fig. (4.9) is devoted to showing the EC of the MIMO network for the CSIR case in the MC system over different impairment levels and different correlation coefficients, while Fig. (4.8) is devoted to showing the EC of the MIMO network for the CSIT case in the MC system over different impairment levels and different correlation coefficients.

Now, the impact of growing the correlation factor on the capacity of the MIMO network for the CSIR case in the MC system with the physical transmitter will be clarified. Figure (4.10) shows the effect of increasing the correlation coefficient on the EC of the MIMO network for the CSIR case in the

MC system with M = 4, N = 4, varying SNR values, and different impairment levels $\kappa_t \in \{0.08, 0.175\}$.

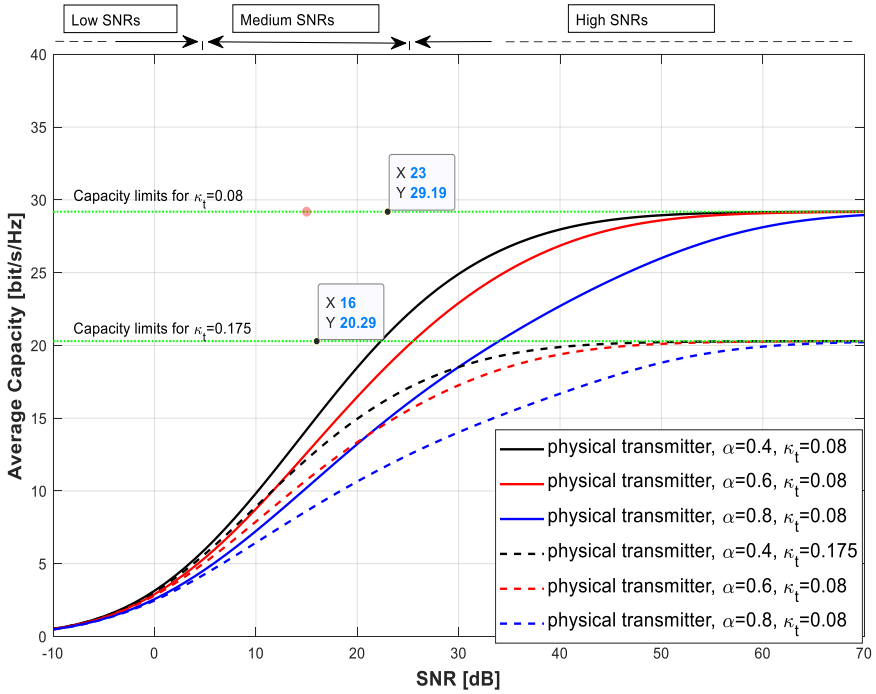

Fig. 4.10: Ergodic capacity of the 4*4 MIMO channel for the CSIR case in the MC system over different impairment levels $\kappa_t \in \{0.08, 0.175\}$ and different correlation coefficients $\alpha \in \{0.4, 0.6, 0.8\}$.

The above figure offers that the capacity limit value of the MIMO channel for the CSIR case in the MC system for any impairment level ($\kappa_t \in \{0.08, 0.175\}$) remains constant, whatever the correlation coefficient value ($\alpha \in \{0.4, 0.6, 0.8\}$). Also, the above figure shows that at low SNRs, medium SNRs, and high SNRs, the capacity of the MIMO channel for the CSIR case in the MC system for any impairment level $\kappa_t \in \{0.08, 0.175\}$ decreases when the correlation coefficient increments. At the same time, the above figure shows that the value of the SNR at which the correlation effect ends increases as the correlation coefficient increases.

Moreover, Table (4.7) displays the ergodic capacity value of the 4*4 MIMO channel for the CSIR case in the MC system over different impairment levels $\kappa_t \in \{0.08, 0.175\}$, different SNR values, and different correlation coefficients $\alpha \in \{0.4, 0.6, 0.8\}$, according to Fig. (4.10).

Table 4.7: The ergodic capacity value for the 4*4 MIMO channel for the CSIR case in the MC system over different impairment levels $\kappa_t \in \{0.08, 0.175\}$, different SNR values, and different correlation coefficients $\alpha \in \{0.4, 0.6, 0.8\}$.

Value of κ_t	SNR value in Db	Ergodic capacity value in bit/second/hertz, $\alpha = 0.4$	Ergodic capacity value in bit/second/hertz, $\alpha = 0.6$	Ergodic capacity value in bit/second/hertz, $\alpha = 0.8$
0.08	5	6.001	5.418	4.611
	10	9.832	8.758	7.243
	20	18.49	16.47	13.22
	30	24.91	22.91	18.51
	40	27.97	26.85	22.71
	70	29.19 (capacity limit)	29.19 (capacity limit)	28.96
0.175	5	5.683	5.102	4.299
	10	8.92	7.892	6.445
	20	14.96	13.35	10.65
	30	18.51	17.26	14.03
	40	19.89	19.38	16.68
	70	20.29 (capacity limit)	20.29 (capacity limit)	20.22

The above table shows that the value of the ergodic capacity when SNR= 70 dB, $\alpha = 0.6$, and $\kappa_t = 0.08$ is equal to 20.29 bit/second/hertz, which is represented the capacity limit. In contrast, the same table shows that the value of the ergodic capacity with the same criteria, but $\alpha = 0.8$, is equal to 20.22 bit/second/hertz, which is not represented the capacity limit. Therefore it can be said that the ergodic capacity needs to more increase in the SNR value to arrive at its limit when the correlation coefficient increases.

Next, the effect of increasing the number of transmitting antennas on the EC of the CMIMOC for the CSIR case in the MC system with the physical transmitter will be clarified. Figure (4.11) presents the EC of the MIMO network for the CSIR case in the MC system with $M = 2$, different N, $\alpha = 0.4$, varying SNR values, and different impairment levels for the transmitter $\kappa_t \in \{0.08, 0.175\}$.

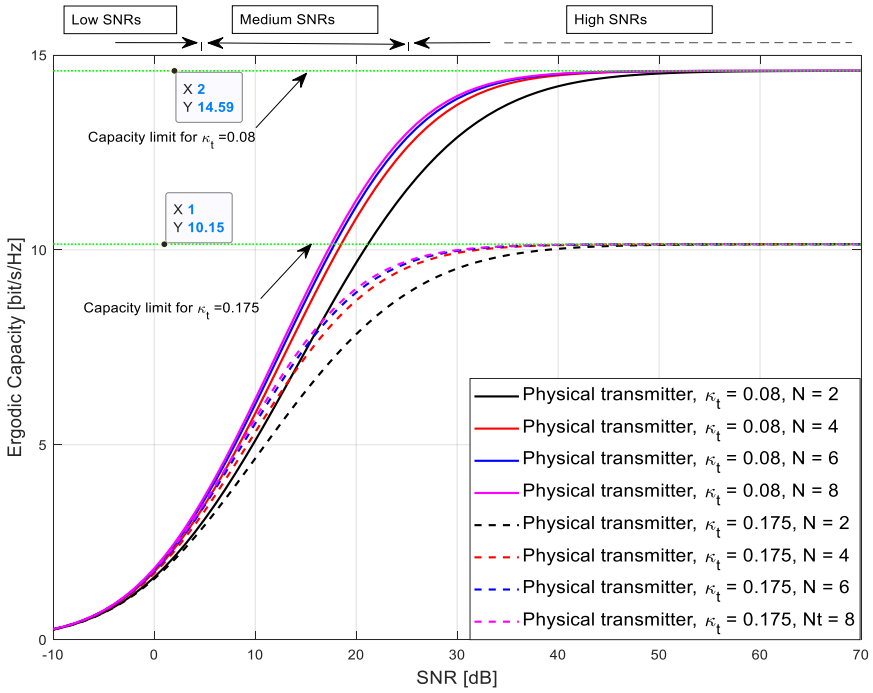

Fig. 4.11: EC of the MIMO network for the CSIR case in the MC system with $M = 2$, $N \in \{2, 4, 6, 8\}$, $\alpha = 0.4$, and different impairment levels for the transmitter $\kappa_t \in \{0.08, 0.175\}$.

The above figure indicated that at any value of the SNR (from the beginning of the SNR range to the value at which the capacity limit begins), the EC of the CMIMOC for the CSIR in the MC system for any impairment level ($\kappa_t \in \{0.08, 0.175\}$) increases as the number of transmitting antennas increases. However, figure (4.11) demonstrates that the improvement in channel capacity that follows from adding several antennas to the sending antennas diminishes

when the same number of antennas is added to the transmitting antennas a second time.

C. SC-MIMO system with CSIT case

Here, the focus will be on showing the effect of the increase in the correlation coefficient on the EC of the MIMO network for the CSIT case in the SC system containing the physical transmitter. Therefore, it can be considered the presence of the MIMO channel with $M = 4$, $N = 4$, $\beta = 0$, and varying SNR values. Figure (4.12) shows the ergodic capacity of this model over different impairment levels and different correlation coefficients,` assuming the information of the channel is obtainable at the receiver and the transmitter.

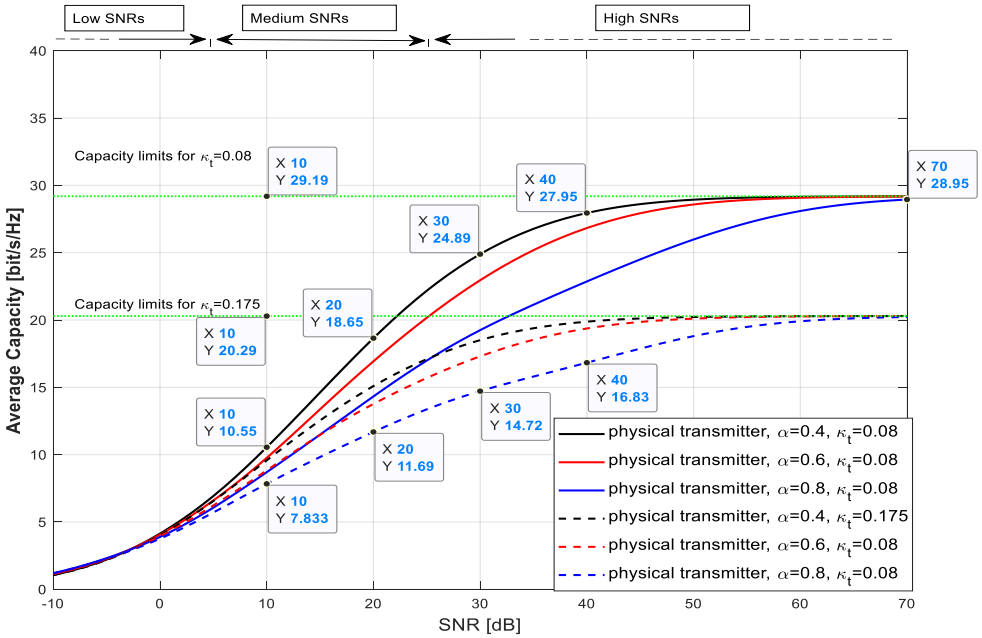

Fig. 4.12: EC of the 4*4 MIMO network for CSIT case in the SC system over different impairment levels $\kappa_t \in \{0.08, 0.175\}$ and different correlation coefficients $\alpha \in \{0.4, 0.6, 0.8\}$.

The preceding figure is nearly identical to Fig (4.10). Consequently, everything discussed in the description for figure (4.10) may be applied to this

figure. The only difference is that figure (4.12) depicts the EC of the CMIMOC for CSIT case in the SC system at various impairment levels, whereas figure (4.8) depicts the EC of the CMIMOC for CSIR case in the MC system at various impairment levels.

II. F-SNRMG Results of the Correlated MIMO Channel in the First Algorithm

In this subsection, the simulation results of the F-SNRMG of the correlated MIMO channel for the CSIT and CSIR cases in the MC system with the physical transmitter will be offered. Also, these results will be compared with the F-SNRMG results of the uncorrelated MIMO channel for the CSIT and CSIR cases in the MC system with the physical transmitter. Thus it can be considered the existence of the MIMO channel with M = 4, N ∈ {4, 8}, β = 1, and varying SNR values. Figure (4.13)` shows the F-SNRMG simulation results of this model for the CSIT and CSIR cases in the MC system over an impairment level of 0.08 and different correlation coefficients α ∈ {0, 0.4}.

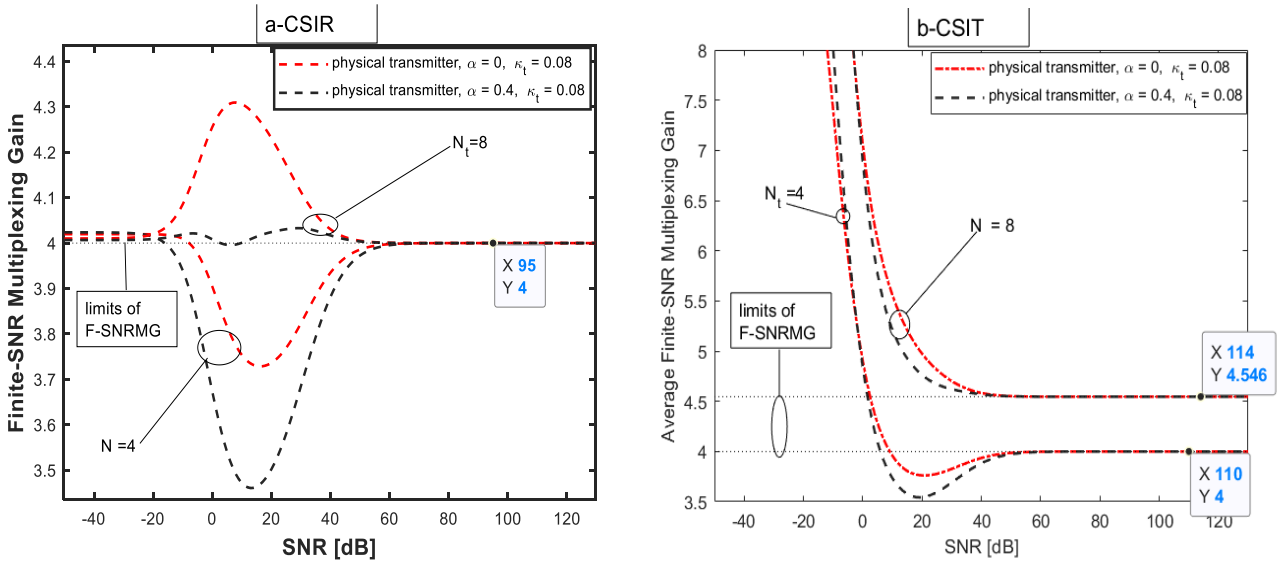

Fig. 4.13: F-SNRMG of the MIMO channel in the MC system with M=4, N ∈ {4, 8}, α ∈ {0, 0.4}, and $\kappa_t = 0.08$: (a) CSIR case, (b) CSIT case

From figure (14.13), it can be seen that the correlation between the channel elements is decreases the F-SNRMG value of the MIMO channel in the low SNRs, medium SNRs, and some value of the high SNRs. However, the same figure is indicates that the limit of the F-SNRMG in the high SNR is not affected by the correlation between the channel elements.

4.3 Results of Second Algorithm

The third chapter mentioned that the second algorithm considers the effect of the physical transmitter and the effect of the physical receiver on the ergodic capacity and finite-SNR multiplexing gain of the MIMO channel. Also, it mentioned that the second algorithm is applied to the uncorrelated MIMO channel and correlated MIMO channel. Therefore, the second algorithm's simulation results can be divided into two parts. The first part is devoted to showing the simulation results of the ergdoc capacity and F-SNRMG of the uncorrelated MIMO channel for the CSIR case in the SC system with the physical transmitter and physical receiver. In contrast, the second part is devoted to showing the simulation results of the ergodic capacity and F-SNRMG of the correlated MIMO channel for the CSIR case in the SC system with the physical transmitter and physical receiver.

4.3.1 The Simulation Results for the EC and F-SNRMG for the UMIMOC in Second Algorithm

In this subsection, the simulation results of the EC of the UMIMOC under the influences of physical transmitter and physical receiver will be offered. These results consist of two figures. The first figure comperes the EC of the UMIMOC for the CSIR case in the SC system having the physical transmitter and physical receiver with the EC of the UMIMOC for the CSIR case in the SC system having the physical transmitter and ideal receiver. The

second figure shows the effect of the increase in the number of transmitting antennas on the EC of the UMIMOC in the second algorithm. Then, the F-SNRMG of the UMIMOC under the second algorithm will be presented.

Initially, it can be assumed the existence of an uncorrelated MIMO channel with $M = 4$, $N = 4$, $\beta = 0$, and varying SNR values. Figure (4.14) shows the ergodic capacity of this technique over the first algorithm and second algorithm with different impairment levels, assuming that the information of the channel is obtainable at the receiver only.

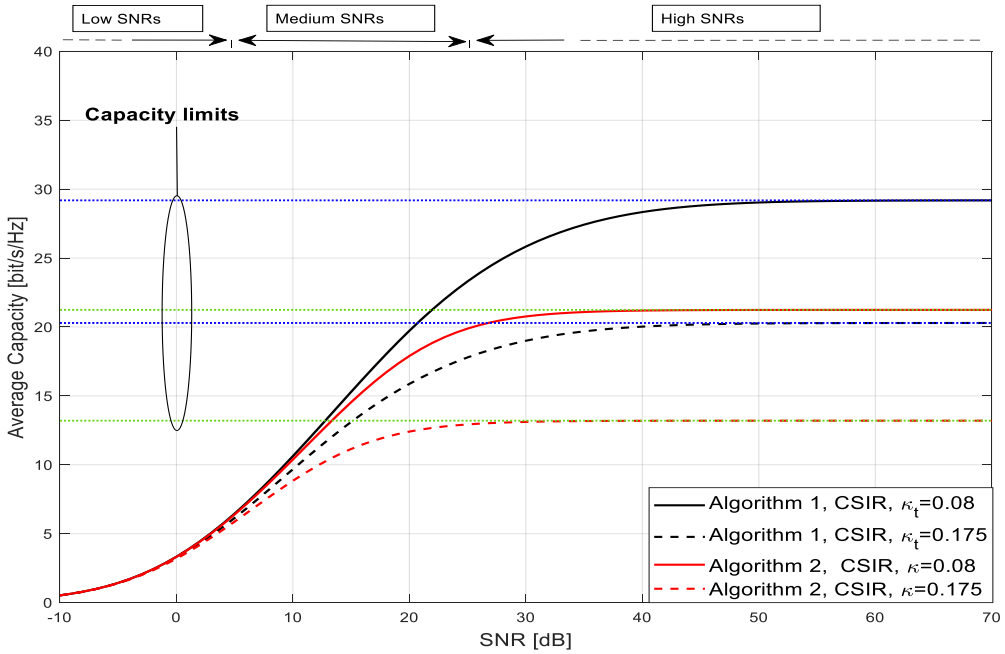

Fig. 4.14: EC of the 4 × 4 UMIMOC over the first algorithm and second algorithm for the CSIR case in the SC system with different impairment levels.

The above figure indicated that in the CSIR case in the SC system, the EC behavior of the UMIMOC in the second algorithm is similar to the EC behavior of the UMIMOC in the first algorithm. However, the above figure shows that in the SC system for the CSIR case for any impairment level, at the low, medium, and high SNRs, the EC of the UMIMOC in the second algorithm is smaller than the EC of the UMIMOC in the first algorithm. Table (4.8)

displays the capacity limit value of the 4×4 uncorrelated MIMO channel over the first algorithm and the second algorithm for the CSIR case in the SC system with different impairment levels.

Table 4.8: The capacity limit value of the 4×4 uncorrelated MIMO channel over the first and second algorithms for the CSIR case in the SC system with different impairment levels

Value of κ_t	**Capacity limit value for the first algorithm in bit/second/hertz**	**Value of** K	**Capacity limit value for the second algorithm in bit/second/hertz**
0.08	**29.19**	**0.08**	**≅ 21.24**
0.175	**20.29**	**0.175**	**≅ 13.2**

The above table indicates that in the CSIR case in the SC system for any impairment level, the capacity limit of the uncorrelated MIMO channel decreases more if the effects of the physical transmitter and physical receiver are taken together into account. Also, it can be seen from above table that the capacity limit of the uncorrelated MIMO channel in the second algorithm is inversely proportional to the impairment level for the transceiver hardware (κ).

Now, the effect of increasing the number of transmitting antennas on the EC of the UMIMOC in the second algorithm will be clarified. Figure (4.15) presents the EC of the UMIMOC in the second algorithm with $M = 2$, different N, varying SNR values, and different impairment levels for the transceiver hardware $\kappa \in \{0.08, 0.175\}$.

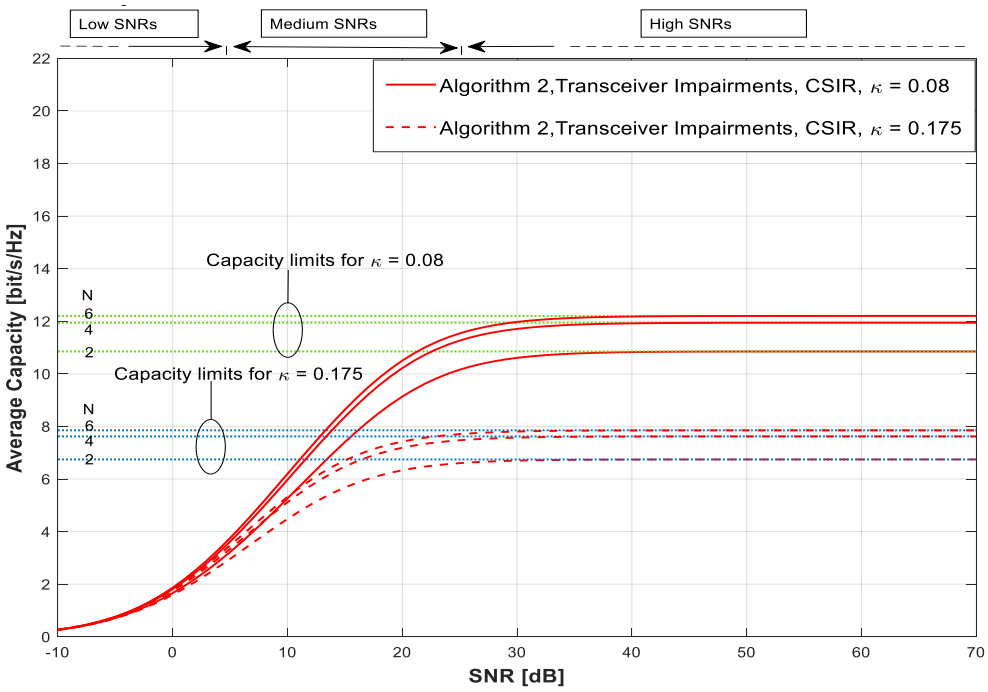

Fig. 4.15: EC of the UMIMOC in second algorithm with $M = 2$, $N \in \{2, 4, 6\}$, and different impairment levels for the transceiver hardware $\kappa \in \{0.08, 0.175\}$.

The above figure illustrates that the EC of the UMIMOC for any impairment level ($\kappa \in \{0.08, 0.175\}$) in the second algorithm is directly proportional to the number of transmitting antennas, which means that at any value of SNR, the ergodic capacity increases by a random amount as the number of the transmitting antennas increases. Also, the figure displayed above shows that this amount of increase in the ergodic capacity, which happens due to the incensement in amount of transferring antennas by a specific quantity, decreases each time the number of transmitting antennas increases again by the same specific number.

In addition, Table (4.9) displays the capacity limit value of the uncorrelated MIMO channel in the second algorithm with $M = 2$, $N \in \{2, 4, 6\}$, and different impairment levels for the transceiver hardware $\kappa \in \{0.08, 0.175\}$.

Table 4.9: The capacity limit value of the uncorrelated MIMO channel in the second algorithm with $M = 2$, $N \in \{2, 4, 6\}$, and different impairment levels for the transceiver hardware $\kappa \in \{0.08, 0.175\}$

Value of κ	Number of transmitting antennas (N)	Capacity limit value in bit/second/hertz
0.08	**2**	**≅ 10.85**
	4	**≅ 11.94**
	6	**≅ 12.2**
0.175	**2**	**≅ 6.744**
	4	**≅7.62**
	6	**≅ 7.851**

The above table shows that the capacity limit value of the uncorrelated MIMO channel in the second algorithm with $M = 2$, $N = 4$, and $\kappa = 0.08$ is almost equal to 11.94 bit/second/hertz. At the same time, the capacity limit value of the uncorrelated MIMO channel in the second algorithm with the same criteria but M = 4 is almost equal to 21.24 bit/second/hertz, as shown in the Table (4.8). Therefore, it can be said that the capacity limit and the EC of the UMIMOC in second algorithm is directly proportional to the number of receiving antennas.

Now, the F-SNRMG of the uncorrelated MIMO channel for the CSIR case in the SC system containing the physical transmitter and physical receiver is compared with the F-SNRMG of the UMIMOC for the CSIR case in the SC system containing the physical transmitter only. Figure (4.16) shows the F-SNRMG of the uncorrelated MIMO channel over the first algorithm and the second algorithm for the CSIR case in the SC system with $M = 4$, $N \in \{4, 8, 12\}$, and impairment level 0.08 ($\kappa_t = 0.08$ for first algorithm, $\kappa = 0.08$ for the second algorithm).

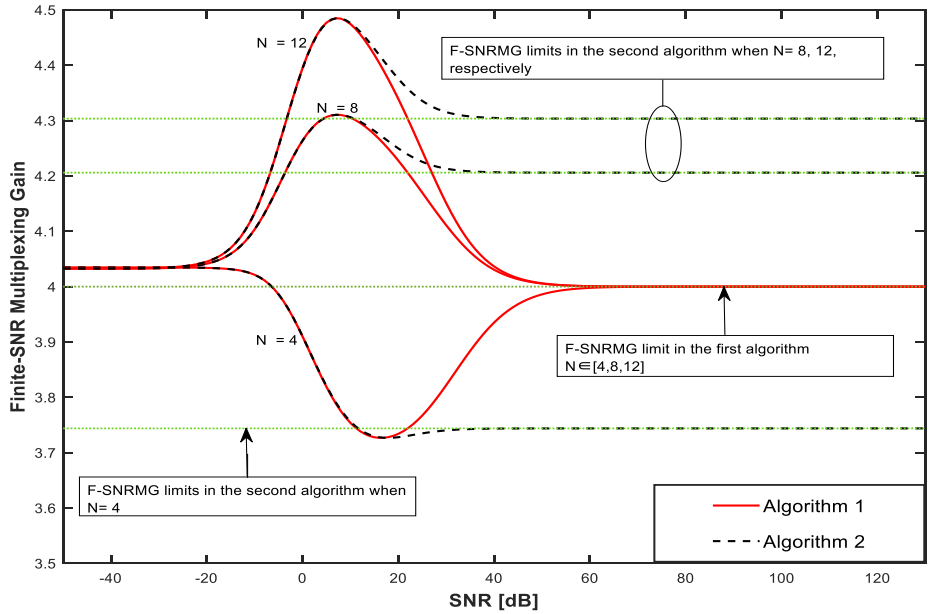

Fig. 4.16: F-SNRMG of the uncorrelated MIMO channel over the first algorithm ($\kappa_t = 0.08$) and second algorithm ($\kappa = 0.08$) for the CSIR case in the SC system with $M = 4$, $N \in \{4, 8, 12\}$.

The critical thing seen from the above figure is that the F-SNRMG limit in the high SNRs for the uncorrelated MIMO channel in the second algorithm is greater than M when $N > M$, but it is smaller than M when $N = M$. This is in contrast to what is found in the first algorithm. The above figure and figure (4.7) show that the F-SNRMG limit in the high SNRs for the uncorrelated MIMO channel for the CSIR case in the SC system having the physical transmitter equals M, whatever the number of transmitting antennas (N).

4.3.2 The Simulation Results for the EC and F-SNRMG for the correlated MIMO Channel in the Second Algorithm

This subsection presents the simulation results of the EC and F-SNRMG of the CMIMOC according to the second algorithm. These results consist of four figures. The first figure compares the EC of the CMIMOC with the EC of the UMIMOC under the impact of the physical transmitter and physical receiver, assuming the system used is the SC-MIMO system, and the

information of channel state are obtainable at receiver only. The second figure shows the effect of the increase in the correlation coefficient on EC of MIMO network under second algorithm, while the third figure shows the effect of the incensement in amount of transferring antennas on the EC of the CMIMOC according to the second algorithm. Finally, the fourth figure compares the F-SNRMG of CMIMOC with the F-SNRMG of UMIMOC according to second algorithm.

Initially, we assumed a 4×4 MIMO channel with $\beta = 0$ and varying SNR values. Figure (4.17) shows the ergodic capacity of this model in the second algorithm over different impairment level $\kappa \in \{0.08, 0.175\}$ and different correlation coefficients $\alpha \in \{0, 0.4\}$.

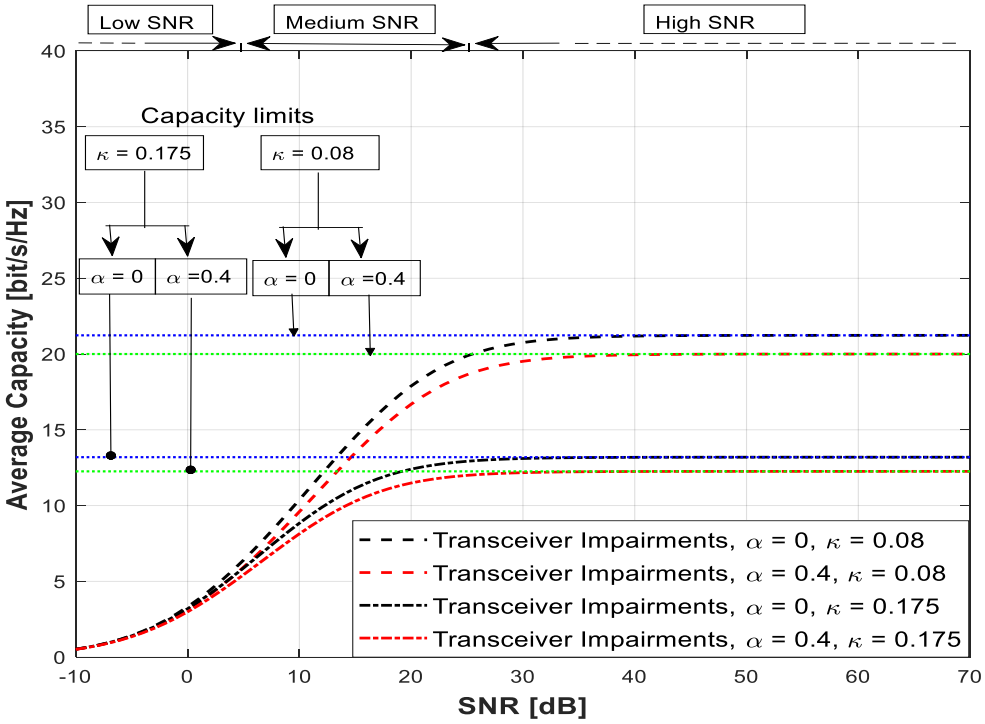

Fig. 4.17: The EC of 4×4 MIMO network in second algorithm over different impairment level $\kappa \in \{0.08, 0.175\}$ and different correlation coefficients $\alpha \in \{0, 0.4\}$.

The above figure shows that in the second algorithm for any impairment level $\kappa \in \{0.08, 0.175\}$ at any value of SNR, the EC of the UMIMOC ($\alpha = 0$) is

greater than the EC of the CMIMOC (α = 0.4). In other words, figure (4.17) illustrates that at any impairment level $\kappa \in \{0.08, 0.175\}$, there is a spacing between the EC of the UMIMOC (α = 0) and the EC of the CMIMOC (α = 0.4). The above figure shows that this spacing started to grow in the low SNRs, but it stopped growing in the high SNRs. Also, from the above figure, it can be seen that the maximum difference between the EC of the UMIMOC and the EC of the CMIMOC decreases as the impairment level increases, so it can be concluded that the effect of the correlation is almost ignored if the impairment level value is very large, taken in to account the antennas configurations and value of the correlation coefficient.

Moreover, Table (4.10) offers the capacity limit value of the 4×4 MIMO channel in the second algorithm over different impairment level $\kappa \in \{0.08, 0.175\}$ and different correlation coefficients $\alpha \in \{0, 0.4\}$.

Table 4.10: The capacity limit value of the 4×4 MIMO channel in the second algorithm over different impairment level $\kappa \in \{0.08, 0.175\}$ and different correlation coefficients $\alpha \in \{0, 0.4\}$.

Value of κ	**Capacity limit value in bit/second/hertz** $\alpha = 0$	**Capacity limit value in bit/second/hertz** $\alpha = 0.4$
0.08	**≅ 21.24**	**≅ 19.98**
0.175	**≅ 13.2**	**≅ 12.24**

The above table demonstrates that the capacity limit of the MIMO channel in the second algorithm is inversely commensurate to the correlation coefficient, impairment level, or both.

Now, it will be clear what happens to the MIMO channel's capacity when the correlation coefficient goes up in an SC system with physical

transmitter and physical receiver. Figure (4.18) shows what happens to the EC of the MIMO network when the correlation coefficient is increased in the SC system with M=4, N=4, different SNR values, and different impairment levels for the transceiver hardware $\kappa \in \{0.08, 0.175\}$.

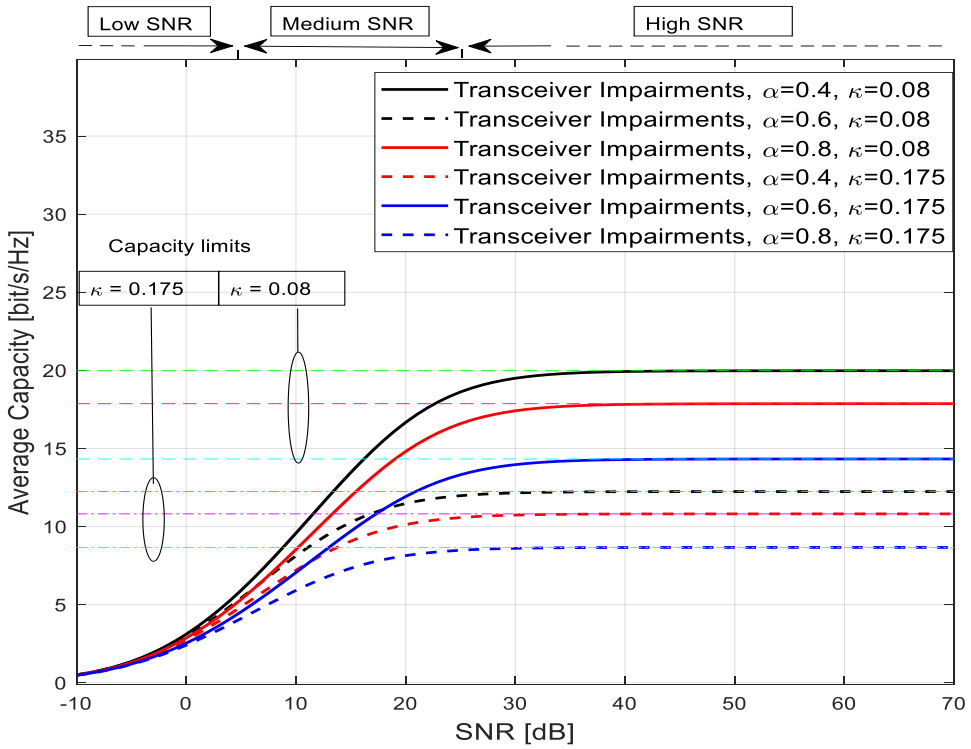

Fig. 4.18: Effect of increasing the correlation coefficient on the EC of the MIMO medium in the second algorithm with M=4, N=4, different impairment levels $\kappa \in \{0.08, 0.175\}$.

The above figure shows that at any value of the SNR, the EC of the MIMO medium for the CSIR case in the SC system having the physical transmitter and physical receiver with any impairment level $\kappa \in \{0.08, 0.175\}$ decreases as the correlation coefficient increases. Also, the above figure proves that the correlation between the channel elements plays an essential role in determining the capacity limit of the MIMO channel for the CSIR case in the SC system having the physical transmitter and physical receiver. Table (4.11) offers the value of the capacity limits found in Fig. (4.18).

Table 4.11: The capacity limit value of the 4×4 MIMO channel in the second algorithm over different impairment levels $\kappa \in \{0.08, 0.175\}$ and different correlation coefficients $\alpha \in \{0.4, 0.6, 0.8\}$.

Value of κ	Capacity limit value in bit/second/hertz $\alpha = 0.4$	Capacity limit value in bit/second/hertz $\alpha = 0.6$	Capacity limit value in bit/second/hertz $\alpha = 0.8$
0.08	**$\cong$ 19.98**	**$\cong$ 17.87**	**$\cong$ 14.33**
0.175	**$\cong$ 12.24**	**$\cong$ 10.82**	**$\cong$ 8.667**

Next, the effect of increment the number of transmitting antennas on EC of CMIMOC for CSIR case in the SC system harboring a physical transmitter and physical receiver is presented; Figure (4.19) shows this effect.

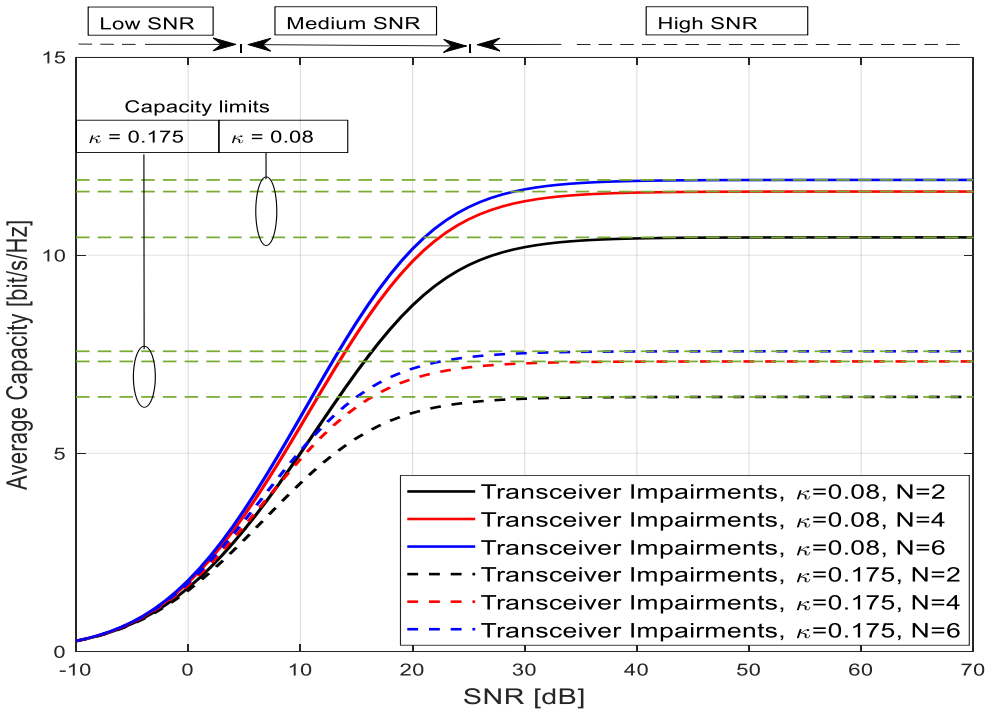

Fig. 4.19: EC of the CMIMOC in second algorithm with $M = 2$, $N \in \{2, 4, 6\}$, $\alpha = 0.4$, and different impairment levels $\kappa \in \{0.08, 0.175\}$.

The above figure indicates that the incensement in amount of transferring antennas affects the EC of CMIMOC in the second algorithm in the same way that it affects the EC of the UMIMOC in the second algorithm.

Therefore, all mentioned in the discussion of Fig. (4.15) can be considered a discussion of the above figure.

Finally, the F-SNRMG of the correlated MIMO channel for the CSIR case in the SC system having the physical transmitter and physical receiver compares with the F-SNRMG of the uncorrelated MIMO channel for the CSIR case in the SC system having the physical transmitter and physical receiver. Figure (4.20) shows this comparison.

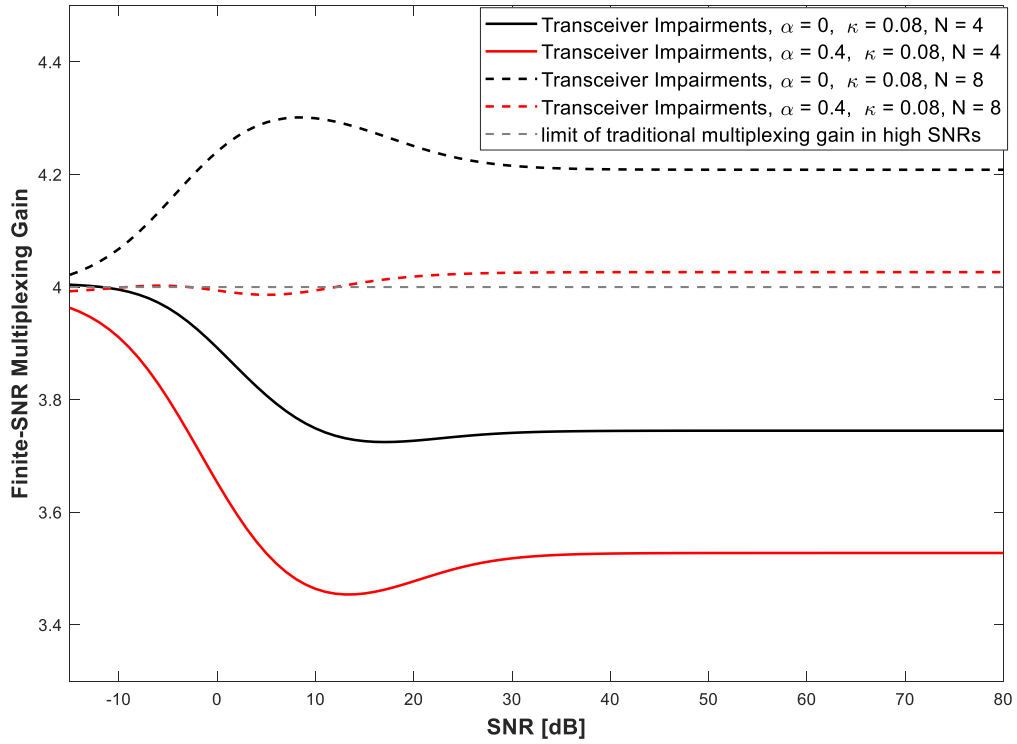

Fig. 4.20: F-SNRMG of the MIMO channel in the second algorithm with $M = 4$, $N \in \{4, 8\}$, $\kappa = 0.08$, and different correlation coefficients $\alpha \in \{0, 0.4\}$.

The above table shows that the F-SNRMG of the MIMO channel for the CSIR case in the SC system having the physical transmitter and physical receiver in any value of SNRs decreases as the correlation coefficient increases. This means that the F-SNRMG limit in the high SNRs is inversely proportional

to the correlation coefficient value. Thus, the above figure indicates that when the N > M, the F-SNRMG limit in the high SNRs may become smaller than M if the value of the correlation coefficient increases, which is in contrast to what is found in the F-SNRMG of the uncorrelated MIMO channel.

4.4 Comparison with related work

In this section, we will be compared the results of the proposed algorithms in this work with the results of the some of the related work such as [13], [15], [19], [24]. The comparison will be created in terms of the ergodic capacity, where the first algorithm for the MC-MIMO system will be compared with [13], [19], [24], and the second proposed algorithm will be compared with the [15]. Table (4.12) offers this comparison. This table shows that the proposed algorithms in this work give accurate results for the EC of the MIMO network, where these algorithms take into account the effect of the correlation between the channel elements. Also, table (4.12) indicates that the ergodic capacity at a specific SNR value, especially in the medium SNRs, may be very negatively affected if the correlation coefficient increases.

Table 4.12: Comparison between the proposed algorithms in this thesis and previous proposed works

The works	Case	Effect factor				Capacity (MC-MIMO) bit/second/hertz				
		κ	***α***	**N**	**M**	**SNR= 10 dB**	**SNR = 20 dB**	**SNR= 30 dB**	**SNR= 40 dB**	**SNR= end dB**
Bharati [24]	CSIT	0.02	0	4	4	11.52	22.07	33.2	40.74	45.15
Bjornson [13]	CSIT	0.05	0	4	4	11.4	21.14	29.17	33.03	34.51
Singal [19]	CSIR	0.05	0	4	4	-	14.166	21.66	26.66	34.61
Propsed algorithm in this work	CSIT	0.08	0	4	4	11.2	19.85	25.85	28.34	29.19
			0.4	4	4	10.56	18.7	24.93	27.97	29.19
		0.175	0	4	4	10.24	15.99	19.02	20.03	20.29
			0.4	4	4	9.638	15.17	18.54	19.89	20.29
Propsed algorithm in this work	CSIR	0.08	0	4	4	10.36	19.72	25.83	28.34	29.19
			0.4	4	4	9.832	18.49	24.91	27.97	29.19
			0.6	4	4	8.758	16.47	22.91	26.85	29.19
			0.8	4	4	7.243	13.22	18.51	22.71	29.19
		0.175	0	4	4	9.679	15.87	19	20.03	20.29
			0.4	4	4	8.92	14.96	18.51	19.89	20.29
			0.6	4	4	7.892	13.35	17.26	19.38	20.29
			0.8	4	4	6.445	10.65	14.03	16.68	20.29

The works	Case	Effect factor				Capacity (SC-MIMO) bit/second/hertz				
		K	α	N	M	SNR= 10 dB	SNR = 20 dB	SNR= 30 dB	SNR= 40 dB	SNR= end dB
Zhang [15]	CSIR	0.15	0	4	4	9.282	13.6	14.56	14.68	14.7
Propsed algorithm in this work	CSIR	0.08	0	4	4	10.38	17.89	20.76	21.18	21.23
			0.4	4	4	9.58	16.67	19.5	19.93	19.98
			0.6	4	4	8.533	14.81	17.41	17.82	17.87
			0.8	4	4	7.062	11.92	13.97	14.29	14.33
		0.175	0	4	4	8.839	12.4	13.11	13.18	13.19
			0.4	4	4	8.125	11.48	12.16	12.23	12.24
			0.6	4	4	7.201	10.13	10.74	10.81	10.82
			0.8	4	4	5.915	8.142	8.608	8.661	8.667

Chapter Five

Conclusions and Future Works

CHAPTER FIVE

CONCLUSIONS AND FUTURE WORKS

5.1 Conclusion

The work provided in this thesis is divided into two algorithms. The first algorithm takes into account only the effect of the physical transmitter on the EC and F-SNRMG in many cases shown in Fig. (3.1). In contrast, the second algorithm considers the effect of the physical transmitter and the impact of the physical receiver on the EC and F-SNRMG in the cases shown in Fig.(3.1). Therefore, the following points represent the important conclusions:

1. When a MIMO system contains a physical transmitter or physical transmitter and physical receiver, its channel capacity at high SNRs reaches a value known as the capacity limit and stops growing.
2. The capacity limit value of the MIMO channel is inversely proportional to the level of the degradation κ.
3. In the first algorithm, the value of the capacity limit for the MIMO channel in the CSIT case increases as the amount of transferring antennas increases. This incensement in the amount of the capacity limit decreases every time the number of transferring antennas is increased by the same number that is added the first time. In contrast, the value of the capacity limit for the MIMO channel in the CSIR case is not affected by the number of transmitting antennas. This statement applies whether the system is MC or SC. While, in the second algorithm, the value of the capacity limit for the MIMO channel in the CSIR case increases as quantity of transferring antennas increase. This incensement in amount of the capacity limit also decreases every time the amount of transferring antennas is increased by same number that was added the first time.

4. In the first algorithm, when M = N, the value of the capacity limit of the MIMO channel is not affected by the type of the system used (SC or MC) or by the nature of the party that owns the channel information, but it is affected by the level of degradation of the transmitter only.
5. When M < N and the channel status information is available in the transmitter, the multi-carrier system achieves a higher capacity limit incident value than the single-carrier system.
6. In general, the capacity limit value for the MIMO channel is directly proportional to the number of receiving antennas.
7. In the first algorithm, the capacity limit value of the MIMO channel is not affected by the correlation coefficient. While in the second algorithm, the correlation between the channel elements plays an essential role in determining the MIMO channel's capacity limit value, where the capacity limit value of the MIMO channel is inversely proportional to the correlation coefficient.
8. In the first algorithm, the MIMO capacity for the CSIR case in the MC system is equal to the MIMO capacity for the CSIR case in the SC system.
9. In both algorithms, the EC of the MIMO network grows with quantity of transmitting antennas. However, this enhancement in channel capacity diminishes when the same number of antennas is added to the transmitting antennas a second time. This point does not include the period at which capacity bound of the MIMO network begins.
10. The capacity of the MIMO network is affect by the value of the correlation coefficient, as the higher the correlation coefficient, the lower the MIMO channel capacity. This point does not include the period at which the capacity limit of the MIMO channel begins.

11. The higher the correlation coefficient, the more power the MIMO channel needs to reach its limit in the high SNRs.
12. In the SC system for the CSIR case for any impairment level κ, at the low, medium, and high SNRs, the EC of the UMIMOC in the second algorithm is smaller than EC of the UMIMOC in the first algorithm.
13. In the MIMO system with a physical transmitter, the value of F-SNRMG at the high SNR rates depends on the party that owns the channel state information. If information of channel is obtainable at the receiver, F-SNRMG limit is equal to M. Whereas if information of channel is obtainable in the transmitter and receiver, the F-SNRMG limit is equal to M when $M = N$ and is greater than that when $N > M$. while, In the MIMO system with a physical transmitter and physical receiver, the F-SNRMG limit in high SNRs for the uncorrelated MIMO channel is larger than M when $\mathbf{N > M}$, while it is less than M when $\mathbf{N = M}$,.
14. In the first algorithm, the F-SNRMG limit value of the MIMO channel is not affected by the correlation coefficient. While in the second algorithm, The F-SNRMG limit in the high SNRs is inversely proportional to the correlation coefficient value.

5.2 Future Works

The following points represent some ideas that may be applied to improving and developing the work proposed in this thesis:

1. The two algorithms proposed may be repeated apply with other types of fading, such as Rician fading, Nakagami fading, and Weibull fading.
2. The two algorithms proposed may be repeated apply with taken into account the cross correlation (mutual compiling).
3. The second algorithm can be developed by including many scenarios such as SC with CSIT, MC with CSIR, and MC with CSIT.

4. The scope of the analysis in both algorithms can be expanded to include the BER, SER, PER, and throughput, leading to whole analysis of system performance.
5. Systems studied in this thesis can be expanded to include MU-MIMO, and downlink systems.
6. Systems studied in this thesis can be expanded to the massive MIMO systems.
7. Study the impact of imperfect CSIT on the EC and F-SNRMG.

References

References

[1] T. Schenk, A. K. Sarangi, and A. Datta, “Capacity Comparison of SISO, SIMO, MISO & MIMO Systems,” in *2018 Second International Conference on Computing Methodologies and Communication (ICCMC)*, Dordrecht: Springer Netherlands, 2018, pp. 798–801.

[2] K. Sengar, N. Rani, A. Singhal, D. Sharma, S. Verma, and T. Singh, “Study and Capacity Evaluation of SISO, MISO and MIMO RF Wireless Communication Systems,” *Int. J. Eng. Trends Technol.*, vol. 9, no. 9, Mar. 2014, doi: 10.48550/arxiv.1403.7774.

[3] P. Yang *et al.*, “Single-Carrier SM-MIMO: A Promising Design for Broadband Large-Scale Antenna Systems,” *IEEE Commun. Surv. Tutorials*, vol. 18, no. 3, pp. 1687–1716, 2016, doi: 10.1109/COMST.2016.2533580.

[4] Lizhong Zheng and D. N. C. Tse, “Diversity and multiplexing: a fundamental tradeoff in multiple-antenna channels,” *IEEE Trans. Inf. Theory*, vol. 49, no. 5, pp. 1073–1096, May 2003, doi: 10.1109/TIT.2003.810646.

[5] J. R. Hampton, *Introduction to MIMO communications*. Cambridge university press, 2013.

[6] W. A. Al-Hussaibi and F. H. Ali, “A Closed-Form Approximation of Correlated Multiuser MIMO Ergodic Capacity With Antenna Selection and Imperfect Channel Estimation,” *IEEE Trans. Veh. Technol.*, vol. 67, no. 6, pp. 5515–5519, Jun. 2018, doi: 10.1109/TVT.2018.2837041.

[7] T. Schenk, “IQ Imbalance,” in *RF Imperfections in High-rate Wireless Systems*, Dordrecht: Springer Netherlands, 2008, pp. 139–183.

[8] D. Tandur and M. Moonen, “Compensation of RF impairments in MIMO OFDM systems,” in *2008 IEEE International Conference on Acoustics, Speech and Signal Processing*, Mar. 2008, pp. 3097–3100, doi: 10.1109/ICASSP.2008.4518305.

[9] E. Telatar, “Capacity of Multi-antenna Gaussian Channels,” *Eur. Trans. Telecommun.*, vol. 10, no. 6, pp. 585–595, Nov. 1999, doi: 10.1002/ett.4460100604.

[10] M. Chiani, M. Z. Win, and A. Zanella, “On the capacity of spatially correlated mimo rayleigh-fading channels,” *IEEE Trans. Inf. Theory*, vol. 49, no. 10, pp. 2363–2371, Oct. 2003, doi: 10.1109/TIT.2003.817437.

[11] C. Studer, M. Wenk, and A. Burg, “MIMO transmission with residual transmit-RF impairments,” in *2010 International ITG Workshop on Smart Antennas (WSA)*, Feb. 2010, pp. 189–196, doi: 10.1109/WSA.2010.5456453.

[12] C. Studer, M. Wenk, and A. Burg, “System-level implications of residual transmit-RF impairments in MIMO systems,” in *Proceedings of the 5th European Conference on Antennas and Propagation (EUCAP)*, 2011, pp. 2686–2689.

[13] E. Bjornson, P. Zetterberg, M. Bengtsson, and B. Ottersten, “Capacity Limits and Multiplexing Gains of MIMO Channels with Transceiver Impairments,” *IEEE Commun. Lett.*, vol. 17, no. 1, pp. 91–94, Jan. 2013, doi: 10.1109/LCOMM.2012.112012.122003.

[14] E. Bjornson, M. Matthaiou, and M. Debbah, “A new look at dual-hop relaying: Performance limits with hardware impairments,” *IEEE Trans. Commun.*, vol. 61, no. 11, pp. 4512–4525, 2013.

[15] X. Zhang, M. Matthaiou, E. Bjornson, M. Coldrey, and M. Debbah, “On the MIMO capacity with residual transceiver hardware impairments,” in *2014 IEEE International Conference on Communications (ICC)*, Jun. 2014, pp. 5299–5305, doi: 10.1109/ICC.2014.6884163.

[16] A. K. Papazafeiropoulos, S. K. Sharma, and S. Chatzinotas, “Impact of Transceiver Impairments on the Capacity of Dual-Hop Relay Massive MIMO Systems,” in *2015 IEEE Globecom Workshops (GC Wkshps)*, Dec.

2015, pp. 1–6, doi: 10.1109/GLOCOMW.2015.7414137.

[17] Kefeng Guo, Daoxing Guo, Yuzhen Huang, Xueling Wang, and Bangning Zhang, "Performance analysis of a dual-hop satellite relay network with hardware impairments," in *2016 25th Wireless and Optical Communication Conference (WOCC)*, May 2016, pp. 1–5, doi: 10.1109/WOCC.2016.7506612.

[18] A. K. Papazafeiropoulos, S. K. Sharma, S. Chatzinotas, and B. Ottersten, "Ergodic Capacity Analysis of AF DH MIMO Relay Systems With Residual Transceiver Hardware Impairments: Conventional and Large System Limits," *IEEE Trans. Veh. Technol.*, vol. 66, no. 8, pp. 7010–7025, Aug. 2017, doi: 10.1109/TVT.2017.2668460.

[19] A. Singal, D. Kedia, N. Jaglan, and S. D. Gupta, "Performance analysis of MIMO-OFDM system with transceiver hardware impairments," in *2017 4th International Conference on Signal Processing, Computing and Control (ISPCC)*, Sep. 2017, pp. 102–105, doi: 10.1109/ISPCC.2017.8269658.

[20] A. Singal and D. Kedia, "Performance Analysis of Antenna Selection Techniques in MIMO-OFDM System with Hardware Impairments: Energy Efficiency perspective," *Int. J. Electr. Comput. Eng.*, vol. 8, no. 4, p. 2272, Aug. 2018, doi: 10.11591/ijece.v8i4.pp2272-2279.

[21] X. Li, M. Huang, X. Tian, H. Guo, J. Jin, and C. Zhang, "Impact of hardware impairments on large-scale MIMO systems over composite RG fading channels," *AEU - Int. J. Electron. Commun.*, vol. 88, pp. 134–140, May 2018, doi: 10.1016/j.aeue.2018.03.010.

[22] A. Papazafeiropoulos, S. K. Sharma, T. Ratnarajah, and S. Chatzinotas, "Impact of Residual Additive Transceiver Hardware Impairments on Rayleigh-Product MIMO Channels With Linear Receivers: Exact and Asymptotic Analyses," *IEEE Trans. Commun.*, vol. 66, no. 1, pp. 105–

118, Jan. 2018, doi: 10.1109/TCOMM.2017.2753773.

[23] J. Li, X. Li, Y. Liu, C. Zhang, L. Li, and A. Nallanathan, "Joint Impact of Hardware Impairments and Imperfect Channel State Information on Multi-Relay Networks," *IEEE Access*, vol. 7, pp. 72358–72375, 2019, doi: 10.1109/ACCESS.2019.2919975.

[24] S. Bharati, P. Podder, N. Gandhi, and A. Abraham, "Realization of MIMO Channel Model for Spatial Diversity with Capacity and SNR Multiplexing Gains," *Int. J. Comput. Inf. Syst. Ind. Manag. Appl.*, vol. 12 (2020), pp. 066–081, Apr. 2020, [Online]. Available: http://arxiv.org/abs/2005.02124.

[25] H. Holma and A. Toskala, *LTE for UMTS: Evolution to LTE-advanced*. John Wiley & Sons, 2011.

[26] W. Jiang and H. D. Schotten, "Neural Network-Based Fading Channel Prediction: A Comprehensive Overview," *IEEE Access*, vol. 7, pp. 118112–118124, 2019, doi: 10.1109/ACCESS.2019.2937588.

[27] E. Basar, "Reconfigurable Intelligent Surfaces for Doppler Effect and Multipath Fading Mitigation," *Front. Commun. Networks*, vol. 2, p. 14, May 2021, doi: 10.3389/FRCMN.2021.672857/BIBTEX.

[28] T. L. Singal, *Wireless communications*. New Delhi: Tata McGraw-Hill Education, 2010.

[29] P. Wang and Y. J. Morton, "Multipath Estimating Delay Lock Loop for LTE Signal TOA Estimation in Indoor and Urban Environments," *IEEE Trans. Wirel. Commun.*, vol. 19, no. 8, pp. 5518–5530, Aug. 2020, doi: 10.1109/TWC.2020.2994037.

[30] A. Farzamnia, N. W. Hlaing, M. Mariappan, and M. K. Haldar, "BER comparison of OFDM with M-QAM modulation scheme of AWGN and Rayleigh fading channels," *2018 9th IEEE Control Syst. Grad. Res. Colloquium, ICSGRC 2018 - Proceeding*, pp. 54–58, Mar. 2019, doi: 10.1109/ICSGRC.2018.8657503.

[31] B. Lee and S. Choi, *Broadband wireless access and local networks: mobile WiMAX and WiFi*. U.S. Library of Congress.

[32] M. V. Jamali *et al.*, "Statistical studies of fading in underwater wireless optical channels in the presence of air bubble, temperature, and salinity random variations," *IEEE Trans. Commun.*, vol. 66, no. 10, pp. 4706–4723, Oct. 2018, doi: 10.1109/TCOMM.2018.2842212.

[33] A. Habib and S. Moh, "Wireless Channel Models for Over-the-Sea Communication: A Comparative Study," *Appl. Sci. 2019, Vol. 9, Page 443*, vol. 9, no. 3, p. 443, Jan. 2019, doi: 10.3390/APP9030443.

[34] J. Y. Taudien and S. G. Bilen, "Correlation Detection of Boundaries in Sonar Applications with Repeated Codes," *IEEE J. Ocean. Eng.*, vol. 45, no. 3, pp. 1078–1090, Jul. 2020, doi: 10.1109/JOE.2019.2903357.

[35] S. K. Das, *Mobile handset design*. John Wiley & Sons, 2013.

[36] S. Dixit and H. Katiyar, "Performance of OFDM in time selective multipath fading channel in 4G systems," *Proc. - 2015 5th Int. Conf. Commun. Syst. Netw. Technol. CSNT 2015*, pp. 421–424, Sep. 2015, doi: 10.1109/CSNT.2015.107.

[37] S. M. Aldossari and K. C. Chen, "Machine Learning for Wireless Communication Channel Modeling: An Overview," *Wirel. Pers. Commun. 2019 1061*, vol. 106, no. 1, pp. 41–70, Mar. 2019, doi: 10.1007/S11277-019-06275-4.

[38] P. Lea, *IoT and Edge Computing for Architects: Implementing edge and IoT systems from sensors to clouds with communication systems, analytics, and security*. Packt Publishing Ltd, 2020.

[39] Q. T. Zhang and S. H. Song, "Exact expression for the coherence bandwidth of rayleigh fading channels," *IEEE Trans. Commun.*, vol. 55, no. 7, pp. 1296–1299, Jul. 2007, doi: 10.1109/TCOMM.2007.900596.

[40] G. Sadeque, S. Mohonta, F. A.-I. J. of Science, and U. 2015, "Modeling

and characterization of different types of fading channel," *Int. J. Sci. Eng. Technol. Res.*, vol. 4, no. 5, p. 1410, 2015, Accessed: Jun. 30, 2022. [Online]. Available: https://www.researchgate.net/profile/Md-Golam-Sadeque/publication/336579078_Modeling_and_Characterization_of_Different_Types_of_Fading_Channel/links/5da6dc28299bf1c1e4c3a501/Modeling-and-Characterization-of-Different-Types-of-Fading-Channel.pdf.

[41] A. L. Imoize, A. E. Ibhaze, A. A. Atayero, and K. V. N. Kavitha, "Standard Propagation Channel Models for MIMO Communication Systems," *Wirel. Commun. Mob. Comput.*, vol. 2021, 2021, doi: 10.1155/2021/8838792.

[42] Z. Jie, L. Liang, and L. Jin, "Performance analysis of space time block code in MIMO-OFDM systems," *2011 IEEE 3rd Int. Conf. Commun. Softw. Networks, ICCSN 2011*, pp. 13–16, 2011, doi: 10.1109/ICCSN.2011.6014377.

[43] R. Xu and F. C. M. Lau, "Performance analysis for MIMO systems using zero forcing detector over fading channels," *IEE Proc. Commun.*, vol. 153, no. 1, pp. 74–80, Feb. 2006, doi: 10.1049/IP-COM:20045281.

[44] M. Matthaiou, N. D. Chatzidiamantis, G. K. Karagiannidis, and J. A. Nossek, "On the capacity of generalized-K fading MIMO channels," *IEEE Trans. Signal Process.*, vol. 58, no. 11, pp. 5939–5944, Nov. 2010, doi: 10.1109/TSP.2010.2058108.

[45] L. G. Ordóñez, D. P. Palomar, A. Pagès-Zamora, and J. R. Fonollosa, "High-SNR analytical performance of spatial multiplexing MIMO systems with CSI," *IEEE Trans. Signal Process.*, vol. 55, no. 11, pp. 5447–5463, Nov. 2007, doi: 10.1109/TSP.2007.896109.

[46] F. Rosas and C. Oberli, "Nakagami-m approximations for multiple-input multiple-output singular value decomposition transmissions," *IET Commun.*, vol. 7, no. 6, pp. 554–561, Apr. 2013, doi: 10.1049/IET-

COM.2012.0400.

[47] S. Markkandan, R. Logeshwaran, and N. Venkateswaran, "Analysis of Precoder Decomposition Algorithms for MIMO System Design," *IETE J. Res.*, pp. 1–8, May 2021, doi: 10.1080/03772063.2021.1920848.

[48] A. Sibille, C. Oestges, and A. Zanella, *MIMO: from theory to implementation*. Academic Press, 2010.

[49] H. Zhang, S. Jin, M. R. McKay, X. Zhang, and D. Yang, "High-SNR performance of MIMO multi-channel beamforming in double-scattering channels," *IEEE Trans. Commun.*, vol. 59, no. 6, pp. 1621–1631, Jun. 2011, doi: 10.1109/TCOMM.2011.050211.100251.

[50] J. G. Andrews, W. Choi, and R. W. Heath, "Overcoming interference in spatial multiplexing mimo cellular networks," *IEEE Wirel. Commun.*, vol. 14, no. 6, pp. 95–104, Dec. 2007, doi: 10.1109/MWC.2007.4407232.

[51] A. M. Lshokry, "Complexity and Performance Evaluation of Detection Schemes for Spatial Multiplexing MIMO Systems," PhD diss., M. Sc. Thesis, College of Engineering Islamic Gaza University, Department of Electrical Engineering, 2010.

[52] S. L. Loyka, "Channel capacity of MIMO architecture using the exponential correlation matrix," *IEEE Commun. Lett.*, vol. 5, no. 9, pp. 369–371, Sep. 2001, doi: 10.1109/4234.951380.

[53] S. H. Lee, X. P. Shi, T. H. Tan, Y. C. Tung, and Y. F. Huang, "Maximizing Channel Capacity of 3D MIMO System via Antenna Downtilt Angle Adaptation Using a Q-Learning Algorithm," *Electron. 2022, Vol. 11, Page 1189*, vol. 11, no. 8, p. 1189, Apr. 2022, doi: 10.3390/ELECTRONICS11081189.

[54] J. Mo and R. W. Heath, "Capacity Analysis of One-Bit Quantized MIMO Systems with Transmitter Channel State Information," *IEEE Trans. Signal Process.*, vol. 63, no. 20, pp. 5498–5512, Oct. 2015, doi:

10.1109/TSP.2015.2455527.

[55] A. Goldsmith, *Wireless Communications*. Cambridge University Press, 2005.

[56] M. M. Haque, M. S. Rahman, and K.-D. Kim, "Performance Analysis of MIMO-OFDM for 4G Wireless Systems under Rayleigh Fading Channel," *Int. J. Multimed. Ubiquitous Eng.*, vol. 8, no. 1, pp. 29–40, 2013, doi: http://dx.doi.org/10.14257/ijmue.2013.8.1.03.

[57] S. Teodoro, A. Silva, R. Dinis, F. M. Barradas, P. M. Cabral, and A. Gameiro, "Theoretical Analysis of Nonlinear Amplification Effects in Massive MIMO Systems," *IEEE Access*, vol. 7, pp. 172277–172289, 2019, doi: 10.1109/ACCESS.2019.2956596.

[58] M. A. Jensen and J. W. Wallace, "A review of antennas and propagation for MIMO wireless communications," *IEEE Trans. Antennas Propag.*, vol. 52, no. 11, pp. 2810–2824, Nov. 2004, doi: 10.1109/TAP.2004.835272.

[59] M. Raja and P. Muthuchidambaranathan, "BER performance of SVD-based transmit beamforming with various modulation techniques," *2010 5th Int. Conf. Ind. Inf. Syst. ICIIS 2010*, pp. 155–160, 2010, doi: 10.1109/ICIINFS.2010.5578715.

[60] M. Raja and P. Muthuchidambaranathan, "Performance analysis of closed-loop MIMO system," *Int. J. Comput. Appl.*, vol. 4, no. 12, pp. 14–19, 2011.

[61] S. Zhang and R. Zhang, "Capacity Characterization for Intelligent Reflecting Surface Aided MIMO Communication," *IEEE J. Sel. Areas Commun.*, vol. 38, no. 8, pp. 1823–1838, Aug. 2020, doi: 10.1109/JSAC.2020.3000814.

[62] Y. Fazea, A. Amphawan, Y. A. Al-Gumaei, A. M. Al-Samman, and W. Mugahed Al-Rahmi, "Modes power equalization based-singular value

decomposition in mode division multiplexing systems for multi-hungry bandwidth applications," *Opt. Fiber Technol.*, vol. 61, p. 102389, Jan. 2021, doi: 10.1016/j.yofte.2020.102389.

[63] Y. Jiang, J. Li, and W. W. Hager, "Joint transceiver design for MIMO communications using geometric mean decomposition," *IEEE Trans. Signal Process.*, vol. 53, no. 10 I, pp. 3791–3803, Oct. 2005, doi: 10.1109/TSP.2005.855398.

[64] M. M. Rana and M. S. Hasan, "An Improved Version of Water-Filling Algorithm for Underground Tunnel Systems: A Comprehensive Literature Review," *Proc. 3rd Int. Conf. Inven. Comput. Technol. ICICT 2018*, pp. 663–667, Nov. 2018, doi: 10.1109/ICICT43934.2018.9034408.

[65] K. Kumar and M. Singh, "Proposed Water filling Model in a MIMO system," *Int. J. Emerg. Technol. Adv. Eng.*, vol. 1, no. 2, pp. 127–131, 2011.

[66] D. Gesbert, H. Bolcskei, D. Gore, and A. Paulraj, "MIMO wireless channels: Capacity and performance prediction," *Conf. Rec. / IEEE Glob. Telecommun. Conf.*, vol. 2, pp. 1083–1088, 2000, doi: 10.1109/GLOCOM.2000.891304.

[67] H. Shin and J. H. Lee, "Closed-form formulas for ergodic capacity of MIMO Rayleigh fading channels," *IEEE Int. Conf. Commun.*, vol. 5, pp. 2996–3000, 2003, doi: 10.1109/ICC.2003.1203954.

[68] G. Fraidenraich, O. Lévêque, and J. M. Cioffi, "On the MIMO channel capacity for the Nakagami-m channel," *IEEE Trans. Inf. Theory*, vol. 54, no. 8, pp. 3752–3757, Aug. 2008, doi: 10.1109/TIT.2008.926467.

[69] I. Yoo, M. F. Imani, T. Sleasman, H. D. Pfister, and D. R. Smith, "Enhancing Capacity of Spatial Multiplexing Systems Using Reconfigurable Cavity-Backed Metasurface Antennas in Clustered MIMO Channels," *IEEE Trans. Commun.*, vol. 67, no. 2, pp. 1070–1084, Feb.

2019, doi: 10.1109/TCOMM.2018.2876899.

[70] T. Ratnarajah and R. Vaillancourt, "Quadratic forms on complex random matrices and multiple-antenna systems," *IEEE Trans. Inf. Theory*, vol. 51, no. 8, pp. 2976–2984, 2005, doi: 10.1109/TIT.2005.851778.

[71] Y. S. Cho, J. Kim, and W. Y. Yang, "MIMO-OFDM Wireless Communications with MATLAB.," p. 457, 2010.

[72] A. M. Elshirkasi *et al.*, "Numerical Analysis of Users' Body Effects on a Fourteen-Element Dual-Band 5G MIMO Mobile Terminal Antenna," *IEEE Access*, vol. 10, pp. 2083–2096, 2022, doi: 10.1109/ACCESS.2021.3139451.

[73] V. K. Minchula and G. S. Rao, "SVD-based IWFA for next generation wireless MIMO communication," *ICT Express*, vol. 4, no. 3, pp. 171–174, Sep. 2018, doi: 10.1016/J.ICTE.2018.01.011.

[74] K. D. Rao, "Channel coding techniques for wireless communications," *Channel Coding Tech. Wirel. Commun.*, pp. 1–394, Jan. 2015, doi: 10.1007/978-81-322-2292-7/COVER.

[75] W. A. Al-Hussaibi and F. H. Ali, "A closed-form approximation of correlated multiuser MIMO ergodic capacity with antenna selection and imperfect channel estimation," *IEEE Trans. Veh. Technol.*, vol. 67, no. 6, pp. 5515–5519, Jun. 2018, doi: 10.1109/TVT.2018.2837041.

[76] M. G. Bakulin, V. B. Kreindelin, and D. Y. Pankratov, "Analysis of the capacity of MIMO channel in fading conditions," in *2018Systems of Signal Synchronization, Generating and Processing in Telecommunications (SYNCHROINFO)*, Jul. 2018, pp. 1–6, doi: 10.1109/SYNCHROINFO.2018.8456962.

[77] V. B. Kreindelin and D. Y. Pankratov, "Analysis of the Radio Channel Capacity of a MIMO System under the Conditions of Spatially Correlated Fadings," *J. Commun. Technol. Electron. 2019 648*, vol. 64, no. 8, pp.

863–869, Aug. 2019, doi: 10.1134/S1064226919080242.

[78] J. Speidel, *Introduction to Digital Communications*. Cham: Springer International Publishing, 2019.

[79] S. Loyka and G. Levin, "Finite-SNR Diversity-Multiplexing Tradeoff via Asymptotic Analysis of Large MIMO Systems," *IEEE Trans. Inf. Theory*, vol. 56, no. 10, pp. 4781–4792, Oct. 2010, doi: 10.1109/TIT.2010.2059570.

[80] A. G. Burr, "Multiplexing gain of multiuser MIMO on finite scattering channels," *Proc. 2010 7th Int. Symp. Wirel. Commun. Syst. ISWCS'10*, pp. 466–470, 2010, doi: 10.1109/ISWCS.2010.5624389.

[81] Y. Wu, Y. Gu, and Z. Wang, "Efficient Channel Estimation for mmWave MIMO With Transceiver Hardware Impairments," *IEEE Trans. Veh. Technol.*, vol. 68, no. 10, pp. 9883–9895, Oct. 2019, doi: 10.1109/TVT.2019.2934167.

[82] X. Li, J. Li, Y. Liu, Z. Ding, and A. Nallanathan, "Residual Transceiver Hardware Impairments on Cooperative NOMA Networks," *IEEE Trans. Wirel. Commun.*, vol. 19, no. 1, pp. 680–695, Jan. 2020, doi: 10.1109/TWC.2019.2947670.

[83] M. Valkama, "Advanced I/Q signal processing for wideband receivers : models and algorithms," Tampere University of Technology, 2001.

[84] S. Mirabbasi and K. Martin, "Classical and modern receiver architectures," *IEEE Commun. Mag.*, vol. 38, no. 11, pp. 132–139, 2000, doi: 10.1109/35.883502.

[85] X. Yang *et al.*, "Hardware-Constrained Millimeter-Wave Systems for 5G: Challenges, Opportunities, and Solutions," *IEEE Commun. Mag.*, vol. 57, no. 1, pp. 44–50, Jan. 2019, doi: 10.1109/MCOM.2018.1701050.

[86] L. Smaini, *Rf analog impairments modeling for communication systems simulation: application to OFDM-based transceivers*. John Wiley & Sons,

2012.

[87] Z. Zhu, X. Huang, M. Caron, and H. Leung, "Blind self-calibration technique for I/Q imbalances and DC-offsets," *IEEE Trans. Circuits Syst. I Regul. Pap.*, vol. 61, no. 6, pp. 1849–1859, 2014, doi: 10.1109/TCSI.2013.2290826.

[88] M. Windisch and G. Fettweis, "Adaptive I/Q imbalance compensation in low-IF transmitter architectures," *IEEE Veh. Technol. Conf.*, vol. 60, no. 3, pp. 2096–2100, 2004, doi: 10.1109/VETECF.2004.1400410.

[89] O. MYLLÄRI, "Digital Transmitter I/Q Calibration: Algorithms and Real-Time Prototype Implementation - Trepo," Master's thesis. Tampere University of Technology, 2010.

[90] E. Cetin, I. Kale, and R. C. S. Morling, "Living and dealing with RF impairments in communication transceivers," *Proc. - IEEE Int. Symp. Circuits Syst.*, pp. 21–24, 2007, doi: 10.1109/ISCAS.2007.378172.

[91] Q. Zou, A. Tarighat, and A. H. Sayed, "Joint compensation of IQ imbalance and phase noise in OFDM wireless systems," *IEEE Trans. Commun.*, vol. 57, no. 2, pp. 404–414, 2009, doi: 10.1109/TCOMM.2009.02.060526.

[92] D. Petrovic, W. Rave, and G. Fettweis, "Effects of phase noise on OFDM systems with and without PLL: Characterization and compensation," *IEEE Trans. Commun.*, vol. 55, no. 8, pp. 1607–1616, Aug. 2007, doi: 10.1109/TCOMM.2007.902593.

[93] A. Mohammadian, C. Tellambura, and M. Valkama, "Analysis of self-interference cancellation under phase noise, CFO, and IQ Imbalance in GFDM full-duplex transceivers," *IEEE Trans. Veh. Technol.*, vol. 69, no. 1, pp. 700–713, Jan. 2020, doi: 10.1109/TVT.2019.2953623.

[94] A. Mohammadian and C. Tellambura, "Joint Channel and Phase Noise Estimation and Data Detection for GFDM," *IEEE Open J. Commun. Soc.*,

vol. 2, pp. 915–933, 2021, doi: 10.1109/OJCOMS.2021.3073348.

[95] M. Li, T. Hao, W. Li, and Y. Dai, "Tutorial on optoelectronic oscillators," *APL Photonics*, vol. 6, no. 6, p. 061101, Jun. 2021, doi: 10.1063/5.0050311.

[96] A. Hajimiri and T. H. Lee, "A general theory of phase noise in electrical oscillators," *IEEE J. Solid-State Circuits*, vol. 33, no. 2, pp. 179–194, Feb. 1998, doi: 10.1109/4.658619.

[97] A. Mohammadian and C. Tellambura, "RF Impairments in Wireless Transceivers: Phase Noise, CFO, and IQ Imbalance - A Survey," *IEEE Access*, vol. 9, pp. 111718–111791, 2021, doi: 10.1109/ACCESS.2021.3101845.

[98] N. N. Tchamov, J. Rinne, A. Hazmi, M. Valkama, V. Syrjala, and M. Renfors, "Enhanced algorithm for digital mitigation of ICI due to phase noise in OFDM receivers," *IEEE Wirel. Commun. Lett.*, vol. 2, no. 1, pp. 6–9, 2013, doi: 10.1109/WCL.2012.091912.120412.

[99] G. Liu and W. Zhu, "Compensation of phase noise in OFDM systems using an ICI reduction scheme," *IEEE Trans. Broadcast.*, vol. 50, no. 4, pp. 399–407, Dec. 2004, doi: 10.1109/TBC.2004.837884.

[100] A. Gersho and R. M. Gray, *Vector quantization and signal compression*, vol. 159. Springer Science & Business Media, 2012.

[101] Q. Gu, *RF system design of transceivers for wireless communications*. Springer Science & Business Media, 2006.

[102] S. Seo and J. Kim, "Efficient Weights Quantization of Convolutional Neural Networks Using Kernel Density Estimation based Non-uniform Quantizer," *Appl. Sci. 2019, Vol. 9, Page 2559*, vol. 9, no. 12, p. 2559, Jun. 2019, doi: 10.3390/APP9122559.

[103] A. Hasso, K. Jacksi, and K. Smith, "Effect of Quantization Error and SQNR on the ADC Using Truncating Method to the Nearest Integer Bit,"

2019 Int. Conf. Adv. Sci. Eng. ICOASE 2019, pp. 112–117, Apr. 2019, doi: 10.1109/ICOASE.2019.8723801.

[104] A. Papazafeiropoulos, E. Bjornson, P. Kourtessis, S. Chatzinotas, and J. M. Senior, "Scalable Cell-Free Massive MIMO Systems: Impact of Hardware Impairments," *IEEE Trans. Veh. Technol.*, vol. 70, no. 10, pp. 9701–9715, Oct. 2021, doi: 10.1109/TVT.2021.3109341.

[105] B. C. Nguyen, L. The Dung, T. M. Hoang, X. N. Tran, and T. Kim, "Impacts of Imperfect CSI and Transceiver Hardware Noise on the Performance of Full-Duplex DF Relay System with Multi-Antenna Terminals over Nakagami-m Fading Channels," *IEEE Trans. Commun.*, vol. 69, no. 10, pp. 7094–7107, Oct. 2021, doi: 10.1109/TCOMM.2021.3100504.

Appendix

```
function ps = function Waterfilling_ (SNR, Invers λ)

N = length (Invers λ);

Invers λ Sorted  = sort (Invers λ,'ascend');

Lagrange coefficients = (SNR+ cumsum (Invers λ Sorted))./(1:N)';

Correct Lagrange select condition = Lagrange coefficients - Invers λ Sorted
(1:end,1)>0 & Lagrange coefficients -[ Invers λ Sorted (2:end,1); Inf]<0;

Water Level = Lagrange coefficients (Correct Lagrange select condition);

D = Water Level - Invers λ;

D(D<0) = 0;

end
```

الخلاصة

في الوقت الحاضر يتَجهُ العالم نحو تَصميم الأجهزةُ الإلكترونيةُ بأقل تكلفة ممكنة. يعود السببُ في هذا التوجه الى أنه في بعض الأجهزة الإلكترونية يتم استخدام العديد من القطع الإلكترونية، والتي قد يصل عددها إلى مئات أو أكثر في جهاز واحد. وكما نعلم أن لا شيء يحدث إلا على حساب شيءُ آخر، لذا فإن تكلفة صنع الأجهزة الإلكترونية تنخفض على حساب جودتها. كما ان هذا التوجه قد طالَ أنظمة الاتصالات اللاسلكية متعددة المدخلات والمخرجات (أي نظام MIMO) ، حيث تحتوي هذه الأنظمة في الظروف الطبيعية على جهاز إرسال واستقبال فعلي على جانب الإرسال أو جانب الاستقبال أو كلاهما. يعاني جهاز الارسال والاستقبال الفعلي الموجود في أنظمة الاتصالات اللاسلكية متعددة المدخلات والمخرجات من العديد من الإعاقات مثل ضوضاء الطور و IQ- عدم الاتزان ،و مضخمات اللاخطية ، وضوضاء التكميم ، إلخ. وبالتالي، سيؤدي جهاز الإرسال والاستقبال الفعلي هذا إلى تشويه الإشارة التي تمر عبره ، مما يؤدي إلى تدهور أداء النظام.

تقترح هذه الرسالة خوارزميتين لتحليل أداء قنوات (MIMO) المتأثرة بخبو (Rayleigh) المسطح في ظل وجود جهاز الإرسال والاستقبال الفعلي. تحللُ الخوارزميةُ الأولى أداء قناة (MIMO) المرتبطة وقناة (MIMO) غير المرتبطة في وجود جهاز الإرسال الفعلي في أربعة سيناريوهات مختلفة: سيناريو (MC-MIMO) مع (CSIT)، وسيناريو (MC-MIMO) مع (CSIR)، وسيناريو (SC-MIMO) مع (CSIT)، وسيناريو (SC-MIMO) مع (CSIR). تأخذ هذه الخوارزميةُ تأثير المرسل الفعلي ليكون ضوضاء تشويه غاوسي مضافة بمتوسط صفر وتباين يُشار إليه بالرمز Υ_t. وبشكل أكثر وضوحًا، يفترض هذا النهج أن قوة التشويه لجهاز الإرسال المادي عند هوائي الإرسال n في نظام (SC-MIMO) يتناسب مع القدرة المخصصة لبث الإشارة عبر نفس الهوائي. بينما في نظام (MC-MIMO)، تفترض هذه الخوارزميةُ أن إجمالي قدرة التشويه للمرسل الفعلي تساوي مجموع قدرة التشويه لكل هوائي إرسال مقسومًا على عدد هوائيات الإرسال.

في المقابل، تحلل الخوارزميةُ الثانية أداء قناة (MIMO) المرتبطة وقناة (MIMO) غير المرتبطة في وجود المرسل الفعلي والمستقبل الفعلي في سيناريو واحد، وهو سيناريو (SC-MIMO) مع (CSIR). تقيّم هذه الطريقة تأثير المرسل المادي بنفس طريقة الخوارزمية الأولى ، وتقوم بتقييم تأثير المستقبل المادي كضوضاء تشويه غوسية مضافة غير مرتبطة بمتوسط صفر وتباين يُشار إليه بالرمز

γ_r. وبشكل أكثر وضوحًا ، تأخذ هذه الخوارزمية في الحسبان أن قوة التشويه للمستقبل المادي عند هوائي الاستقبال m في نظام SC-MIMO تتناسب مع متوسط قدرة الإشارة المستقبلة عبر الصف m من مصفوفة القناة.

بالإضافة الى ذلك، فإن الخوارزميتين المقترحتين في هذه الدراسة تحلل أداء قنوات MIMO المرتبطة وغير المرتبطة من حيث السعة (ergodic (EC)) وكسب مضاعف (SNR) المحدود (F-SNRMG). بالإضافة إلى ذلك، فأن كلا الخوارزميتين تستخدم نموذج (Kronecker) لحساب الارتباط بين عناصر القناة. كما أن مستوى الانحطاط المستخدم في عمليات المحاكاة لهذه الخوارزميات هو إما 0.08 أو 0.175 أو كليهما.

تتمثل أهم نتائج العمل في أن سعة قناة MIMO في الخوارزميات الأولى والثانية في معدلات (SNR) العالية تتوقف عن النمو عند قيمة تسمى حد السعة ، ولا يمتلك معامل الارتباط في الخوارزمية الأولى تأثيرًا على قيمة حد السعة ، بينما في الخوارزمية الثانية ، يلعب معامل الارتباط دورًا مهمًا في تحديد قيمة حد السعة.

وزارة التعليم العالي والبحث العلمي
جامعة بابـل / كلية الهندسة
قسم الهندسة الكهربائية

تحليل أداء القنوات متعددة المدخلات-متعددة المخرجات مع ضعف جهاز الإرسال والاستقبال

رســـالـــــة
مقدمة الى كلية الهندسة في جامعة بابل
كجزء من متطلبات نيل درجة الماجستير في الهندسة/ الهندسة الكهربائية/إلكترونيك

من قبل
مُحَمَّد عدي عبدالله حسون

اشـراف
الدكتورة وسن هاشم يعقوب

1444هـ 2022م